Imaging Magnetic Focusing in a Two-Dimensional Electron Gas

A dissertation presented

by

Katherine E. Aidala

to

The Department of Division of Engineering and Applied Sciences

in partial fulfillment of the requirements

for the degree of

Doctor of Philosophy

in the subject of

Applied Physics

Harvard University

Cambridge, Massachusetts

July 2006

Thesis advisor

Robert M. Westervelt

Author

Katherine E. Aidala

Imaging Magnetic Focusing in a Two-Dimensional Electron Gas

Abstract

The most direct way to understand how electrons move through semiconductor heterostructures is to spatially image their motion. The two-dimensional electron gas has proved its interest for both device applications and studies of fundamental physics, and offers many more opportunities as we better understand these systems. We wished to examine electron motion in magnetic fields, both to study fundamental physics (e.g. quantum Hall and spin-orbit coupling) and to design future devices (e.g. for spintronics and quantum information processing), and we successfully imaged the magnetic focusing of electron waves. To this end, much of my time at Harvard was spent building the He-3 cooled scanning probe microscope (SPM), which reaches 470 mK and can apply up to a 7 Tesla magnetic field perpendicular to the electron motion, or 3 Tesla parallel to the electron motion.

Prior to my work on this microscope, we created a V-shaped imaging interferometer that uses a backscattering technique to map out electron flow and interference. A negative charge is placed on the SPM tip, fully depleting the electrons below. Some electrons will backscatter and return to the QPC along the path they came, changing the conductance of the QPC. By scanning the tip above the surface and associating a change in conductance with each point, we image electron flow. We used this

backscattering technique to look at flow from a QPC in a perpendicular magnetic field, and observed the decay of the measurable change in conductance with tip position. A perpendicular field breaks time reversal symmetry such that the electron may not have a path to return to the QPC after being scattered.

To image the magnetic focusing of electron waves, we developed a new technique that can image electrons transmitted from one QPC to another, taking advantage of the adjustable strength of our tip voltage induced scatterer. We source current through one QPC and measure the transmission through a second. We bring the tip close to the surface of the heterostructure and place a voltage on the tip, creating an area of reduced (or increased) density of electrons beneath. This area deflects the electrons away from their initial trajectories, changing the transmission between the QPCs. By scanning the tip with a small voltage applied and measuring the change in transmission at each tip location, we can image the originally transmitted trajectories. We see clear images of the skipping orbits of magnetic focusing. By scanning the tip with a large voltage applied, we enhance interference effects and see fringes in our images. Simulations agree well with the experimentally obtained images.

Contents

Chapter 1

Introduction

1.1 Motivation and Overview

As the size of electronic devices shrinks, the quantum nature of the electron can be exploited to engineer novel devices. New applications are possible, with great interest in spintronics [53, 5] and quantum information processing [31, 6]. These coherent devices fall into two main categories: closed systems, which confine electrons (i.e. quantum dots) and allow manipulation of individual charge and spin, and open systems in which transport is dominated by ballistic electrons. I have concentrated mostly on open systems. The study of open, ballistic, systems can shed light on the fundamentals of transport in real systems, as well as lead to novel applications involving quantum electron optics and coherent control of electrons. The most basic question in these open systems is, "Where is the electron as it moves through the system?"

The most direct way to answer this question is to spatially image the electron flow.

It is no trivial task, for in many structures of interest (i.e. two-dimensional electron gas), electrons are buried beneath the surface under layers of semiconductors. Conventional imaging techniques like scanning electron microscopy, transmission electron microscopy, and scanning tunneling microscopy, cannot access these electrons. Scanning probe microscopy has the potential to affect the behavior of these electrons through a conducting tip that capacitively couples to the electrons. Electric charges and forces can be measured with scanning probe techniques, as well as magnetic fields. However, the ability to affect the electron behavior or to measure a force or charge does not necessarily lead to images that can be confidently interpreted. Good characterization of the imaging technique with theoretical modelling is necessary to relate the experimentally obtained images to actual electron flow.

The Westervelt group uses a low temperature scanning probe microscope (SPM) to locally scatter electrons while measuring transport properties through the system. We have imaged coherent electron flow from a quantum point contact (QPC), revealing both the modal structure of the QPC [46] and the branched nature of the flow [45]. We have used the SPM to image local electron density [25] and single electron quantum dots [18]. These experiments were done in a home-built SPM that can reach 1.7 K and lacks the ability to apply a magnetic field.

I have studied a V-shaped imaging interferometer [24], the topic of Chapter 3, using a QPC as a source of electrons. Flow from a QPC is imaged with excellent resolution by placing a charge on the SPM tip to deplete the electrons beneath. We measure the conductance across the QPC and scan the tip above the surface. Electrons are locally backscattered from this depleted area, and those that return through

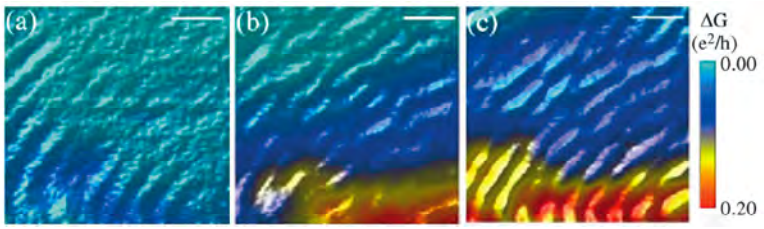

Figure 1.1: Enhancement of fringes when the reflecting gate is energized. The gate is at 0 V,−0.4 V, and −0.8 V left to right, with the gate fully depleting the electrons with $V = -0.8$ V. The scale bars are 50 nm long. (Reproduced from [24], see Chapter 3 for more information)

the QPC will decrease the conductance. By associating a change in conductance with each location of the tip, we can map out the electron flow. Areas of large electron flow will backscatter many electrons and change the conductance considerably. Areas of little or no flow will backscatter few electrons and the conductance will remain fixed. We see interference fringes throughout the images that are generated in this manner, due to the many backscattered paths the electrons can take. We introduced a gate on the surface of the structure that, when energized, will backscatter electrons. Turning on this gate enhances the fringes (Fig. 1.1) and allows us to control these paths to create an electron interferometer.

The desire to image physical systems that require lower temperatures and/or a magnetic field fueled my interest in building a second scanning probe microscope. A photo of this microscope is shown in Figure 1.2. This microscope reaches 470 mK, with a perpendicular magnetic field up to 7 Tesla or a parallel magnetic field up to 3 T. This microscope is well suited for the study of magnetic focusing, quantum Hall systems, large quantum dots or small quantum dots in magnetic fields, and spin-orbit coupling, to name just a few. The design of this new microscope is the topic of chapter 2, and the appendices are intended to serve as a manual for the operation of

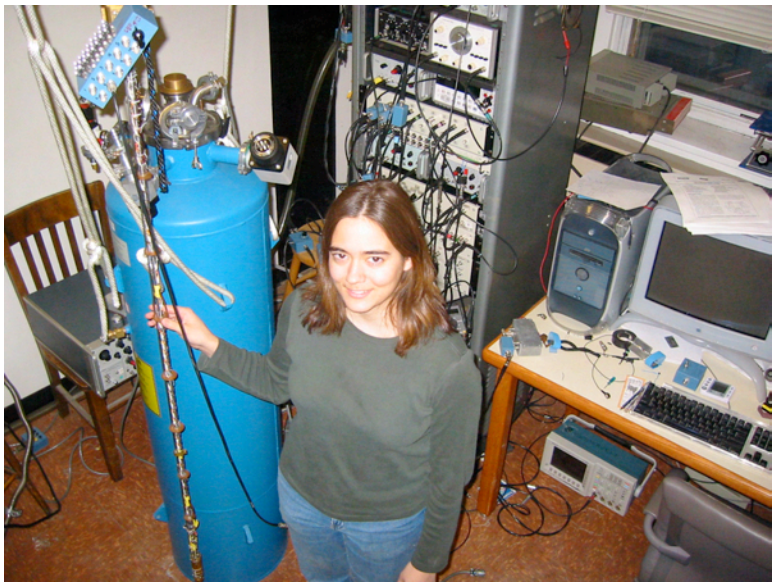

Figure 1.2: Experimental setup for the He-3 cooled scanning probe microscope.

this SPM.

We imaged electron flow in a perpendicular magnetic field, as described in Chapter 4. We began by using the same backscattering technique, with the electron traveling from the QPC, to the tip, and back. However, a perpendicular magnetic field breaks time reversal symmetry, and the electron cannot follow the same path to return to the QPC. As expected, we are unable to observe the flow as the magnetic field is increased.

We developed a new technique to image flow in a perpendicular magnetic field, which is flexible enough to image flow between any two points defined by QPCs in an open system. We source electrons from one QPC and measure the transmission through a second QPC. The tip is still used as a scatterer, but one that we control the scattering strength of to our advantage. A small negative voltage on the tip slightly lowers electron density below and acts as a diverging lens. A large negative

voltage serves as a strong scatterer and can backscatter the electrons that hit it. (In a sufficiently strong magnetic field, the electrons will curve around and continue their forward motion). This adjustable scatterer that we create with the tip deflects the electron trajectories, changing the transmission. By scanning the tip and recording the change in transmission at each point, we are able to image electron flow.

We developed this technique through imaging the magnetic focusing of electron waves. Electrons that emerge from one QPC will follow a circular orbit determined by the magnetic field. If a second QPC is placed after half an orbit, electrons that leave the first QPC with a small spread in angles will reconverge at this second QPC, resulting in high transmission. Introducing the tip as an adjustable scatterer deflects the electron trajectories and allows us to image the transmitted flow that was present before introducing the tip. A relatively weak scatterer leads to a good image of transmitted flow (Fig. 1.3), while a strong scatterer enhances the interference that we see in the image (Fig. 1.4). Chapter 4 shows the experimental images and theoretical simulations of this imaging technique.

There are many exciting directions to take now that we have a SPM that reaches 470 mK and has the ability to apply a magnetic field. Parisa Fallahi and I have imaged a single electron quantum dot in magnetic fields up to 6.5 Tesla. See her thesis [17] for details. Preliminary work has been done with Stefano Roddaro and the new students in the lab on a quantum Hall system, and a collaboration has recently been established with Leonid Rokhinson to study spin-orbit coupling in a two-dimensional hole gas. I expect these and many more experiments to provide stunning images of electron flow in the future.

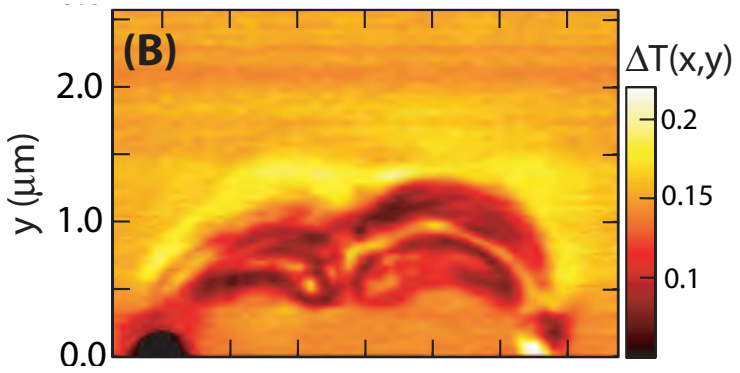

Figure 1.3: Experimental image of magnetic focusing, near the second focusing peak, revealing the electron bouncing along the wall between two quantum point contacts (dark and light circles). This image is obtained by using the tip to slightly deflect electrons, changing the transmission between the two point contacts. See Chapter 4 for details.

1.2 Background

Before describing my work at Harvard, I will present the common background to the experiments. All the imaging that I have done involves electrons confined in a two-dimensional electron gas and quantum point contacts. Additionally, I add a brief history of the scanning probe microscope with references to the existing present day low temperature scanning probe microscopes.

1.2.1 Scanning Probe Microscopy

Scanning probe microscopy (SPM) is a relatively general term that applies to a class of microscopes that share the common factor of having a sharp and controllable tip located close to or in contact with a surface (see [29] for a comprehensive, introductory review). The invention of the scanning tunneling microscope (STM) in 1981 [8] led to rather rapid progress on different types of SPM. The difficulty is in keeping

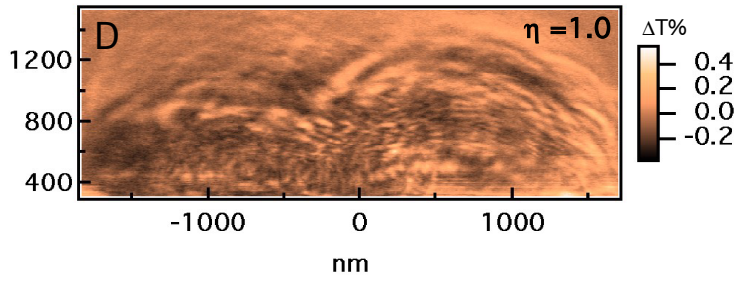

Figure 1.4: Experimental image of magnetic focusing, near the second focusing peak showing the two semicircles that result from the electron bouncing along the wall (below the image) between the two quantum point contacts. This image is obtained with the tip acting as a strong scatterer, enhancing interference fringes. See Chapter 4 for details.

a small, sharp tip close to a surface in a controlled fashion, such that the tip does not crash into the surface and break, or damage itself or the surface. The STM uses the tunneling current between a sharp metallic tip and a conductive substrate to measure the distance between tip and surface, and a piezotube or piezostacks to control the tip-sample separation. The tunneling current measures the density of states in the substrate and is capable of yielding atomic resolution. However, STM cannot be performed on non-conducting surfaces, nor can it probe deep within a structure. Near field scanning optical microscopy was invented in 1984 [26, 35], which uses near field optics to beat the resolution limit of far field optical microscopy. A narrow aperture is brought in close proximity of the surface of interest and scanned to generate an image. In 1986, the atomic force microscope was invented [7]. It was first used to take topographic images of material, capable of atomic resolution. A flexible cantilever is brought directly into contact with the surface and dragged across the surface. The cantilever's deflection changes as it goes over bumps and troughs, and this deflection is measured. Since the first images, numerous modes of operation have been devel-

oped, from new topographic imaging modes with less contact with the surface (i.e. tapping mode) to magnetic force measurements performed with a magnetic tip, to scanned gate microscopy, which is what we use in the Westevelt lab. A charged tip acts as a local and moveable gate that influences charged carriers below the tip. To date, the commercially available low temperature scanning probe microscopes leave room for improvements, and cryogenic scanning probe microscopes are best built in the lab.

There are several groups that use scanning probe microscopes to examine buried electrons in nanostructures at low temperatures, and many more in development that have yet to publish results. The Westervelt group has imaged electron flow in open systems [45, 46, 24] and closed systems [18, 9]. Klaus Ensslin's group at ETH, Zurich, has a similar system that they have used to image a quantum dot [34] and electrons in the quantum Hall regime [22]. McEuen's group at Cornell has a low temperature system tht they have used as a scanned gate microscope [54] and in other modes, like electric force microscopy [28]. A similar mode of electric force mircroscopy was used by Weitz et al. [50] to image the voltage drops in quantum Hall systems. Charles G. Smith's group at the University of Cambridge has a scanned gate setup and has imaged electrons in open systems [14] and large quantum dots [13]. A more recent system has been constructed by David Ferry's group at Arizona State University [3, 4]. Ray Ashoori's group at MIT employs a somewhat different imaging mechanism by measuring a capacitance between the scanning probe tip and the sample. When imaging in the quantum Hall regime, incompressible strips can be visualized as well as tunneling through a impurities in an incompressible strip created by the tip [42]. As a

final system of note, Yacoby has used a scanned single electron transistor to generate images with excellent charge sensitivity [55, 27]. There are other groups that do low temperature scanning tunnelling microscopy that I am not including here.

1.2.2 Two - dimensional electron gas and the quantum point contact

Confining electrons to two dimensions leads to fascinating physics (e.g. quantum Hall effect) as well as useful transport properties that can be exploited for electronic devices (e.g. high electron mobility transistor (HEMT)). Heterostructures are used to control the properties of electrons, through band structure engineering. Layers of different materials are grown on top of one another, designed so that the band discontinuities at the interfaces will confine electrons. Molecular beam epitaxy (MBE) is a common technique to grow high quality interfaces in these heterostructures. Though simple in concept, it is difficult to do right. Material sources are heated up so that molecules will travel through a vacuum space and land on the substrate of choice. Atomic monolayers can be deposited in a controlled fashion, generally using reflection high-energy electron diffraction (RHEED) within the MBE system to measure the deposition of the monolayers.

Figure 1.5 sketches the material layers and the energy band diagram at the top of the heterostructure structure for the GaAs/AlGaAs structure used in the magnetic focusing experiment of Chapter 4. From the top down, there is a 5 nm cap layer that resists oxidation. There is 20 nm of $Al_{0.3}Ga_{0.7}As$ followed by a delta doped layer of silicon atoms, and continued by another 22 nm of $Al_{0.3}Ga_{0.7}As$. 1000 nm of GaAs is

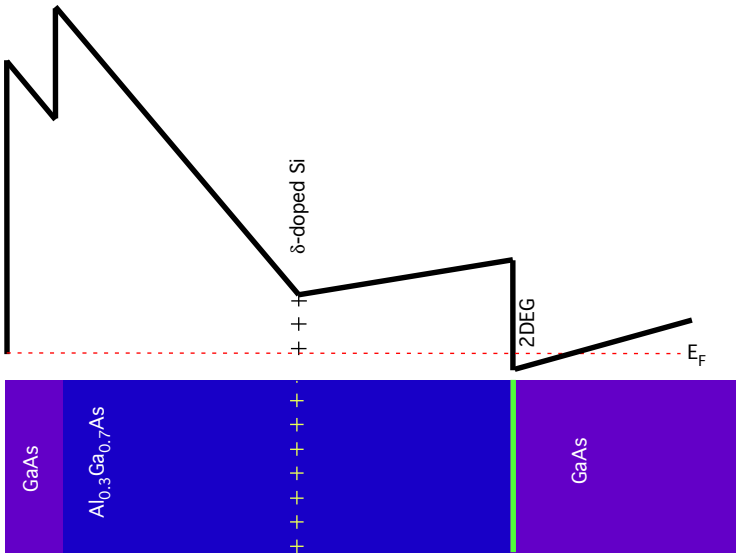

Figure 1.5: Structure of the GaAs/AlGaAs heterostructure used in the magnetic focusing experiment of chapter 4. A δ - doped silicon layer is found 22 nm above the 2DEG formed at the interface of GaAs and AlGaAs, which is 47 nm below the surface. The red dashed line indicates the Fermi level.

found below the AlGaAs, then a 20 period superlattice, 100 nm GaAs buffer, and the intrinsic GaAs substrate. The electrons are confined by the effective triangular well between the $Al_{0.3}Ga_{0.7}As$ and GaAs, 47 nm below the surface and 22 nm below the delta doped silicon layer.

The Fermi level is indicated by the red dashed line in Figure 1.5, and is determined by the donor layer of silicon atoms. Each silicon atom has four valence electrons, only three of which are bound in the crystal structure, which leaves one electron to be ionized. These electrons both satisfy the surface states and fall into the well that exists between the GaAs and AlGaAs. This well can be treated as a triangular box, and the energy levels associated with it can be found by solving Schroedinger's equation as if a particle in a box. To be truly two-dimensional, only the lowest energy

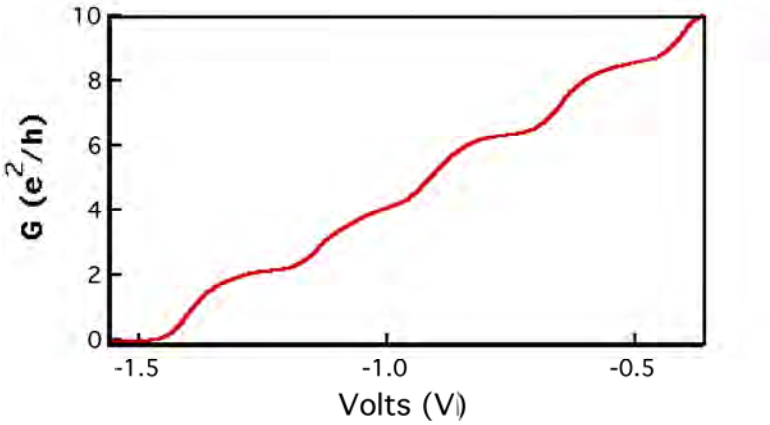

Figure 1.6: Typical conductance vs. voltage sweep of a quantum point contact (QPC). As the voltage becomes more negative, the QPC narrows and the conductance is reduced. Clear steps of $2e^2/h$ are seen here at 1.7 K.

level is occupied with electrons. See [15] for a good discussion.

One strives to have as perfect a crystal lattice as possible to have high mobility in a two-dimensional electron gas (2DEG). Impurities must be avoided, but even without unintentional impurities, the presence of the charged donor atoms 22 nm away from the surface affects the mobility. The electrons are always traveling through a potential profile that is determined largely by this donor layer. Small angle scattering limits the mobility in these samples. Generally speaking, the farther away these donor atoms are from the 2DEG, the higher mobility the sample will have. The structure shown here (Fig. 1.5) and used in the magnetic focusing experiments has mobility $\mu = 500,000\ Vcm/s^2$ and density $n = 3.8 \times 10^{11} cm^{-2}$.

Electrons can be further confined by a quantum point contact (QPC), first discovered in 1988 [49, 51]. Flow from a QPC is coherent and collimated. Two gates separated by a small distance can be defined on the surface with electron beam lithography and metal is evaporated into the lithographically defined pattern (see Chapter

2). Figure 1.6 shows a typical conductance versus voltage plot, taken at 1.7 K from one of the QPCs used in the magnetic focusing experiment of Chapter 4. When a sufficiently negative voltage is placed on the gates, the electrons below the gates are fully depleted, forcing electrons to travel between the split gates. Applying a more negative voltage continues to narrow the path between the gates, reducing the conductance. When the channel is on the order of the electron wavelength, it is possible to see quantized conductance steps of $2e^2/h$, with sufficiently low temperature and an adiabatic constriction. As a pinched off QPC opens up, individual modes are added, each of which carries $2e^2/h$ of conductance. This can be easily derived from the cancellation of the group velocity and the density of states in one dimension. The conductance, G, is given by

$$G = \frac{2e^2}{h} \sum T_i \tag{1.1}$$

In a QPC with no scattering at 0 K, the transmission coefficient, T, will be 0 or 1, and the steps would be abrupt as individual modes are added.

Chapter 2

Experimental Techniques

Construction of the new He-3 scanning probe microscope occupied a large portion of my time at Harvard. I describe the electronics and mechanical setup in this chapter, leaving some circuit diagrams to the appendix. Additionally, I include a brief account of sample fabrication (Section 2.5) and remarks on the low-noise electrical measurements that are necessary and details of the measurements that I performed (Section 2.4). The bulk of this chapter contains details of the electronics and the cryostat. Diagrams that are not needed for description but only if a significant repair or reconstruction is required are found in the appendix E.

2.1 The He-3 Scanning Probe Microscope

Scanning probe microscopy is a relatively recent development, with the scanning tunneling microscope invented in 1981 [8], and the atomic force microscope in 1986 [7].The challenge is to maintain a small (< 10 nm) distance between a sharp and

delicate tip and the sample surface. This is accomplished by feedback and good control over the tip-sample distance with piezotubes that can move in X, Y, and Z, where Z is always the vertical direction in this thesis. Operating a scanning probe microscope at low temperatures creates additional challenges, as thermally cycling a complex electrical-mechanical system is non-trivial. Vibration isolation is necessary, and sufficiently fast data acquisition is needed to perform experiments in a reasonable amount of time. When the first Westervelt microscope was built, a fast digital-analog converter that could output ±10V was not available, and it is still essentially unavailable with suitable ground isolation for low-noise measurements. We used the same design for the DAC that is described in Brian LeRoy's thesis [23] in part to remain compatible with the software that was written to drive the AFM. We now have DACs available from the electronic design lab at Harvard and IGOR programs to run them, which is something to consider for the next generation microscope. Additionally, with improvements in the speed of digital signal processing (DSP), it is worth considering options that use DSP to provide some functions that we perform with analog circuits. Noise must always be a consideration in evaluating the options.

Here I present the inner workings of the He-3 scanning probe microscope. Photos of the system are presented in Figure 2.1, 2.2, 2.3, and 2.4. Figure 2.5 is a schematic overview.

2.1.1 Overview

The scanning probe microscope can be thought of as three large circuits: the cantilever; the high voltage; and the device leads. These circuits share common

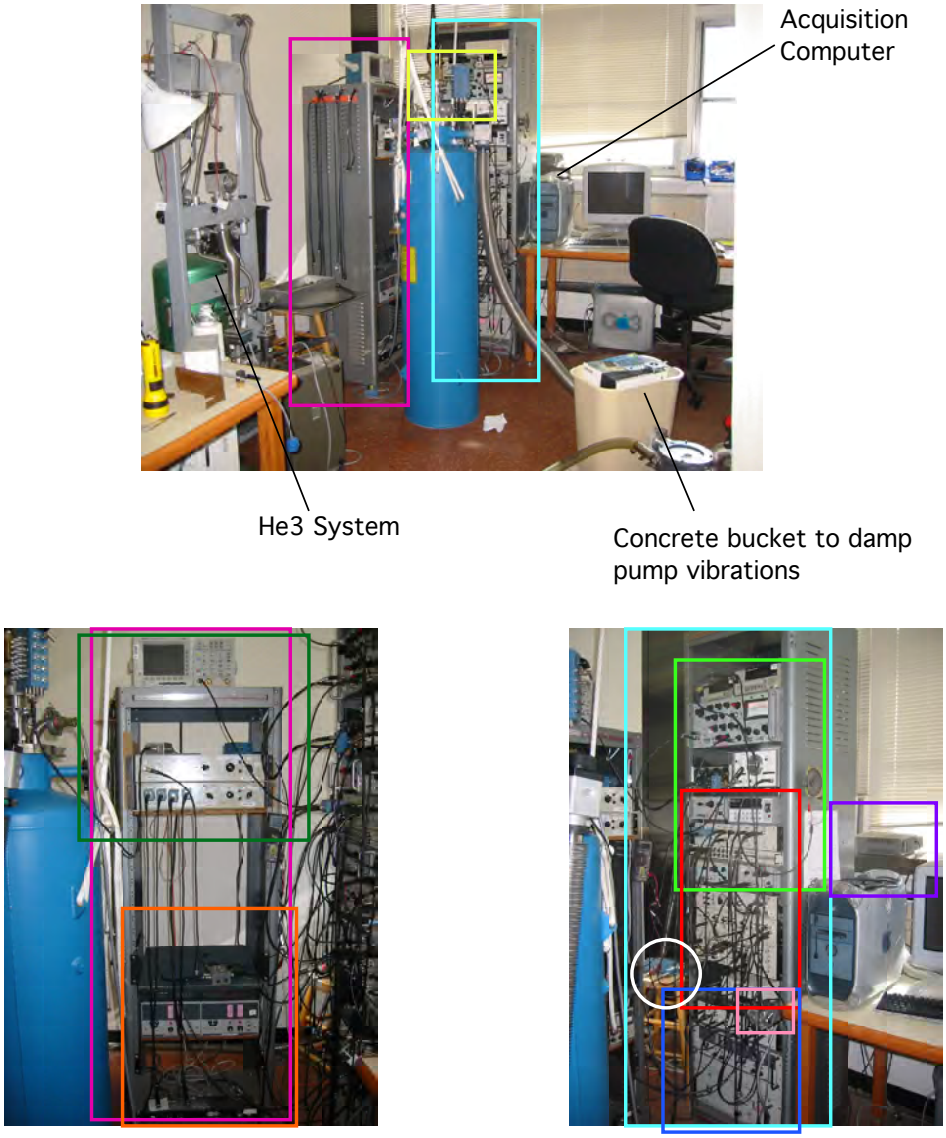

Figure 2.1: Photos of the He-3 system in McKay 204. The boxes indicate areas with closer photos and are color coded. The lower right image is repeated in more detail in Fig. 2.2. The lower left is in Fig. 2.3. The contents of the home-built electronics boxes are included in this chapter and in Appendix E.

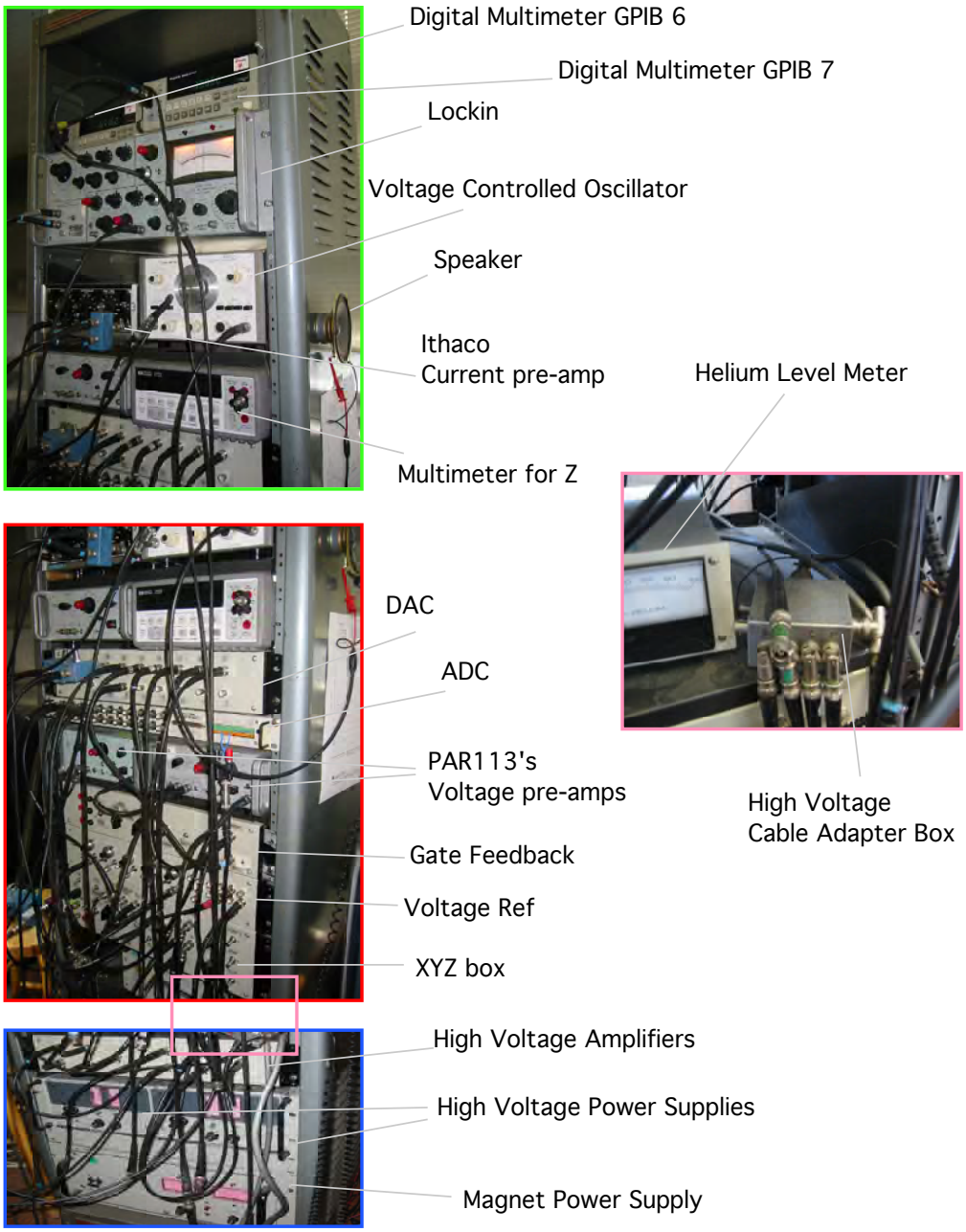

Figure 2.2: Photo of most of the electrical equipment of the He-3 microscope.

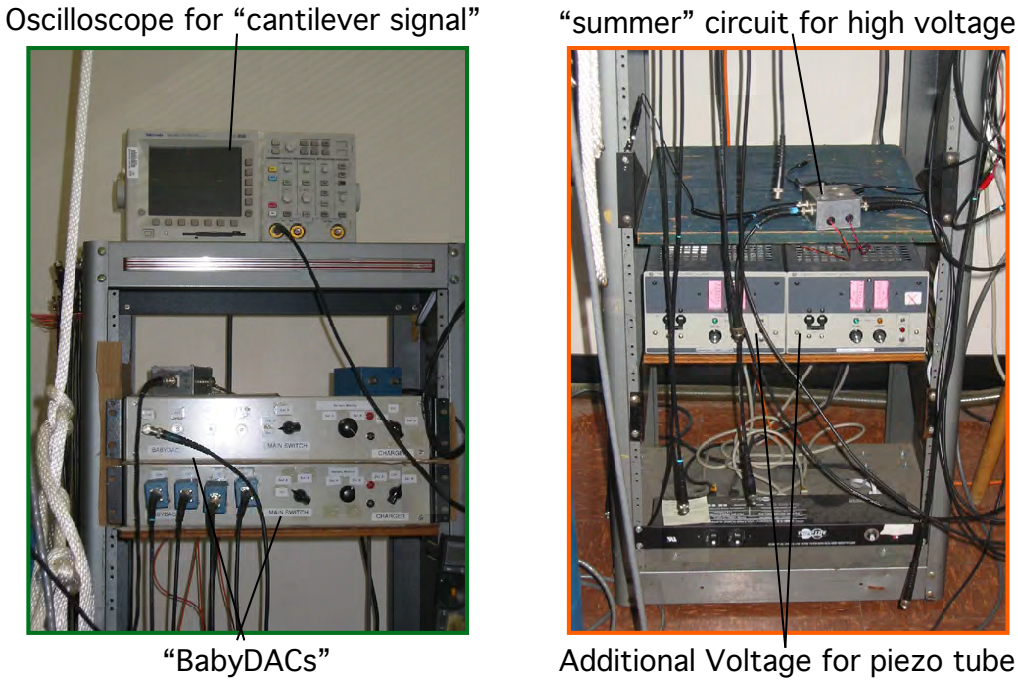

Figure 2.3: Photo of shorter electronics rack for the He-3 microscope.

elements, like the digital analog converter box, and both the cantilever and high voltage lines are part of the feedback circuit. Figure 2.5 sketches these relationships, while Figures 2.1, 2.2, 2.3, and 2.4 show photos of the actual instrument.

The dunker stick has three Fisher connectors: one 24 pin that connects to the 24-pin switcher box that controls the device leads; and two ten-pin connectors (see Figure 2.4). The blue outlined ten-pin connector attaches to the high voltage, and the yellow outlined connector controls additional low voltage lines, including the cantilever bridge circuit. The 24-pin connector is relatively straightforward. BNCs are connected directly from whatever is supplying a voltage to the device to the 24-pin switcher box, and signals measured from the device are connected directly with BNCs to whatever pre-amplifier is desired. The pinout of the 24-pin connector is shown in

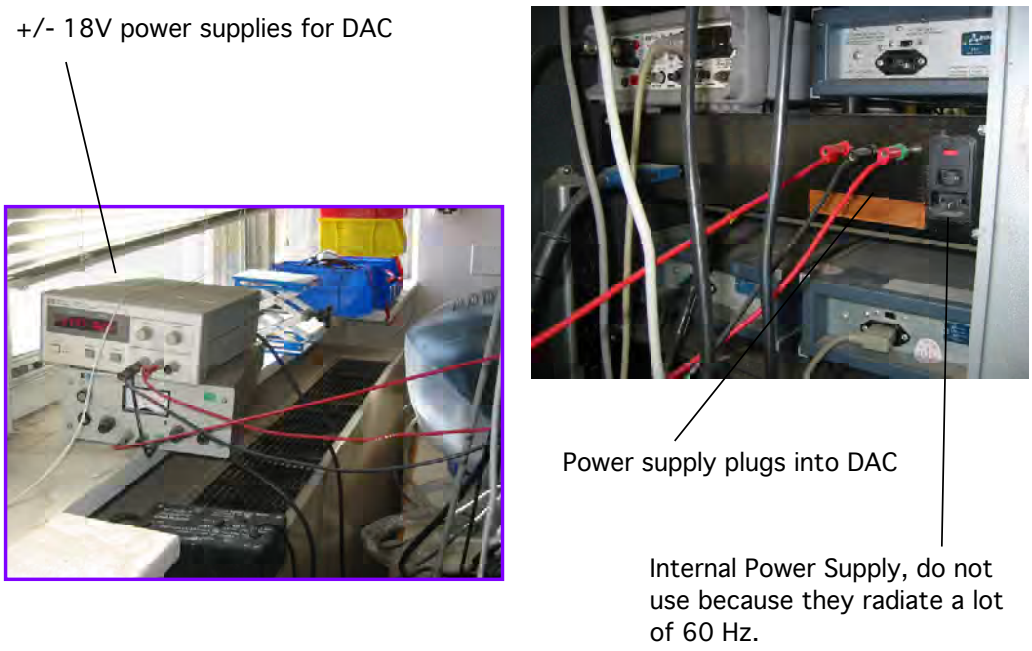

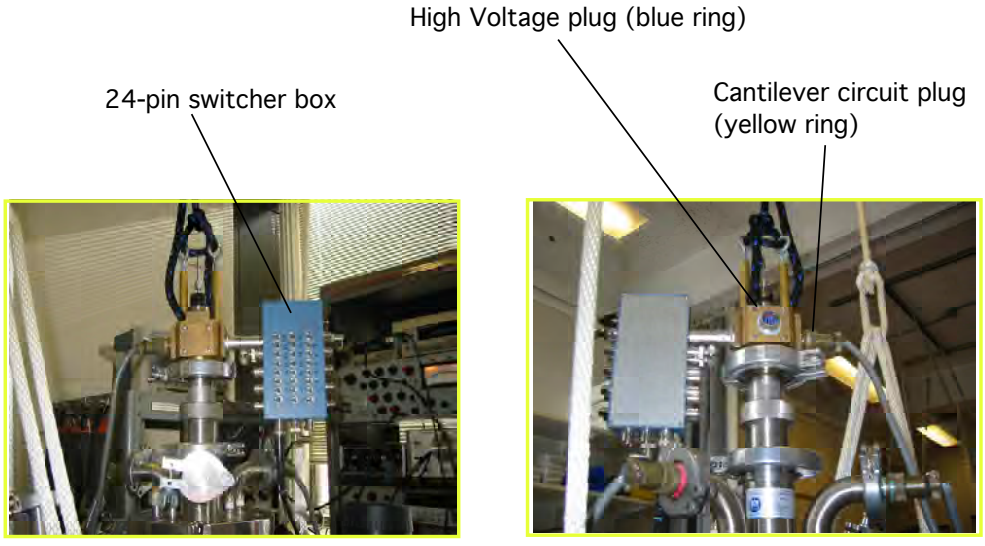

Figure 2.4: Photos of the back of the tall electronics rack and the dunker stick inside the blue dewar.

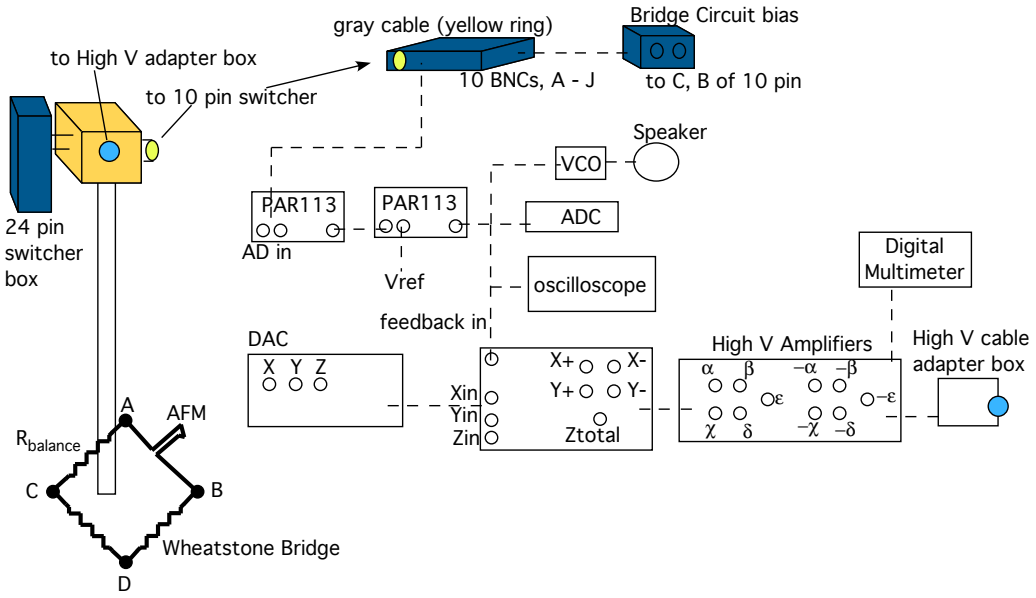

Figure 2.5: A schematic of the overall electrical setup for the He-3 SPM. Dotted lines indicate at least one connection exists between the boxes, and the yellow and blue Fisher connectors attach through a cable to the yellow and blue circles indicated in the diagram.

Figure 2.6.

Cantilever circuit

The gray cable bundles the ten wires leading from the dunker stick connector (Figure 2.4) to the ten pin switcher box (Figure 2.7), labeled A - J. Four of the leads on the dunker stick (A - D) are attached to the Wheatstone bridge circuit, sketched in Figure 2.5. The bridge circuit provides a sensitive way to measure a small change in resistance. A bias voltage is applied between B and C, and the voltage difference is measured between A and D. The resistor $R_{balance}$ is chosen to approximately match the resistance of the AFM cantilever and must have similar thermal drift. The measured voltage difference should be near zero. The bias comes from a small blue box with a

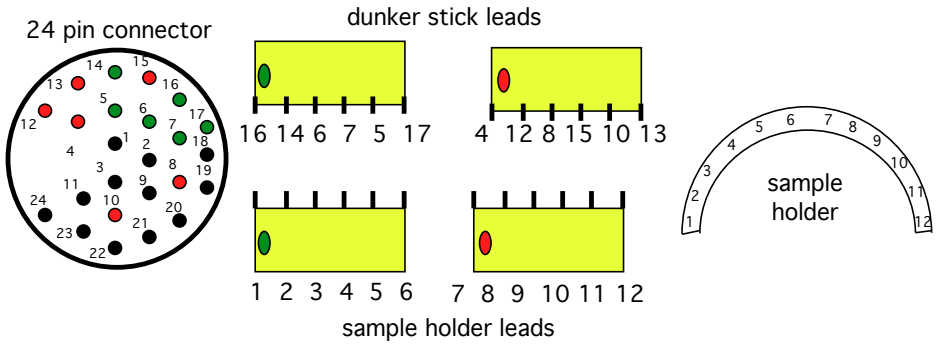

Figure 2.6: Pinout of the 24-pin Fisher connector at the top of the dunker stick, which connects to the sample leads. The connections at the bottom of the dunker stick are indicated, as well as the connections of the sample holder.

battery and variable gain setting (see Figure 2.7), which also adds the tip voltage bias to the circuit. Two PAR113 voltage pre-amplifiers are used to measure the voltage difference (Fig. 2.2). Two are necessary because the cantilever and balance resistor are not perfectly matched. In order to obtain a gain of 100,000 and avoid overloading the pre-amp, the first is set to 500 and the output fed into the second. An arbitrary reference voltage is used to essentially zero the difference, and the second gain is set to 200. Small changes in resistance are now easily detectable. The output of the second pre-amp is what I refer to as the "cantilever signal" that plays a vital role. It is a measure of the deflection of the cantilever.

The cantilever signal is passed to multiple places. It is read directly in through the analog digital converter and can be plotted by the AFM program as the tip is scanned. It is fed to the voltage controlled oscillator (VCO) and converted to a triangle wave at a given frequency (about 1 kHz), which is then connected to a speaker. It is also fed to an oscilloscope. This signal provides the most information about what is happening at the tip, and the combination of the audio information and visual

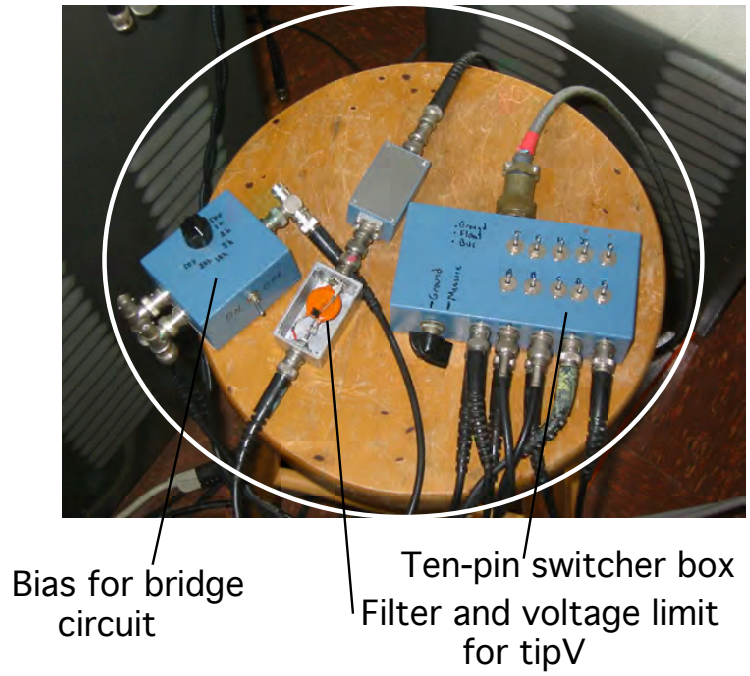

Figure 2.7: The 10-pin switcher box that carries low voltage connections to the dewar. The tip circuit, thermometer, and LED are connected through here.

display on the oscilloscope is extremely useful. The cantilever signal is also the input to the feedback of the XYZ box. The feedback strives to keep its two inputs equal. The reference input is grounded. The output of the feedback is summed into the Z output, changing the height of the tube, which brings us to the high voltage circuit.

But first, there are a few more connections to discuss on the low voltage ten-pin connector. There are leads that are connected to a thermometer and an LED. The thermometer is a calibrated silicon diode from Lakeshore, to which you source a current and measure a voltage (the Keithley source meter is convenient for this). The LED is a GaAs diode that should be able to excite additional carriers in GaAs, or otherwise be used for photoconductive effects. However, I have yet to see any results from turning on this diode; it may be positioned too far away from the sample. Figure 2.8 shows the pinout of the low voltage ten-pin connector on the dunker stick.

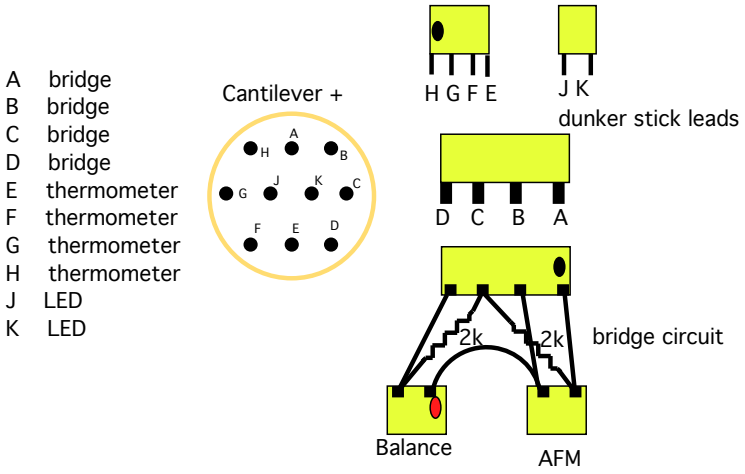

Figure 2.8: Pinout of the low voltage ten-pin connector, and the leads to the wheatstone bridge circuit at the bottom of the dunker stick.

High voltage circuit

The blue outlined connector on the dunker stick leads to the piezo tube. There are ten pins on the connector, though only five are used for the tube, and two more are wired to mini-coaxial cables for future use (e.g. oscillating the tip in Z with an additional piezo). The five high voltage lines are connected to the four quadrants of the tube, +X, +Y, -X, -Y, and the inside electrode of the tube, Z.

The gray cable that connects to the dunker stick attaches to a small silver box that exists to adapt the five BNC leads carrying the high voltage to this ten-pin connector (Figure 2.2). The total Z voltage that goes to the tube is read on the digital multimeter from this point. The Z voltage provides useful information about how extended or retracted the tube is, if there is drift, etc. The high voltages come from the high voltage amplifiers, which take in a voltage from -10 V to 10 V and multiply by -30. The input to the amplifiers comes from the XYZ box. X and Y are fed in from the digital analog converter (from the computer), and X and Y are negated so that X, -X, Y, and -Y are all output from the XYZ box. Z can be input from the DAC and summed with the output of the feedback and the plane (see section 2.2.1). To summarize, X, Y, and Z are input from the computer, through the DAC, negated and summed as needed, amplified, and passed through an adapter to the dunker stick. The pinout at the dunker stick is shown in Figure 2.9.

Feedback summary

The cantilever deflects when it hits a bump. This results in a change in resistance that is amplified by the PAR113's. This amplified signal is fed into the feedback

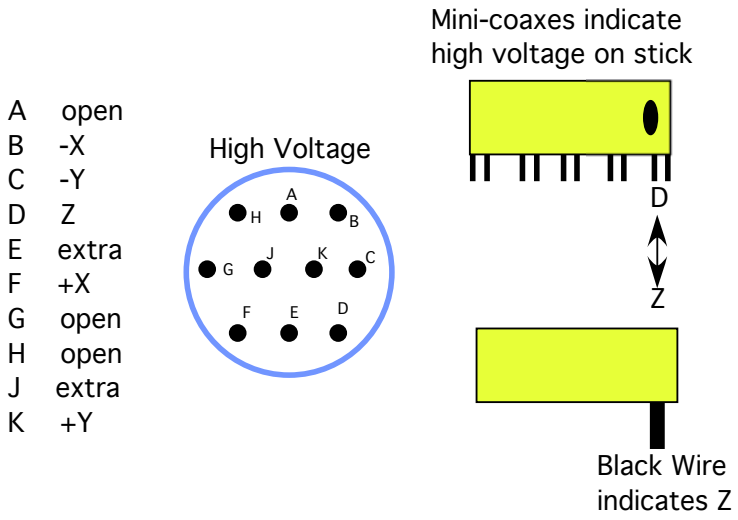

Figure 2.9: Pinout of the high voltage Fisher connector at the top of the dunker stick, and the leads to the bottom.

input. The output is sent to the Z voltage on the tube. The tube will extend or pull back as needed. This changes the cantilever signal, which changes the feedback, etc.

2.2 Electronics

Five of the main electronic boxes are home-built. These are the "XYZ box," the "High Voltage Amplifier Box," the "Voltage Reference Box" (also known as the "ramper box" or "summer box"), the Digital Analog Converter (DAC) and the "Gate Feedback Box". The gate feedback is identical to the XYZ box with only the feedback circuit hooked up, and I'll cover the slight difference in the XYZ box section.

Excluding the high voltage box, all the circuits were made with PCAD, in Jim MacArthur's Instrument Design Lab. I have reproduced the layout in this thesis in case it is ever needed for debugging in the future (see appendix E), and provided a

CD with these diagrams for easier use. The circuit is first put together schematically in PCAD and then the printed circuit board (PCB) layout is done by hand in PCAD. It takes about a week to get the boards, and at the time of writing 3 copies cost $100 (minimum order). Surface mount chips are easy to solder to these printed circuit boards, as are through-hole components. To correctly read these circuit diagrams, you need to be aware of the "net" labels, which appear in rectangular boxes. Different portions of a circuit are connected at the points with the same NET label.

2.2.1 XYZ box

The XYZ box is composed of four parts: the feedback circuit, the X chunk, the Y chunk, and the overall summing of the different parts. As this was the first PCB that I designed, there were a few non-fatal flaws. First, you should not solder wires from the physical box that holds the circuit directly to the printed circuit board. The points labeled "TP" indicate such connections. You should always make the board easily removable for future access or replacing by using connectors that can be taken apart and reassembled as needed. If you look at the actual board, you will notice a few thin wires that are soldered on and a few scratches though printed wires. There was an error in the wiring in the original design that I fixed afterwards by cutting and rewiring. The schematics I have included are correct, though you should double check the layout if you wish to reproduce the boards.

The box contains two "ON" switches; one tuns on the ± 18 V supply, the other the ± 9 V supply(Fig. 2.10). Both are batteries. The 9 V batteries can be checked with the lower two BNCs, below the ON switches. There should be 18 V between

Figure 2.10: Photo of the XYZ box, below the voltage reference box, with all the regular BNC connections.

the two, with each pin to ground measuring 9 V. The box must be opened up to replace these. The 18 V batteries are checked with the three BNCs above it. There should be 18 V across all three, with the center BNC splitting the value into 12 V and 6 V, which are the individual batteries being used. The knob below the ON switches toggles between the two (±) sets of batteries. You check only one at a time, and charge only one set at a time. To charge, flip the "charge" switch up. You can charge while running the box, though this may introduce noise to the system. It is a good habit to always charge one set of batteries when you turn off the box.

Feedback circuit

Figure 2.11 is a schematic of the feedback portion of the XYZ box. It is this part of the PCB that is wired in the gate feedback box, with one difference (the direction of the limiting diode). This is a proportional integrator feedback circuit, in that it multiples the input by a factor (that you can change) and then integrates, or averages, over a certain time (that you can control). The input is differential, comparing a reference voltage to, in this case, the cantilever signal. There is no gain in this input stage to an inverting op-amp. The second stage is the gain stage. There is a knob on the box for coarse gain and one for fine gain. Looking at the circuit, you can see that the total gain is $(R_{fine\ gain})/(R_{coarse\ gain})$ such that decreasing the fine gain or increasing the coarse gain will lower the sensitivity of the feedback. The coarse gain is labeled on the box by the resistors that the knob switches between; the fine gain is labeled as the fine gain. The next stage of the feedback is the integrator. There are three capacitor values to choose from, the larger capacitor averaging more.

The capacitor is rarely changed from 1 μF, and if changed, generally lowered. If there are oscillations in the circuit, first try lowering the proportional gain. If you need to stop the oscillations, turn the fine gain down to zero, and they should cease (do NOT scan like this, there is 0 gain which means no feedback!). The zener diodes across the integrator clamp the output from going above 12 V. These diodes also add a large resistance in parallel with the capactor, which prevents the feedback from railing if there is any offset current in the op-amp.

The last stage of the feedback allows you to choose whether or not to invert the feedback. The switch controlling this is labeled "invert". This generalizes the feedback circuit. The direction of the output depends on the task at hand. Finally, there is an optional limiting diode. For example, i f you wish to prevent the feedback from going above a certain value, you can set the value at the BNC input labeled V_{limit}. You would do this if you want to be able to pull the tube back (lower voltage) in case you hit something, but not be in contact the rest of the time. This can be used to carefully find gates, if desired, such that the tube will pull back if it hits a gate and be slightly above the surface for the rest of the area.

In the gate feedback box, the direction of this limiting diode is flipped. Generally, you would want to limit the output from suddenly going too negative (protective diodes should always be on your gate voltage lines to avoid a large positive voltage). We found one device that was very sensitive to sudden jumps in gate voltage, and had to ramp the feedback to the correct value as opposed to initializing by railing the feedback box before finding the correct value. It is generally a good idea to avoid sudden changes of voltages on your gates.

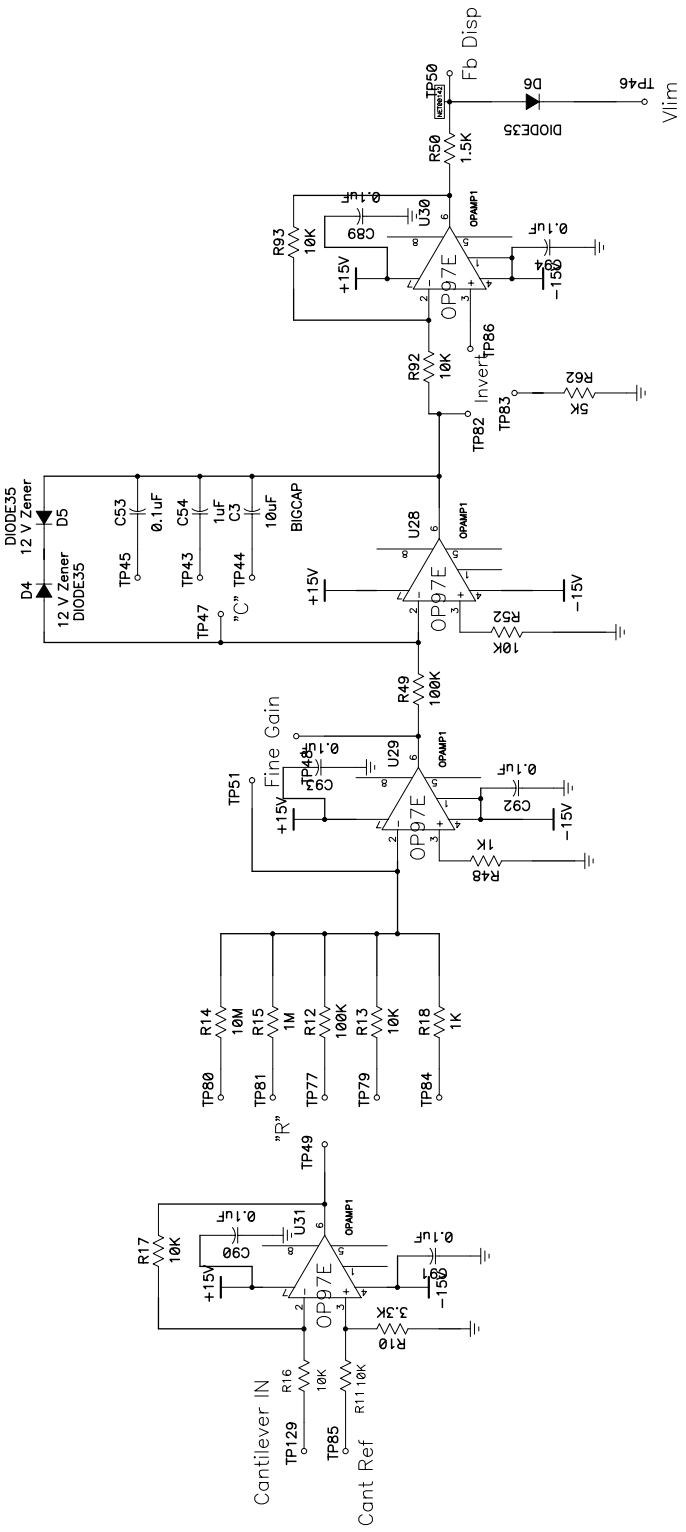

Figure 2.11: Schematic from the printed circuit board CAD program (PCAD) of the feedback portion of the XYZ box.

Plane circuits

The sample is generally not perfectly horizontal as mounted, causing a constant plane in the area scanned. Though the feedback can handle the plane, we take care of the plane with the XYZ box. It is important to have the plane on when accurately finding the surface, such that the "Zguide" (see Appendix 1) is relatively small and precise. The formula for a plane is $Ax + By = Cz$. We implement this with an analog circuit. Figures 2.12 and 2.13 show the schematic circuit. The circuits are identical, though laid out as reflections of each other (across a horizontal axis). The plane circuit also serves to take an X [Y] voltage in and provide both ±X [Y] out.

X_{IN} and Y_{IN} are labeled on the the box, and are provided from the DAC. These are taken in with a differential amplifier of gain 1, and compared to ground. There is an optional X and Y offset that can be added in the next stage, though I must say I've never used them and included them because they exist on the old system. This stage also has a switch that can be closed to add a time constant, but this capacitor is generally left open. τ_x and τ_y label these switches. At this point, the initial signal has been inverted twice, so +X or +Y is taken after this stage. There is an additional inverting stage from which -X and -Y are obtained. To make the "Ax" and "By" parts of the plane, there is a variable gain amplifier. -X [-Y] is the input, and the gain is between 2 and 0. This provides -2X to 0 or -2Y to zero. When they get added to +X and +Y, the overall range of coefficients is $\pm X$ and $\pm Y$, or an A and B of -1 to 1. The variable gain is provided by potentiometers whose knobs are labelled "Plane X" and Plane Y".

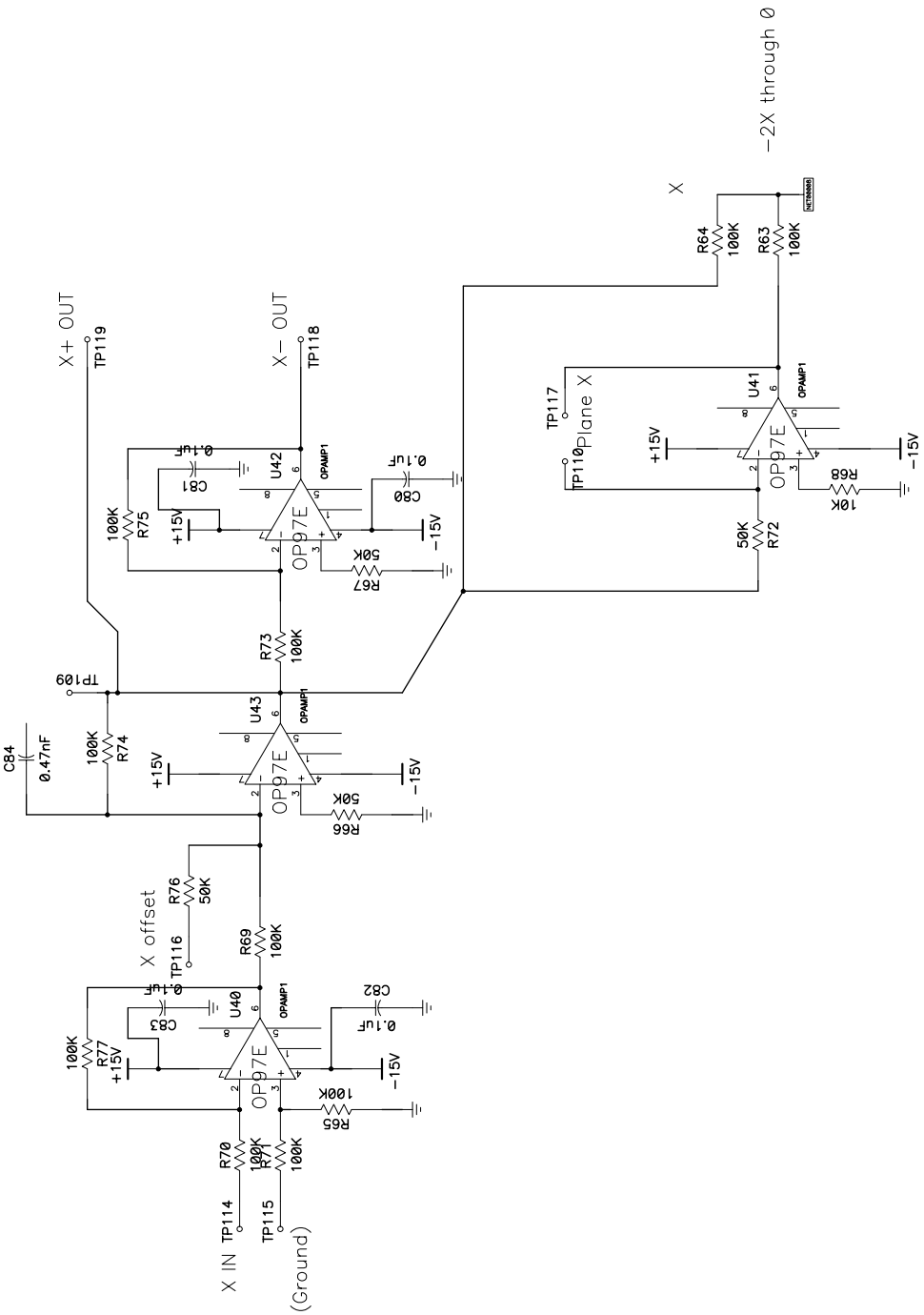

Figure 2.12: PCAD schematic of the X part of the XYZ box.

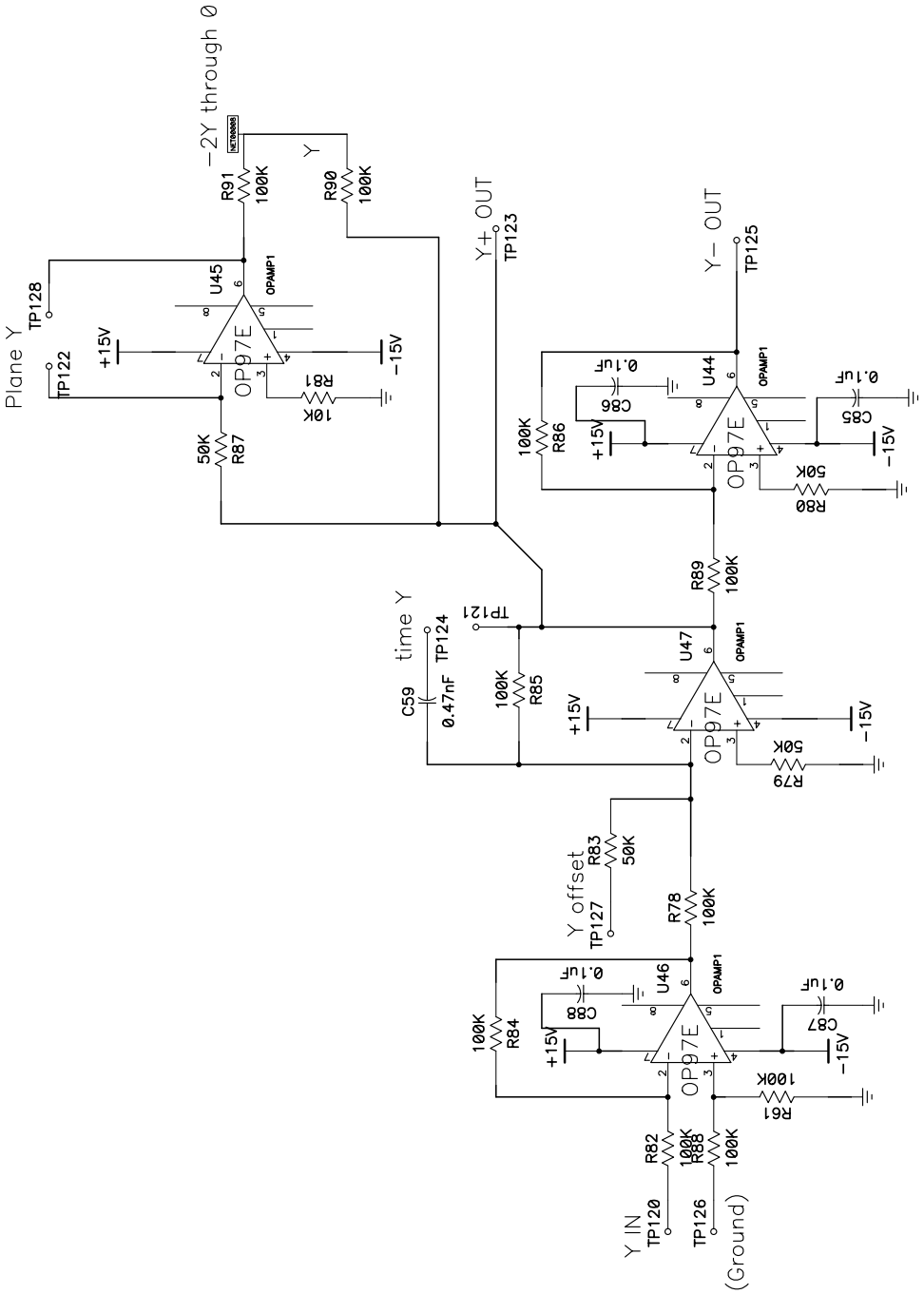

Figure 2.13: PCAD schematic of the Y part of the XYZ box.

Summation circuit

The final part of the XYZ box sums the overall voltages that are output on Z. $\pm X$, $\pm Y$, and Feedback Out have all been provided by the plane and feedback circuits. What remains is Z. Starting from the left in the schematic of Figure 2.15, the ±9V provide the Z offset. There is a potentiometer that selects this offset, and it should be set to zero by default. This Z offset is then added to the X and Y plane components in the next stage (NET00008). Then Z_{IN}, Z_{plane}, and Feedback are passed through potentiometer switches and summed together. These potentiometers serve to gently turn on and off the three components. They are not as sudden as a mechanical switch, which would be bad for the piezotube. The schematic for these "soft switches" is in Figure 2.14. They are on X and Y as well, but are placed at the output of the DAC. Z_{IN} is labeled as TipH, which corresponds to the value in the control software. TipH is output as channel 3 on the DAC, which is input to Z_{IN} on the XYZ box.

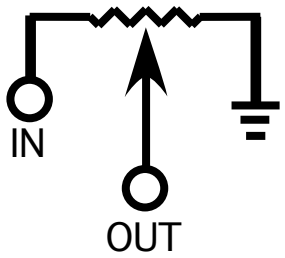

Figure 2.14: Schematic of the "softswitch" that controls the voltages to the piezo tube.

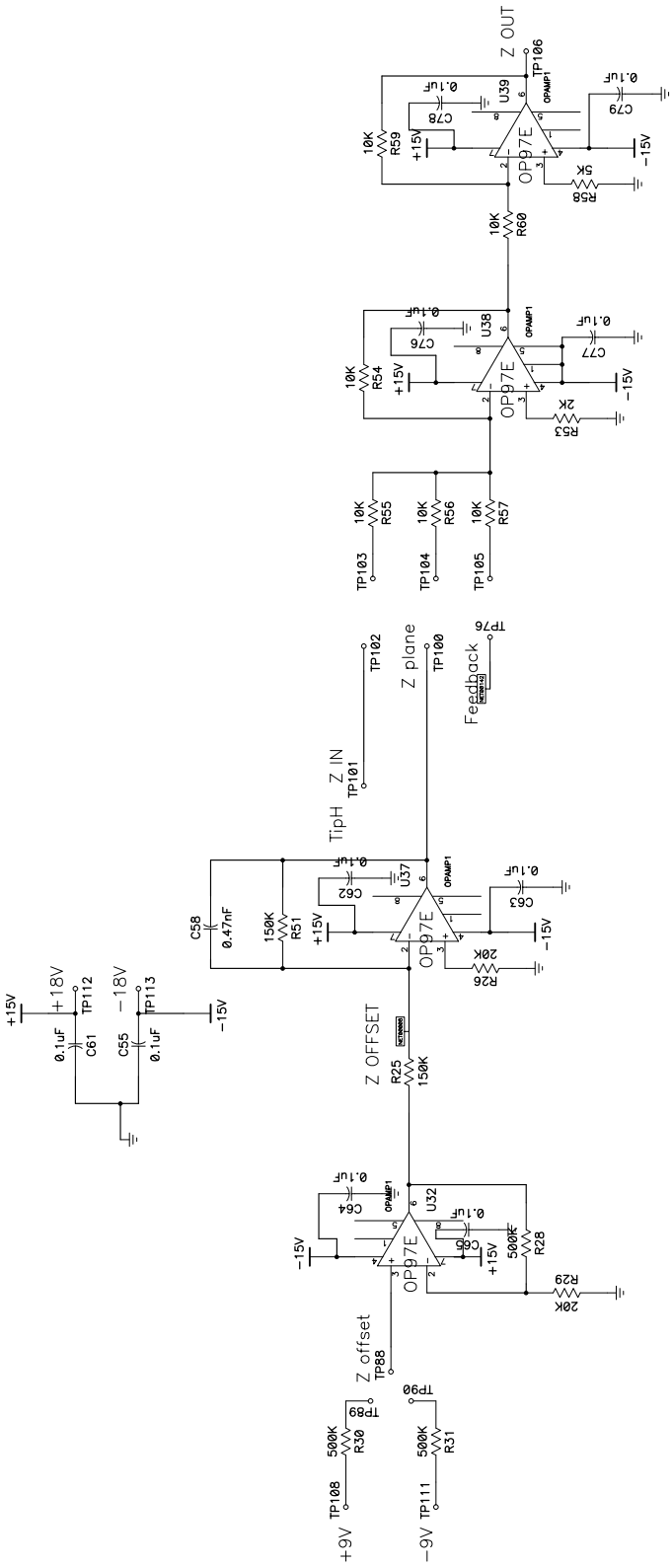

Figure 2.15: PCAD schematic of the final summation of the Z output in the XYZ box.

2.2.2 High Voltage Amplifiers

Apex Microtech makes good quality high voltage amplifiers. We use the PA85 for this application, because they have a large output voltage, a reasonable current, a large input differential, a built-in current limit, and a linear output stage. They can output ± 250V. An earlier attempt to use amplifiers that are cheaper and had higher output voltages was less successful, though they were functional when written in Brian LeRoy's thesis [23], where you will find a description of the PA97. These are class C amplifiers, and without a current limit. The lack of a current limit was probably its downfall, as we destroyed multiple amplifiers over time, possibly as the result of short circuiting them. Eventually, we moved back to the tried and true PA85's. It is possible that the PA94 or 95 would be good choices, as they are class AB (linear output stage) and have programmable current limits. They have a larger output voltage range than the PA85. They would also be compatible with the PCBoard I designed for the PA97's.

The PA85's are soldered together in a "bird's nest." You can see these "nests" in Figure 2.16. The components are soldered directly to the socket of the amplifier. This reduces the stray capacitances that may exist between lengths of wire. It is possible they can be put on a PC Board, designed with adequate heat sinking. The PA85s are mounted on the exterior of the metal box, attached to heat sinks. The circuit is as recommended by the company, and shown in Figure 2.17, including input voltage protection, a current limiting resistor, a compensation R-C network to determine the roll-off frequency of the open loop gain, and an input R-C network for additional compensation. All are written up in Mark Eriksson's thesis [16], and are in literature

available from APEX Microtech [30].

Figure 2.16: Photo of the inside of the high voltage box. Five amplifiers are soldered directly to the sockets for the amplifiers.

2.2.3 DAC

The digital analog converter box is described in Brian LeRoy's thesis [23]. It is programmed by a PCI digital output board made by National Instruments. Inputs pass through a digital isolation chip (Burr-Brown ISO150), from which the lines go to the converters, the address decoder and the control logic. There are sixteen channels on the box, the first eight of which are commonly used and are written into various software commands. The second eight can be accessed with the command "setvout mio16x [ch] [volts]". (For a glossary of software commands, see LeRoy's thesis [23].) These voltages can be swept by writing a macro in the script, or by programming a function in the AFM code. The DAC runs off of external power supplies that do not appear to add noise to any of the measurements I have performed, though the box could be converted to battery power if desired in the future. Initially, smaller power supplies were placed inside the DAC box, but these radiated considerable 60 Hz noise

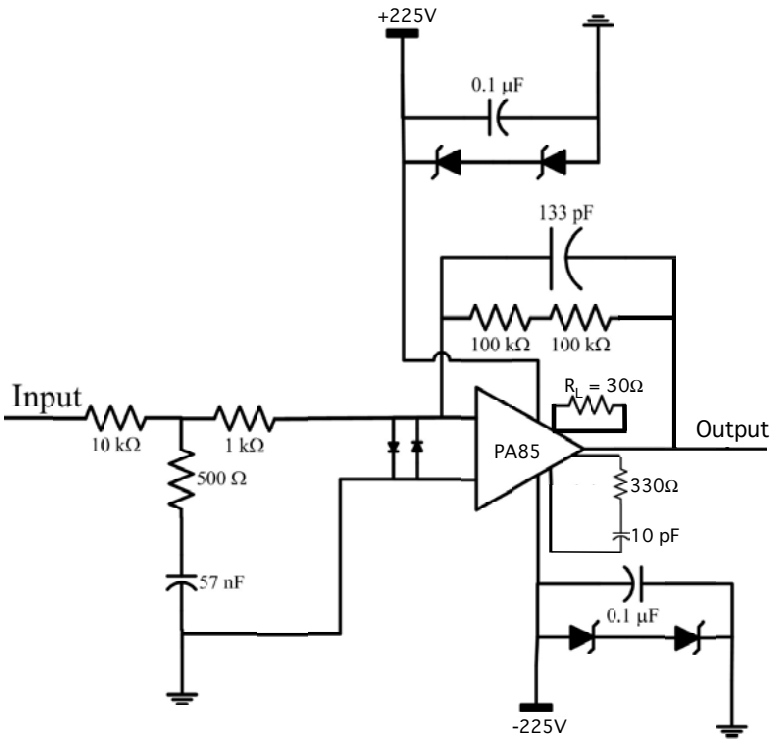

Figure 2.17: Schematic of the high voltage amplifier circuit of the PA85.

that was showing up in scans. The external supplies are connected through the back of the box (Figure 2.4).

If the control software is upgraded in the future, a DAC box from the instrument design lab would be an improvement as they are optically coupled to the computer, can run continuously off batteries, and can be purchased ready to use. This change would involve considerable rewriting of all the data acquisition code.

The circuit diagram and layout are included at the end of the thesis in Ap. E.2.

2.2.4 Voltage Reference Box

The Voltage Reference Box is a straightforward circuit that provides five variable voltage outputs and will sum up to four inputs together. The circuit diagram is included in the appendix E.2, and a photo in Figure 2.10. MAX6325 voltage references are used to provide a reliable 2.5 V reference, which is then modified with a knob to a potentiometer that determines the value (0 to max), and a switch that sets the maximum output. There are two switches associated with each voltage output. The left switch determines the sign of the output (- is to the left, + to the right) or turns off the output (center position). The right switch controls the output range. Left is smallest (-0.56 V to 0.56 V), center is mid-range (-2.05 V to 2.05 V) and the right is the largest (-6.17 V to 6.17 V). These outputs are used for the reference voltage on the second PAR113, and are generally useful whenever an arbitrary fixed voltage is required.

The righthand side of the box contains three summer circuits. These circuits are regularly used for the gate voltage, to add together the DAC "gatev" output

and the "vguide" if gate feedback is being used. They are general purpose summers and can be used anytime voltages are being added together. This box is sometimes called the "summer box" for obvious reasons, and the "ramper box" in older theses for historical reasons (before computers ramped voltages, earlier versions of this box performed that function).

The batteries are charged through the back of the box. The two sets of banana plugs should each have 12 V across them. If this box is not charged, the cantilever signal will be unstable or will not be usable.

2.3 Mechanical Design

I inherited the mechanical design from Brian LeRoy and Mark Topinka, and the cryostat is described in Brian LeRoy's thesis [23]. I will describe the important parts of the system and highlight the changes that I have been involved with.

2.3.1 The AFM

The AFM consists of the "cage" that contains the piezo tube (Figure 2.18), on top of which the sample is mounted, and the "head" that houses the cantilever (Figure 2.19). The head is mounted to the cage on three screws and held by three springs (Figure 2.20). These three screws allow for motion of the cantilever in the Z direction. The tip points to one of the screws, which directly raises and lowers the tip. The other two are needed to align the cantilever chip parallel to the sample, ensuring that the tip comes into contact with the sample and not the side of the cantilever chip. The top of the head has two screws which allow for coarse positioning of the tip in

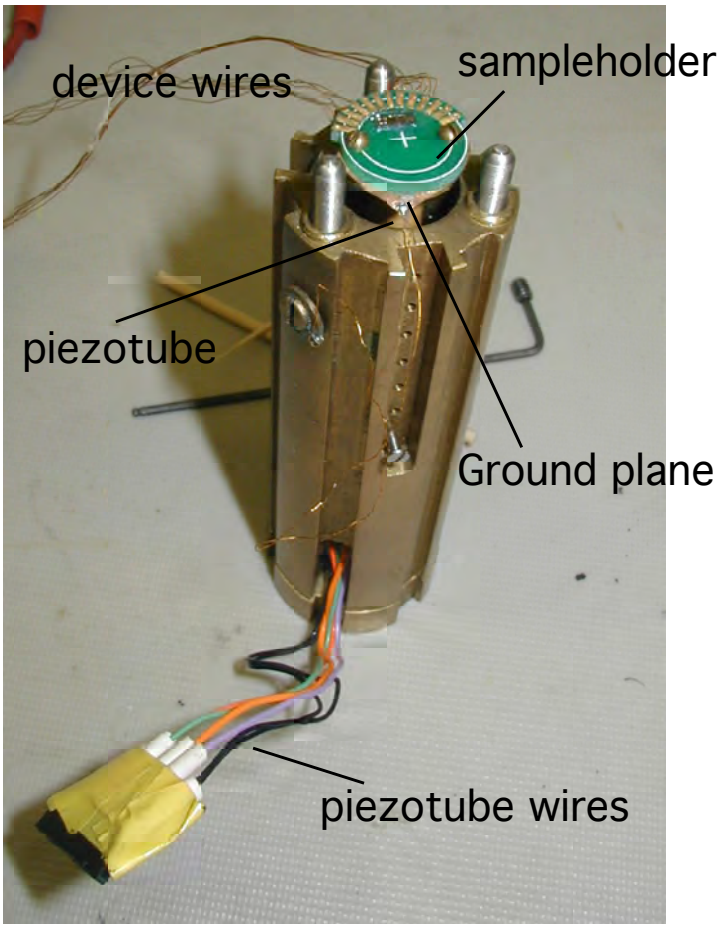

Figure 2.18: Photo of the cage of the AFM.

X and Y. The X and Y screws are valuable for positioning at room temperature, but cannot be accessed at low temperature. Low temperature coarse positioning should be designed for our system, whether through using a commercially available product or designing our own mechanism. There are two heads available for the AFM; the older has limited motion in X and Y and holds the tip in place with a set screw, and the newer has a greater range of motion in X and Y and holds the tip in place by a more effective screw. Space is tight in the AFM, and the ground plane could only go directly on top of the piezotube sample mount (as opposed to capping over the sides on the old AFM) and very thin wires were needed on the sample holder.

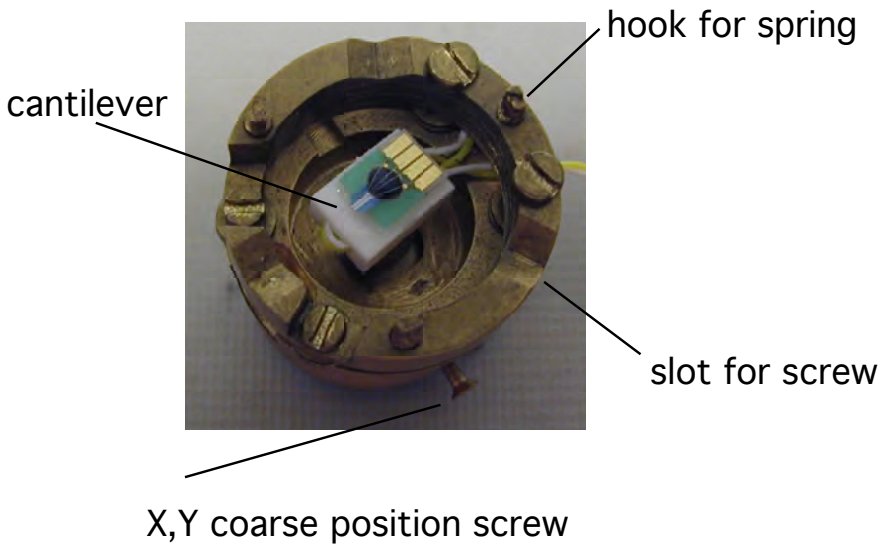

Figure 2.19: Photo of the cantilever mounted in the head of the AFM.

The sample holders were redesigned to use the PC Board program and place smaller pads and holes closer together than the holders that had previously been made and etched in the lab. A photo of the sample holder is in Figure 2.18 and

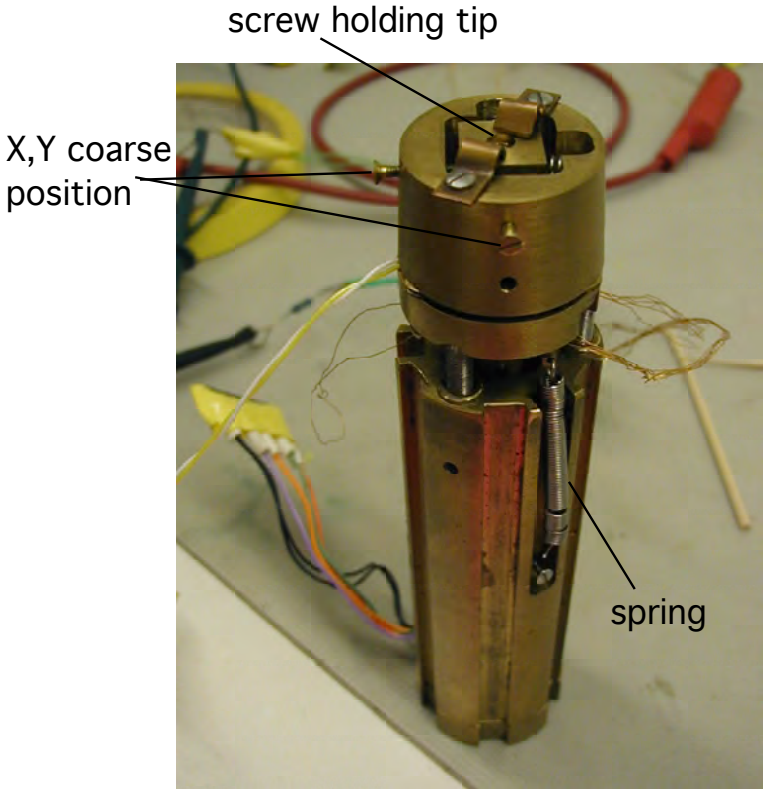

Figure 2.20: Photo of the assembled AFM.

the PCAD schematic is shown in Figure 2.21. The FR 40 printed circuit board (the default board) does not appear to create any problems when cooled down. The sample no longer sits on a conductive surface, which would prevent a backgate from shorting, but also prevents using the sample holder as a backgate if that is desired. Plating the bonding pads with gold (we have switched to electrodeless plating solution) is straightforward.

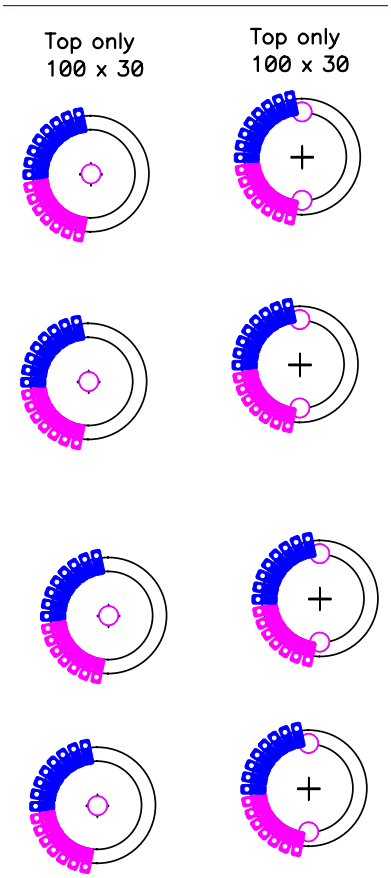

Figure 2.21: The printed circuit board design for the sample holders. The left is for the old system, with the hole for the screw in the middle. The right is for the new system, with the holes on the edge and the cross indicating the center for positioning purposes.

The lab recently used the last of its old tips purchased many years ago from Park

Scientific. Figure 2.19 shows the new tip. The tip comes mounted on the green board and with an attached balance resistor. At the time of writing, we have not tested the balance resistor, though one expects it to have similar thermal drift as the cantilever because it is made out of the same material. There are four bonding pads on the cantilever chip. Looking closely at Fig. 2.19, you will see gold wires passing over a black blob. The electrical connection to the tip breaks when cooled down, presumably under this dark material, and we wirebonded to the tip over this blob to assure good electrical connection. The tip appears to conduct at low temperatures, but showed some unusual behavior that suggested it did not conduct well out to the end of the tip. Coating these tips is advisable.

2.3.2 The dunker stick and dewar

The AFM plugs into microtech connectors at the base of the dunker stick (Figure 2.22). The dunker stick is wired to three Fisher connectors at the top. There are copper baffles along the length of the stick to reflect heat radiation, and the wires are looped around the stick to increase heat sinking and minimize electromagnetic pickup. The high voltage lines are stainless steel coaxial cables to help prevent possible voltage spikes from being picked up by nearby wires, and to more safely shield the high voltages. There are 1 $k\Omega$ resistors at the bottom of the sample leads to minimize heat conduction and to serve as low pass filters. Part of the dunker stick center is hollow (thin tube of of stainless steel), as are parts of the coarse positioning stick, to minimize heat conduction. There is a 16:1 gear (10/1 planetary gearbox from Faulhaber in Clearwater, FL) that we broke apart and cleaned in TCE to remove the

lubrication that would otherwise freeze, and then pushed back together. This gear has been functional for the past three years, and I've cleaned it once. The gear allows finer control over the Z approach.

The dunker stick is inserted into either the He-3 insert, or the open bottomed insert that is placed directly into He4. There is a superconducting solenoid magnet that provides up to a 7 Tesla perpendicular field, or a split coil magnet that can provide up to 3 Tesla parallel field. This 3 T magnet has not yet been tested.

The dewar has one chamber that is filled with Helium (Figure 2.23). There are resistors placed at the top of the magnet, the bottom copper baffle on the dunker stick, and at the top baffle. These change in resistance as the dewar is filled with liquid nitrogen, before the helium level meter can be used. The location of the helium level meter is indicated in Figure 2.23. There are two connectors at the top of the dewar, one to the resistors and the other to the helium level meter.

2.3.3 Cooling the AFM

Appendix C serves as a manual with instructions on how to cool the microscope. I will describe the procedure briefly here to allow discussion of improvements that should be made.

The AFM is assembled, the tip is aligned optically above the device, and the AFM is mounted at the bottom of the dunker stick. To cool to He-4 temperatures, the dunker stick is placed inside the open-bottom insert. Place the insert, with the dunker stick, into the dewar. To cool the dewar, first pump out all the air to prevent the "dirt" in the air from sticking to the device and the AFM. Then fill the dewar

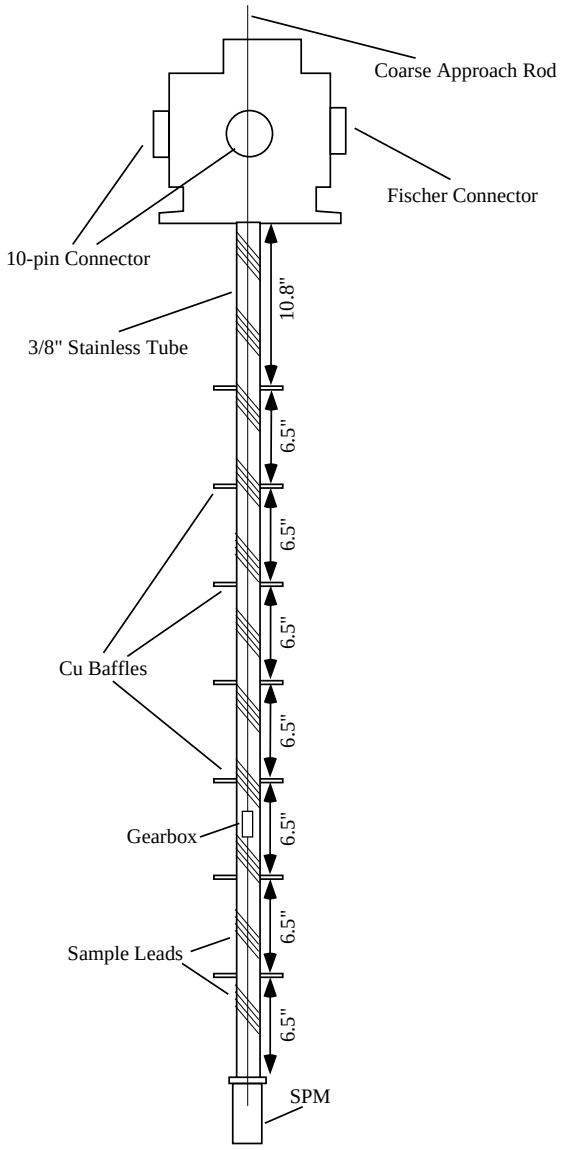

Figure 2.22: Schematic of the dunker stick.

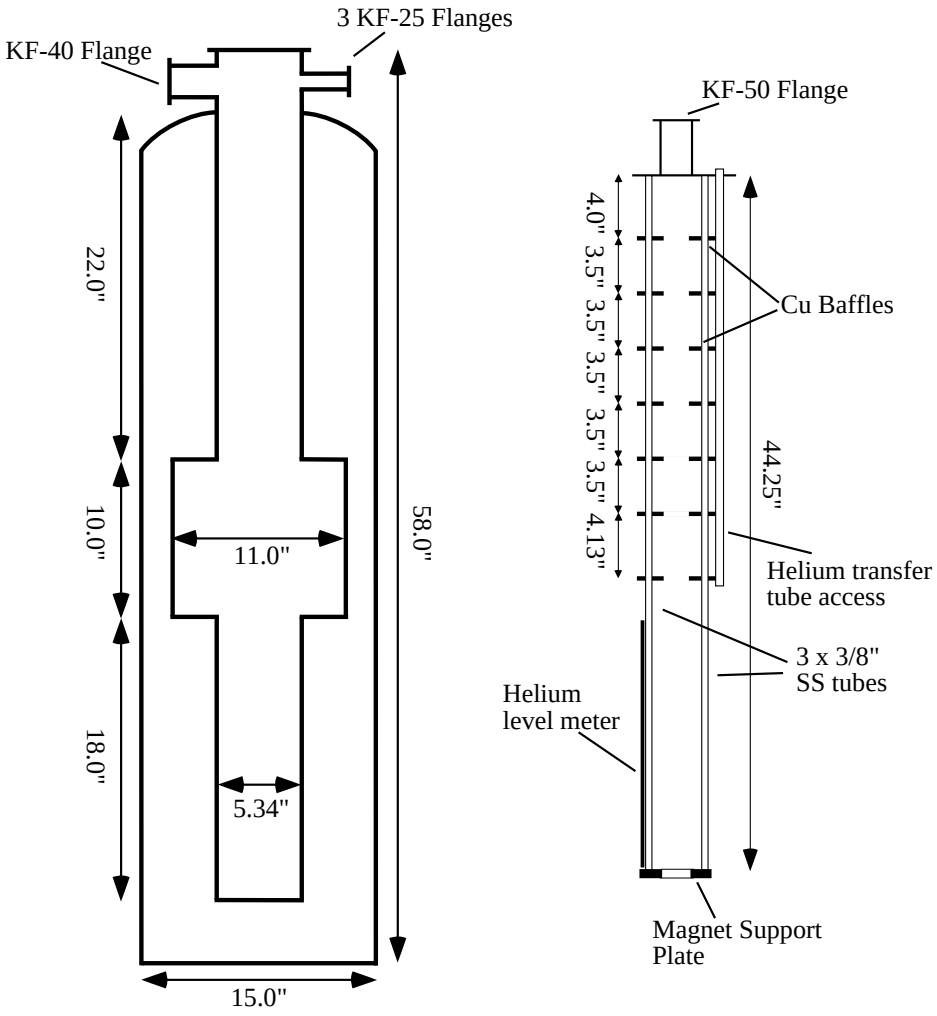

Figure 2.23: Schematic of the dewar and magnet support in the He-3 system.

with nitrogen gas to above atmosphere, and then fill with liquid nitrogen. This uses the large heat capacity and latent heat of vaporization of liquid nitrogen (as opposed to the relatively small heat capacity of liquid helium) to cool from room temperature to 77K. Allow the system to hold the liquid nitrogen so that the magnet and dewar are cooled. Push out all the nitrogen with helium gas, and then fill with liquid helium. The microscope and your device is now cold. To warm up, simply lift the insert so that the device is at the top of the dewar, which is essentially at room temperature, and wait at least two hours while the sample is still in helium and comes to room temperature.

If the dewar is already cold, it is tempting to simply put the insert back in. (For example, you may have warmed up to simply move the XY position of the tip and are ready to cool down within a half hour.) This may lead to dirt being deposited on the sample as it cools. To avoid this, place the insert at the top of the dewar such that the AFM is still at room temperature, and open up the flange at the top of the insert that holds the dunker stick to the insert. As you slowly lower the insert, most of the air will be pushed out the top as the helium boils off.

A valve system at the top of the dewar that allows you to pump out the insert before cooling would be an improvement. The primary valve must mate to both the dewar and the insert, and allow the insert to pass through when open. Additionally, there must be an outlet included to access the space for pumping. An additional valve at the outlet is necessary to allow the space to be sealed off again once in vacuum, before the primary valve is opened, allowing helium to fill the space. Alternatively, a new insert can be designed with the inlet/outlet at the top, but the valve at the top

of the dewar is still needed to selectively close off the space. One concern with any of these designs is the added height to the dewar/insert combination, which is already close to the ceiling.

When cooling to He-3 temperatures, the dewar is cooled as described above, and the sealed insert is pumped out before He-3 is added. With the insert in the dewar, a rotary pump is used to pump on the He-4 belly to bring it to 1.7 K. Once the dewar is at 1.7 K, He-3 can be condensed in the insert and pumped on to reach about 470 mK, as tested. The dewar is designed with a 15 L belly to hold the He-4. Without pumping, the hold time is about two and a half days, and depends on whether you fill beyond the 100% value on the helium level meter or stop before it is entirely covered (the meter tends to stop for a while around 98%, perhaps from the cold vapor before being fully covered). When pumping on a very full dewar, the hold time will be over 24 hours.

The entire dewar can be lifted from the floor with a manual winch. One must take care that the dewar is aligned correctly and the system is not jolted when it no longer contacts the floor. Nylon ropes suspend the dewar and damp most vibrations, however appropriate springs may provide improved vibrational damping. Additionally, a box like the blue box for the old microscope could be built to damp acoustic noise.

There is a pulley with a ratchet that holds the dunker stick. This aids the handling when inserting the dunker stick into the He-3 insert and the insert into the dewar. It is almost possible for one person to do it, though two is advised. If the pulley and ratchet could be raised a few inches, it would be much easier.

2.4 Low noise measurement

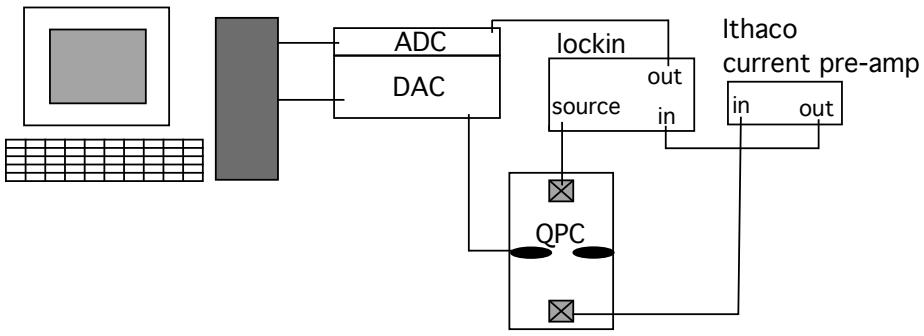

Figure 2.24: Experimental setup to measure conductance through the QPC. The computer controls the voltages on the gates through the DAC, the lockin sources a small ac signal, and the current pre-amp amplifies the resulting current and converts it to a voltage that goes back into the lockin. The voltage is read into the computer through the ADC. The lockin sets the ground reference. The 24 pin switcher box that all leads pass through is not shown.

For all of our devices, we have a twenty-four pin switcher box that attaches to a Fisher connector (at the top of the dunker stick, see Figure 2.5 and 2.6). There is a switch to ground or float all of the leads, and individual switches on each lead to either ground, float, or bus that lead. The bus is a wire that runs along each lead, so that by applying a voltage to one and bussing that lead will place the voltage on the bus. Any other switch that is turned to "bus" will then have that voltage applied to its lead. We are able to keep the gates grounded and free from electric shock with this box when not in use. Care should always be taken to keep oneself grounded when touching anything connected to the device.

Measuring conductance through a QPC is relatively straightforward, and schematically shown in Figure 2.24. The gates are attached to outputs from the DAC, which are controlled by the software written largely by Mark Topinka. Brian LeRoy's thesis

[23] contains a glossary of the available commands. The lines to the gates run through a low pass filter and a divider and protection diode to prevent applying too large a negative voltage or a positive voltage to the gates. All of the ohmics on the 2DEG are floated at the 24 pin switcher box, and the lockin is connected to an ohmic on one side of the QPC, and an ohmic on the other side of the QPC is attached to the Ithaco current preamplifier, the output of which is run back into the lockin. Generally the lockin is set to 1 V with a 10^{-3} divider, to apply an ac signal of 0.1 mV. The current preamplifier is then set to a sensitivity of 10^{-7} A/V. The lockin range can be set to 500 mV given these values, and converted into conductance. The lockin continuously measures conductance as the charged SPM tip is scanned above the surface, changing the measured conductance and mapping electron flow.

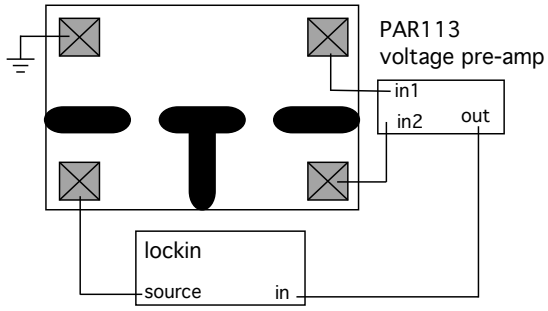

Figure 2.25: Experimental setup to measure magnetic focusing. The DAC and ADC are not shown. The lockin sources an ac signal across one QPC, the voltage across the other is measured. The ground reference is taken from the lockin.

Figure 2.25 shows the schematic for the magnetic focusing measurement, in which the voltage across the second quantum point contact is measured. I use "first QPC" to indicate the source of electrons and "second QPC" to indicate the collector. Once again, the DAC controls the gates of the QPCs. The lockin is attached to one ohmic, and an ohmic on the other side of that QPC, in the common area between the two,

is grounded. Two ohmics, one on either side of the collector QPC, are run to the PAR116 voltage pre-amps to measure the voltage across the collector QPC, the output of which is input to the lockin. Once again, 0.1 mV is sourced from the lockin, which leads to a voltage across the second QPC in the 5 - 10 microvolt range.

A magnetic field is applied by a voltage controlled current supply, found at the bottom of the electronics rack (Fig. 2.2). A voltage from 0 - 1 volts is applied to the appropriate pins on the back of the current supply, through a box that connects the BNC to two wires. This corresponds to the 0 to 50 Amp range of the current supply. Thick wires are run from the output of the current supply to the magnet leads on the dewar. The positive lead passes through a small (0.1 Ω) resistor, whose voltage drop is measured to accurately record the magnetic field. The "sense" leads from the power supply are connected to the magnet leads at the dewar, bypassing the resistor. These leads measure the voltage drop across the magnet, and are used to set the voltage limit at the power supply to prevent quenching the magnet if one accidentally ramps the current too quickly. The voltage limit will be reached and the current supply will stop increasing the current until the voltage is lower than the limit. The magnet is a large inductive load and has been tested with a limit of 2 V across its leads.

There are certain common techniques to low noise, cryogenic measurements that should be followed to assure good data and avoid harming your device. One of the most straightforward is to protect your sample. Never apply sudden voltages, and do not apply positive voltages to a gate. You can protect from accidental positive voltages by putting a diode to ground along the line. The largest positive voltage

that will get through will be the voltage drop across the diode. Also, always keep yourself grounded before touching any of the device leads or any of the equipment. Shocking the device can kill it, as can shocking an electronics box that then rails a voltage that goes to the device.

Ground loops must be avoided. There should be one point of common ground, from which all parts of the experiment take their reference. Differential inputs to amplifiers help to avoid ground loops, and isolation amplifiers can be used to break loops by transmitting the electric signal optically or capacitively rather than through a common ground. The lockin can be used with a differential input, though usually we take the lockin ground as the reference point because it is difficult to float. All instruments that can be floated (run off batteries) should be. Sometimes the blue dewar makes a weak connection with ground through the floor; raising it will remove this connection. Additionally, care must be taken to isolate the digital ground from analog ground. Rapid swinging of voltages from high to low can affect the ground line, and consequently affect the low noise measurements. Optically coupling to the computer, or another form of isolation, reduces this concern. Pumps must be isolated from the device ground, and a plastic o-ring and clamp must be used to avoid connecting the grounds through the vacuum hoses. Generally, the computer, the pumps, and the experiments should be plugged into different circuits in the wall. This also helps in case you blow a fuse with the pump; you will not kill the power to your device or piezo tube.

Electromagnetic pickup can be problematic. There are numerous sources at many frequencies that exist. Some instruments (particularly power supplies) radiate con-

siderably at 60 Hz from the transformers, and are often close to the measurements. A current carrying loop can pick up this signal from the flux through the area of the loop. We see this especially in our cantilever signal, because a large loop is formed from the wires going to two sides of the bridge circuit, and the two wires coming back. The most practical way to remove this 60 Hz pickup is to have twisted pairs of wire, so that the area of the total loop is minimized. There are also "sweet spots" in the room that will have lower pickup - we see this on the cantilever signal, even when the wires are twisted, and we see the immediate effect of turning on the high voltage power supplies. You can move around the twisted pair and untwist sections until you are satisfied with the signal. Using triax cables or otherwise shielding your signals is the best way to eliminate the electromagnetic pickup, and having the entire setup inside a shielded room will eliminate outside signals.

The best way to avoid a noisy signal is to avoid picking up the noise in the first place. However, filtering often is the realistic solution. There are filters built in to the voltage pre-amplifiers, and the lockin will remove a great deal of the noise if you set the filters correctly. You must be careful not to lose any meaningful information from your measurement. Pick your lockin frequency in a range where there is less noise, and select your filter as needed. We also always place a low-pass filter on our signal lines to both remove higher frequency pickup, and avoid sudden changes or spikes to the voltage on the gates. Some amount of low-pass filtering may exist due to unintentional capacitance and resistance (e.g. capacitance of the coaxial cables and resistance of the wires and device).

2.5 Sample fabrication

Most of the sample fabrication has been written up in past theses [23, 43, 11]. The basic steps have not changed. (1) The sample is cleaved. (2) PMMA is spun on the chip. (3) Trenches are written and etched if there is a back gate. (4) Ohmic contacts are defined with electron beam lithography. (5) NiAuGe contacts are evaporated. (6) The PMMA is lifted off. (7) The contacts are annealed. (8) PMMA is spun again and the device is written with electron beam lithography. (9) The device is evaporated. (10) The PMMA is lifted off. (11) The device is mounted and wirebonded.

First one carefully cleaves the sample into approximately 2 x 3 mm chips. The chips cannot be much larger than this or they will not fit on the sample holder. The chips are cleaned in TCE, Acetone, and Methanol, with ultrasound, and three layers of PMMA are spin coated. The lower two layers have lower molecular weight than the third, creating an undercut in the profile for better liftoff, and three layers help to avoid defects in the PMMA. Trenches or ohmics are then written with electron beam lithography. Photolithography could be used for these steps if desired. If using trenches or defining a mesa, the sample is wet-etched in a mixture of Citric Acid and Hydrogen Peroxide (10:1 ratio), the PMMA is lifted-off, three more layers of PMMA are spun, and ohmics are written. Once ohmics are written, the sample is placed in the evaporator and Ni-Au-Ge contacts are deposited (50 Å Ni, 50 Å Au, 250 Å Ge, 400 Å Au, 100 Å Ni, 400 Å Au). After lifting off the PMMA, the contacts are annealed. Two layers of PMMA are spun and the gates of the device are written with electron beam lithography. Only two layers are used for better resolution with the lithography, still with the bottom layer of lower molecular weight to create the

appropriate undercut profile for better liftoff. We deposit 100 Å of Cr over the entire chip, then remove the sample from the evaporator and cover the device area, but none of the bonding pads, with aluminum foil. The sample is then returned to the evaporator and another 50 Å of Cr and 400 Å of Au is evaporated onto the bonding pads. After liftoff, the sample is mounted and wirebonded and ready to use.

The only changes in procedure is the use of the Rapid Thermal Annealer (RTA) to anneal the ohmic contacts, and the use of the new JEOL 7000F electron beam writer. The RTA anneals many samples at once and takes about twenty minutes. The procedure to use the RTA is in appendix A.2. It reliably creates ohmic contacts, though a recipe has not been established to contact the 2DEG but not the backgate, if structure has one. The old annealer in 211 still works best for this purpose until effort is put into developing a reliable recipe. The new JEOL 7000F is easier to use and more often available than the older JEOL. The focus is much better and the current is always on. A high current is available, allowing us to continue writing our ohmics and other large patterns with e-beam lithography instead of photolithography. The procedure for using the new JEOL is in appendix A.1.

Chapter 3

V-shaped Imaging Interferometer

Previous work in the Westervelt lab used a liquid helium cooled scanning probe microscope (SPM) to image electrons flowing from a quantum point contact (QPC) [45, 46]. A negative voltage is placed on the conducting SPM tip, such that the electrons beneath the the tip are fully depleted, and the tip is scanned above the area near the QPC while the conductance across the QPC is measured. Electrons that encounter this area are backscattered, changing the conductance through the QPC. Coherent electron flow can be mapped out in this way.

We designed and fabricated an imaging V-shaped interferometer that uses a semi-circular metal gate on the surface as one "mirror" and the tip as the second. Electrons are scattered off these two mirrors back to the QPC. This interferometer uses the motion of fringes to distinguish between electrons that bounce once or twice off the "mirror" of the interferometer. Electrons that pass through the interferometer have a range of wavelengths, associated with the thermal distribution of energy and centered at the Fermi energy. Electrons will dephase relative to one another over the

thermal length, l_T, such that interference will not be observed for pathlengths that differ by more than the thermal length. We can verify which paths contribute to the observed interference by watching the shift in the fringes with the change in location of the gate.

In this chapter, I will first review in Section 3.1 the relevant knowledge gained from earlier work [45, 46, 40], including a discussion of the thermal length in Section 3.1.1. I will then discuss the V-shaped imaging interferometer and what we have learned and demonstrated about electron interference in the device: first, our ability to enhance the fringes by providing additional backscattered paths (Section 3.2.1); second, the motion of the fringes as we move a "mirror" of the interferometer (Section 3.2.2); and last, the decay of the fringes as the electron paths that interfere differ on order of the thermal length, l_T (Section 3.2.3). This chapter is based on the PRL [24] and Nano Letters [20] publications.

3.1 Coherent electron flow

Topinka and colleagues imaged coherent electron flow from a quantum point contact (QPC) in a two-dimensional electron gas (2DEG) [45, 46]. This was done by bringing a conducting scanning probe microscope (SPM) tip near the surface of the GaAs/AlGaAs heterostructure. A voltage can be placed on this tip, which capacitively couples to the 2DEG. By placing a sufficiently negative voltage on the tip, the area beneath is fully depleted of electrons; all electrons that encounter this area will be scattered. Some electrons that come from the QPC and encounter this depleted region beneath the tip will be directly backscattered back through the QPC, conse-

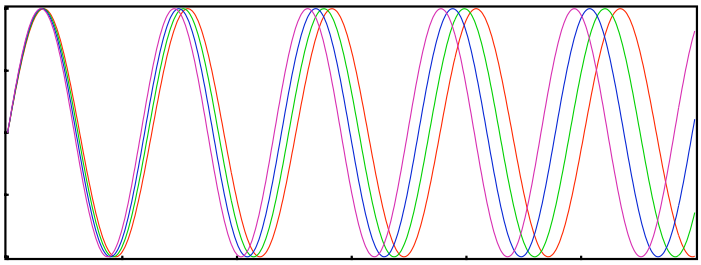

Figure 3.1: Four sine waves start together at the left. Though each sine wave is coherent, due to their slightly different frquencies they will not show interference effects after a number of periods. The interference is averaged over all the frequencies and will not be visible.

quently reducing its conductance. By measuring the conductance across the QPC while scanning the tip position, the electron flow will be mapped. When the tip is over an area of large flow, the conductance will be reduced by more than when the tip is over an area of small flow. Interference effects can be seen due to the coherent nature of the electron flow.

3.1.1 Decoherence and thermal averaging

A particle that can take multiple paths to the same location will interfere with itself, provided the particle has not decohered along the paths. Electron-electron and electron-phonon scattering are two contributions to the decoherence of a single electron in a two-dimensional electron gas. The coherence length, l_ϕ, characterizes this single particle decoherence. For GaAs/AlGaAs, l_ϕ is on the order of 20 microns at 4 K.

Our measurements of conductance are an ensemble average of many electrons that each interferes with itself. Though each electron is coherent with itself within l_ϕ, the

average over all the electrons can lead to no visible interference. The average phase is effectively randomized due to the spread in energy of the electrons. For a finite temperature, there will be some distribution in the wavelengths of the electrons. Figure 3.1 demonstrates how a spread in wavelength leads to the inability to see periodic fringes. Though the waves start in phase, after a few periods they are no longer in phase and interference that occurs at each individual wavelength will not be visible once one sums over all the individual wavelengths. The thermal distribution of wavelengths at a finite temperature is given by the Fermi distribution, or rather, the derivative of the Fermi distribution

$$-f' = [1 + e^{(\frac{E-E_F}{kT})}]^{-2} \frac{1}{kT} e^{(\frac{E-E_F}{kT})} \tag{3.1}$$

which can be well approximated by a Gaussian,

$$-f' = \frac{1}{4kT} e^{-(k-k_0)^2 l_T^2} \tag{3.2}$$

where

$$l_T = \frac{\hbar v_F}{\pi kT} = \frac{\hbar^2 k_0}{\pi mkT}. \tag{3.3}$$

This is the distance that it takes two waves separated in energy by the standard deviation of the Gaussian to drift one radian out of phase. In a model that assumes a single scattering event (an electron travels from the QPC and scatters once off the tip or an impurity and returns), this corresponds to the amplitude of the fringes decaying as

$$A(r_t, r_i) \propto \frac{1}{r_i r_t} e^{\frac{-(r_i - r_t)^2}{l_T^2}} \tag{3.4}$$

in which the pathlength difference between the tip location, r_t, and the other scatterer, r_i, determines the amplitude. The r^2 falloff of the signal is expected for the roundtrip

paths of the electrons coming from a QPC and being backscattered back through the QPC. For a more detailed derivation, see [40].

3.1.2 Imaging by backscattering

Previous experiments used a backscattering technique to image electron flow from a quantum point contact [46, 45, 44]. We bring a liquid helium cooled scanning probe microscope tip to within ten nanometers above the surface of a GaAs/AlGaAs heterostructure. We place a voltage on the tip that capacitively couples to the electrons and fully depletes the electrons directly below the tip, creating a disc that scatters electrons. The diameter of this disc is roughly twice the distance of the tip to the 2DEG, about 100 nm for most of our experiments. To image flow, electrons are sourced through a quantum point contact and the charged tip is scanned above the surface (Fig. 3.2). The conductance is measured across the QPC as the tip is scanned, and the change is conductance is recorded for each location of the tip. Electrons that directly hit the tip will backscatter back through the QPC, changing the conductance. When the tip is over an area of high electron flow, many electrons are backscattered through the QPC and the conductance is reduced. When the tip is over an area of no flow, the conductance does not change. By associating the change in conductance with each location of the tip, the electron flow is mapped.

Figure 3.3 shows a typical image of flow from a quantum point contact taken with this backscattering method. Fringes are visible, which are due to the multiple backscattered paths that the electrons can travel to return to the QPC, where they interfere. As the relative strength of the fringes remains constant with distance,

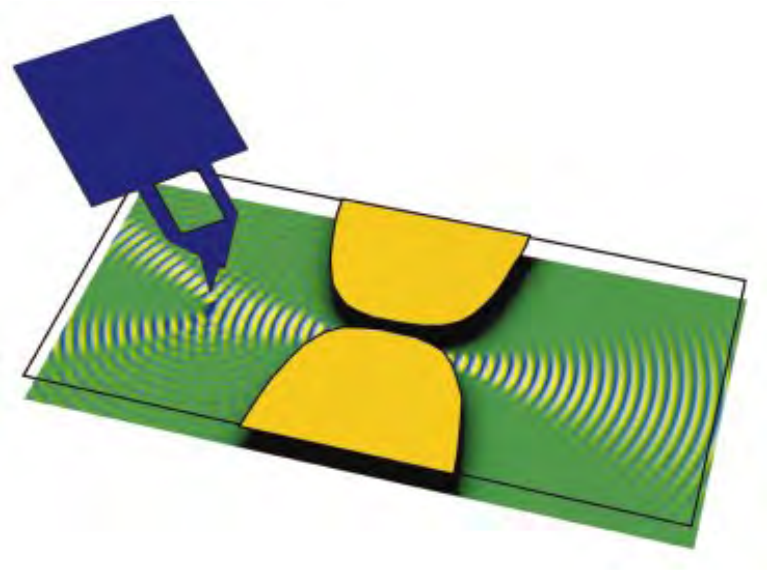

Figure 3.2: A scanning probe microscope (SPM) is brought near the surface of a two-dimensional electron gas. Current flows through a quantum point contact (the yellow gates), and a voltage is placed on the SPM tip. This voltage can deplete the electrons beneath the tip (indicated by the dark spot below the tip) and backscatter any electrons that hit this area. Flow is coherent from the quantum point contact, indicated by the periodic structure in the schematic. (Reproduced from [45].)

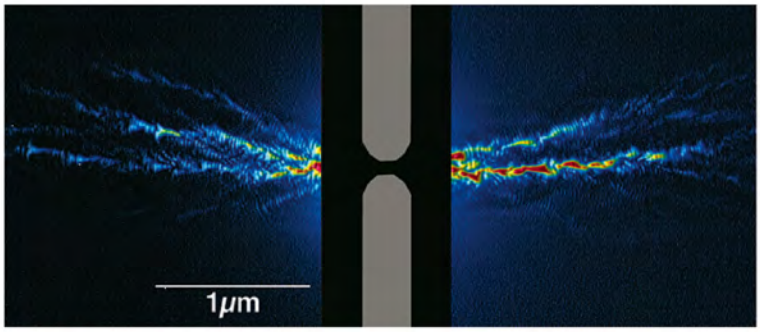

Figure 3.3: Image of electron flow from a quantum point contact. The red indicates a large decrease in conductance, the dark blue no change in conductance, and consequently high flow and no flow, respectively. Reproduced from [44] .

and given the finite temperature and thermal length (Eq. 3.3), one must hypothesize that backscattering impurities exist throughout the area scanned. These impurities provide the multiple paths to return to the QPC that are comparable in length to the paths that go to the tip and back to the QPC. The next section describes an interferometer that was initially designed to test this hypothesis.

3.2 V-shaped Interferometer

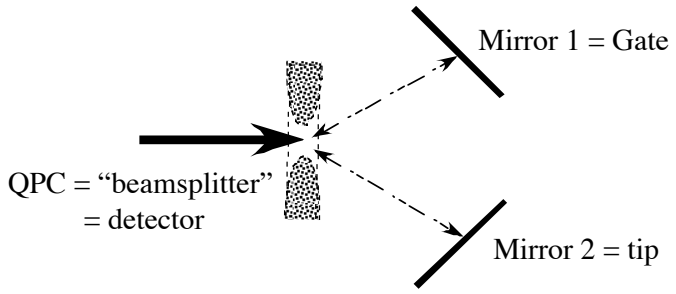

Figure 3.4: The quantum point contact can be viewed as a beamsplitter, from which the electron can take two paths. The first mirror is the gate that is patterned on the surface, and the second mirror is the tip that can be moved over a large distance. The backscattered electrons from these two mirrors converge again at the QPC, which serves as a detector as well.

Electrons taking multiple paths will interfere when these paths reunite, providing they are coherent. This section describes an experiment in which a gate was used to introduce many new paths to enhance interference and to create an interferometer. Figure 3.4 shows how a quantum point contact can be viewed as a beamsplitter, from which an electron can take a path to either of two mirrors. The first mirror is the gate, and the second is the tip which is introduced for this experiment. The QPC also serves as the detector, because this is where the multiple paths converge

and interference takes place. We measure the conductance across the QPC, and any changes due to backscattering and interference are recorded. Because of the geometry, we refer to this as the "V-shaped interferometer." The imaging mechanism is the same as described in the previous section, and sketched in Fig. 3.5A.

3.2.1 Enhancement of fringes

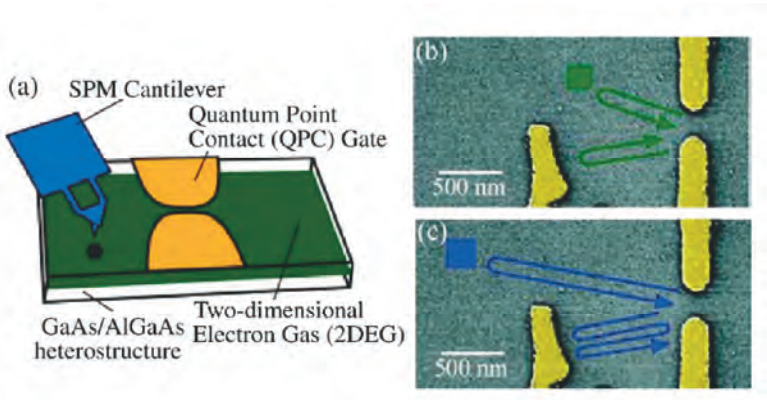

Figure 3.5: Geometry of the V-shaped interferometer. (A) depicts a schematic of how a charged SPM tip is brought close to the surface of the 2DEG and can backscatter electrons. (B) and (C) are SEM micrographs of the device (color added). (A) indicates two paths that the electron can take that are of comparable length, and the green box is where the "single bounce" images are taken. (C) indicates a different two paths that the electron can take, this time both are twice as long as in (B). The blue box indicates where the "double bounce" images are taken. (Reproduced from [24].)

To make the V-shaped electron interferometer, we fabricated a sample that included the standard quantum point contact and added a metal gate (Fig. 3.5) that serves as a mirror. This gate was designed to be a circular arc that pointed back towards the QPC, causing a large number of trajectories to be reflected back to the QPC with the same phase. In addition to creating an electron analog to an optical interferometer, we sought to confirm the idea that the fringes persisted throughout

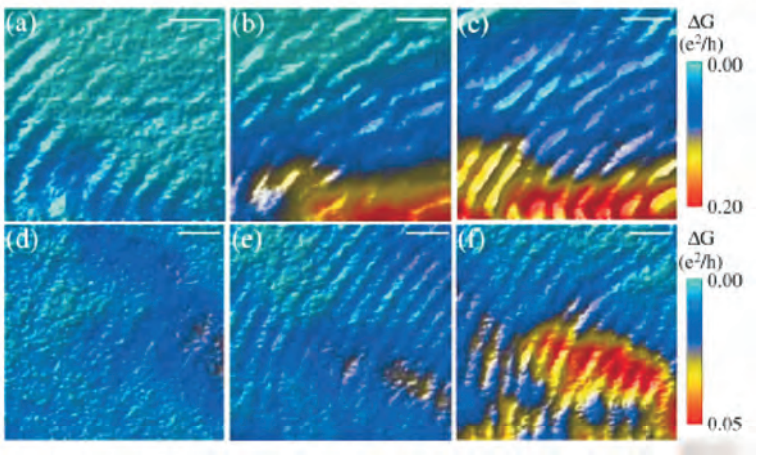

Figure 3.6: Enhancement of fringes when the reflecting gate is energized. (A) - (C) are taken in the green area of Fig 3.5, (D) - (F) are taken in the blue area. (A) and (D) are taken with the voltage on the reflecting gate = 0.0V. (B) and (E) at -0.4 V, where the gate just begins to deplete, and (C) and (F) at -0.8V, showing considerable enhancement of the fringes in both locations. The scale bars are 50 nm long. (Reproduced from [24].)

the images due to additional backscattered paths that are caused by random impurities. This gate allowed us to turn a set of "impurities" on and off, and to confirm that additional paths enhance the fringes, even when farther from the QPC than the thermal length, l_T.

Figure 3.6 confirms that energizing the gate does enhance the fringes. The top row of images are taken at the "single bounce" location indicated in Fig. 3.5B, and the bottom row at the "double bounce" location (Fig. 3.6C). Fig. 3.6A and 3.6D are taken with zero volts on the reflecting arc. Fringes are visible, presumably due to random impurities that backscatter electrons. Fig. 3.6B and 3.6E are taken just as the reflecting gate begins to deplete, and some enhancement of the fringes is seen. Fig. 3.6C and 3.6F are taken with the reflecting gate fully depleted, and the fringes are noticeably enhanced. As the gate begins to deplete the electrons beneath, it adds to

the number of backscattered paths, and strengthens the fringes. The rows are taken at locations that are separated by more than the thermal length, l_T. Because of this, we hypothesize that different paths off the gate (bouncing once or twice) contribute to the interference signal, which we confirmed and is described in Section 3.2.2. A simulation of this effect is shown in Figure 3.7. This is a quantum mechanical simulation of full tip scans, without the reflecting gate energized (Fig. 3.7 A,C) and with it depleting the 2DEG below and contributing many backscattered paths (Fig. 3.7 B,D). The images are at the radius of the reflecting gate (Fig. 3.7 A,B) and twice the radius (Fig. 3.7 C,D). In both cases, the fringes are strongly enhanced when the reflecting gate is energized. The transmission through the QPC is calculated using an inverse Green function technique and each pixel in the image is obtained by calculating the thermally averaged conductance through the QPC with the tip located at that point.

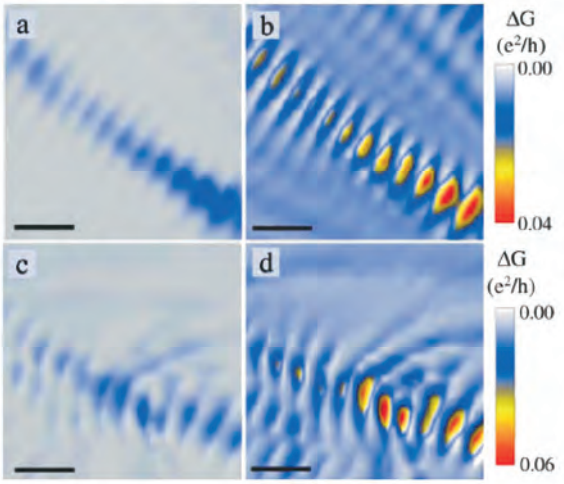

Figure 3.7: Quantum mechanical simulations of the electron flow with (B,D) and without (A,C) the reflecting gate energized. (A) and (B) are taken at the radius of the reflecting gate. (C) and (D) are taken at twice the radius. In both cases, the fringes are strongly enhanced when the reflecting gate is energized. The scale bars are 50 nm long. (Reproduced from [24].)

3.2.2 Motion of Fringes

We can differentiate between some paths of the electrons based on the interference that we observe. The fringes exist past where the thermal length, $\lambda_T \approx 179nm$ at 4.2 K (Eq. 3.3), suggests they would be averaged out. It is not the total pathlength that the electrons travel that matters, but the pathlength difference between the two or more paths, as seen from Equation 3.3. The reflecting gate is placed one micron away from the QPC. The "single bounce" imaging location is about one micron away, corresponding in length to electrons that travel from the QPC to the reflecting gate and back, as is sketched in Fig. 3.5B. The "double bounce" imaging location is two microns away from the QPC, corresponding to the distance electrons travel when going from the QPC, bouncing off the reflecting gate, boucinging again off a QPC gate, again off the reflecting gate, and back to the QPC, as sketched in Fig. 3.5C.

Figure 3.8: Snapshot of a thermal wavepacket returning from one bounce off the distant mirror and two bounces off the closer mirror. (Left) A node has developed at the QPC from the interference between the two, resulting in little flow back through the QPC. (Right) The outer mirror is shifter by about $\lambda/4$ relative to the right snapshot, otherwise the two are identical. This results in an antinode at the QPC and more flow back through the QPC. (Reproduced from [20].)

Figure 3.8 demonstrates how we can differentiate the two paths that correspond to a single bounce and double bounce scenario by moving the mirror and watching the position of the fringes shift. In the case of one bounce, the fringes should shift by a full period when the mirror moves one half the wavelength (due to the round trip path). For two bounces, when the mirror shifts $\lambda_F/4$ the fringes should shift by a full period. Fig. 3.8 is a snapshot of a wavepacket simulation performed by Eric Heller, taken when the flux from the farther mirror is reaching the QPC. When the outer mirror is in the first position, a node develops at the QPC and this deconstructive interference results in a small change in conductance. When the outer mirror is moved by about a quanter of the wavelength, an antinode develops and much more flow back through the QPC is observed.

We are able to experimentally observe this change in the interference pattern as the position of the mirror is changed, shown in Figure 3.9. The reflecting gate moves when the voltage is changed. Putting a more negative voltage on the gate causes the classical turning point of the electrons that hit it to extend farther beyond the lithographically defined gate, moving the reflection point towards the QPC. The left column of panels in Figure 3.9 (A - E) display the single bounce case, taken at the same distance from the QPC as the gate. The right column of panels display the double bounce case, at twice the distance from the QPC as the gate. The three colored dots are in the same location throughout the column, and serve as guides to the eye. Each row corresponds to a different voltage on the reflector gate, equivalent to a different position of the mirror. The single bounce case moves through about a half a period while the double bounce case moves through about a full period. The

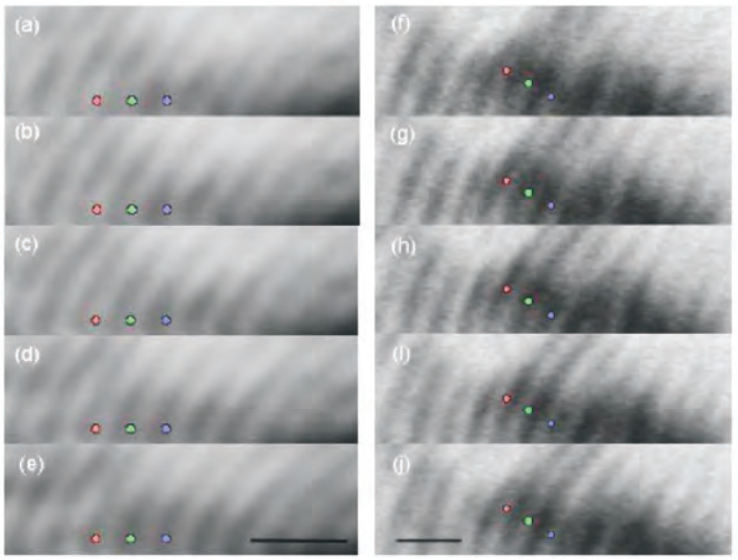

Figure 3.9: Two series of images of electron flow showing the motion of the interference fringes with the motion of the reflecting gate. Each row is taken for a different voltage on the reflecting gate, from -0.72 V to -0.80 V in steps of -0.02 V. (A) - (E) are images recorded at the same distance as the reflector gate. (F) - (J) are taken at twice the distance. The dots are guide to the eye to see that the fringes move twice the distance for the same motion of the reflector gate. The scale bars are 50 nm long. (Reproduced from [24].)

fringes do indeed move twice as fast in the double bounce case.

Though the single bounce and double bounce trajectories always exist coming from the reflecting gate, we can differentiate between the two due to the finite temperature. The thermal length of about 170 nm tells us that unless the paths returning to the QPC are within about 200 nm to either side of the tip, averaging over the thermal distribution will destroy any periodic signal. This allows us to identify the single bounce and double bounce case. Thinking in the time domain is simpler, in which a wavepacket is lauched from a QPC and propagated through the system. The wavepacket has a width that is equal to the thermal length, and a speed that is given by the Fermi velocity. In order to interfere, the returning flux must overlap as it

travels back through the QPC.

Fig 3.10 displays two time snapshots of a wavepacket released from the QPC, from a simulation by Eric Heller, that demonstrates the overlap in time that is needed to see interference. Initially we see a propagating wavefront some distance from the QPC. On the right, the waves have been scattered from the two impurities that are closest to and equidistant from the QPC. The backscattered amplitude is about to arrive at the QPC, where it can interfere because it arrives at the same time. For comparison, it is clear that the backscattered amplitude from the upper right impurity that has just begun its trip back to the QPC will not arrive in time to interfere with the signal from the closer impurities.

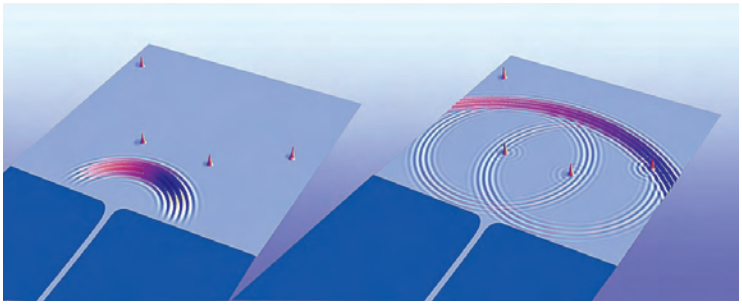

Figure 3.10: Backscattered electrons must return at approximately the same time to interfere at the QPC. The left panel shows a thermal wavepacket emerging from a QPC. It encounters two impurities that are equidistant from the QPC, which scatter the amplitude. The backscattered amplitude arrives at approximately the same time at the QPC, where it will interfere. The amplitude scattered from the farther away impurities will not interfere with the closer impurities because it will arrive too late. (Reproduced from [20].)

3.2.3 Expected fringe decay

Thinking about wavepackets in the time domain leads to a description of this system as an interferometer with a time resolution of a half picosecond at 4 K. The time resolution is determined by the thermal length, andactually goes up as the temperature increases. Fringes will only be present if their backscattering sources are within a thermal length of where the tip is located. As the temperature increases, the thermal length decreases, and a smaller area contributes to the fringe signal. Correspondingly, the time difference that separates the paths is smaller. As the temperature is increased, eventually incoherent scattering events will become dominant, reducing the single electron coherence length, l_ϕ.

Figure 3.11 demonstrates the validity of the thermal wavepacket picture. We heated up the electrons by using an arbitrary waveform generator to provide a time-varying signal that reproduces the distribution of electrons for a given temperature (because we lacked a variable temperature cryostat). The amount of time at a given voltage is determined by the probability of the electron having that energy for the desired temperature. In this way, we were able to reproduce the thermal distribution of the electrons. Fig. 3.11A is the schematic of the device, with the area scanned shown as the long rectangle that is positioned near the radius of the reflecting gate. The scans below correspond to 1.7 K (Fig. 3.11B), 4.2 K (Fig. 3.11C), and 8.4 K (Fig. 3.11D). The fringes are more quickly smeared out (averaged over) as the temperature is increased. The position of the reflecting gate is obvious by looking at these images, where it clearly contributes to a strong interference signal when the tip is at a comparable radius.

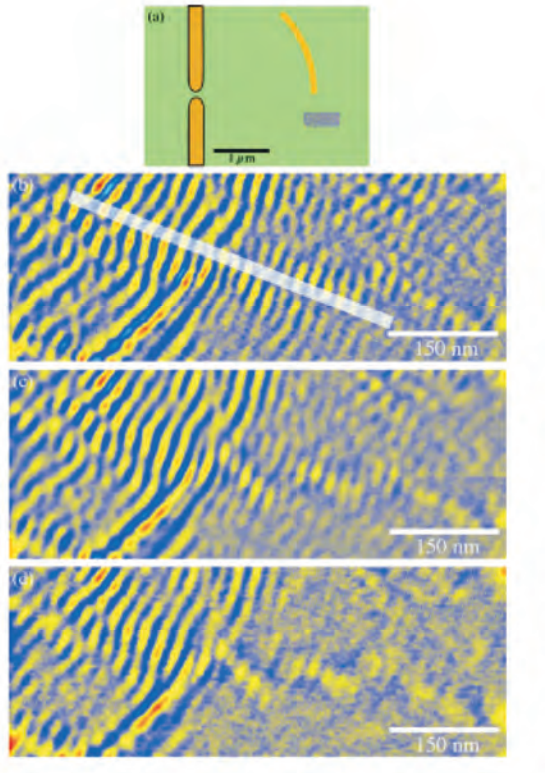

Figure 3.11: Demonstration of the thermal averaging of fringes for different temperatures. (A) Schematic diagram showing the location of the images of flow. (B) 1.7K (C) 4.2 K, (D) 8.4K. The fringes are robust near the radius of the arc, and decay more rapidly as the temperature is increased. (Reproduced from [20].)

Equation 3.4 describes quantitatively how the fringe amplitude should decay for the different temperatures. Figure 3.12 displays this envelope function on top of linesamples that are obtained from the data at a number of temperatures. The white line in Figure 3.11 shows the location of these linesamples. The envelope serves mostly as a guide to the eye, with the height and central location being fixed to the data. It is clear that not only do the fringes decay more rapidly with higher temperature, they do so at the expected rate. A perfect match would be difficult as there are uncontrolled scattering sites other than the reflecting gate.

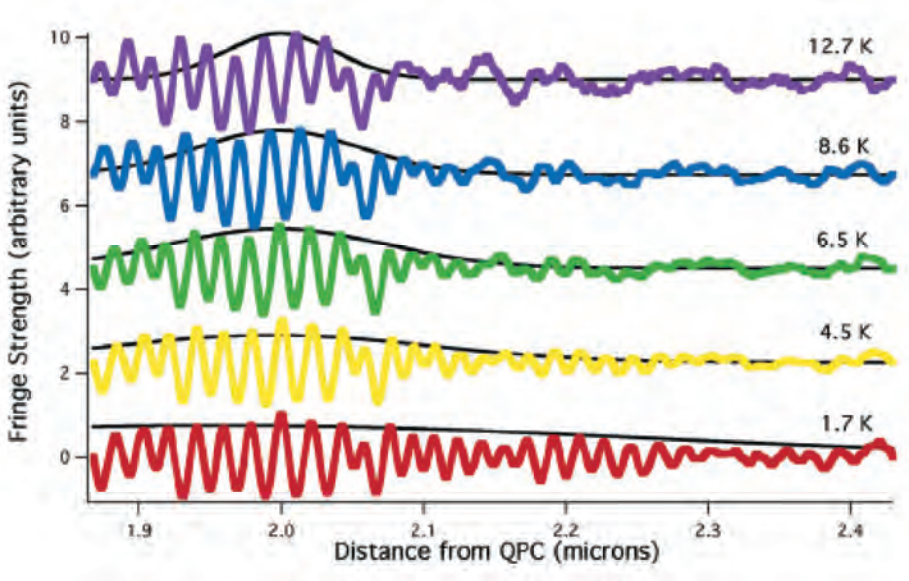

Figure 3.12: Plot of the strength of the measured signal taken along the line shown in Fig. 3.11. Five temperatures are shown with the expected decay in fringe strength indicated by the black envelope function. The strength of the signal decays more quickly away from the reflecting gate for higher temperatures. (Reproduced from [20].)

3.3 Summary

We have made an imaging V-shaped interferometer by using a metal gate on the surface as one "mirror" and the tip as the second. Energizing the semicircular gate creates many new backscattered paths to the QPC that are in phase and enhances the fringes. At 4.2 K, the thermal length is about 200 nm, and we can use this to distinguish paths that the electrons take. If the electron bounces once off of the reflecting gate and returns to the QPC, electrons that scatter from the tip at approximately the same distance from the QPC will interfere. If the electron bounces twice off of the reflecting gate, electrons that scatter from the tip at twice the radius from the QPC will interfere. We are able to confirm this by moving the mirror and watching the shift in fringes. Raising the temperature decreases the thermal length and increases the time or space resolution of the system. The fringes will be strong near the radius of the reflecting gate and decay past that. Higher temperatures have a faster decay in the fringes.

Chapter 4

Imaging electrons in a magnetic field

In our desire to study the basic physics of electron transport and to develop novel devices, we must consider what happens when electrons move in magnetic fields. Understanding the coherent flow of electrons in magnetic fields may lead to novel devices for quantum information processing [31, 6] and spintronics [5, 53], as well as allow us to understand fascinating physical regimes, for example, in quantum Hall systems. The most direct way to investigate electron waves in these systems is to spatially image them. Scanning probe microscopy (SPM) has been used successfully in the past to investigate electrons in 2DEGs, primarily in no or very small magnetic field [46, 13, 34, 14], or a strong magnetic field in the quantum Hall regime [55, 42]. In the absence of a magnetic field, electron flow from a quantum point contact (QPC) in a 2DEG shows strong branching behavior [44]. The flow was previously observed by backscattering the electrons to the point of origin at the QPC, using a strongly

energized SPM tip. However, when a moderate magnetic field is present, this simple imaging mechanism is unavailable, and a new approach is needed is order to image flow in these important systems.

We developed a new technique to study the magnetic focusing geometry, in which two quantum point contacts are located side by side, within the mean free path of the electron. Magnetic focusing has proven to be of great utility in understanding ballistic electron flow in metals [38, 47] and in a two-dimensional electron gas (2DEG) [48]. This geometry has been used more recently as a spin-detector, to measure electrons emitted from a quantum dot [19] or spin-polarized electrons resulting from strong spin-orbit coupling and birefringent reflection [37, 12].

The first section (4.1) of this chapter discusses what happens when you turn on a magnetic field and image by backscattering. The rest of this chapter discusses the magnetic focusing experiment, in which two QPCs are used and the tip changes the transmission between them. This new imaging technique is flexible enough to image between any two points in a 2DEG where quatum point contacts are defined. We take advantage of the tip to act as an adjustable strength scatterer to either image the flow transmitted before the tip is introduced, or to enhance interference effects. All simulations shown in this chapter were done by Robert E. Parrott, unless otherwise noted. Additional detail can be found in his thesis [33]. This chapter includes the content of [2] and [1].

4.1 Backscattering in a magnetic field

Chapter 3 discusses how electron flow can be imaged by bringing the tip of a scanning probe microscope close to the surface of a 2DEG and placing a negative voltage on the tip (see Figure 3.2). When this voltage is sufficiently negative, it will deplete the electrons below and scatter electrons into many angles. Only those trajectories that are directly backscattered, scattered by π, will return to the QPC of origin and change the conductance through the system. Measuring the change in conductance that results from this backscattering maps out the electron flow.

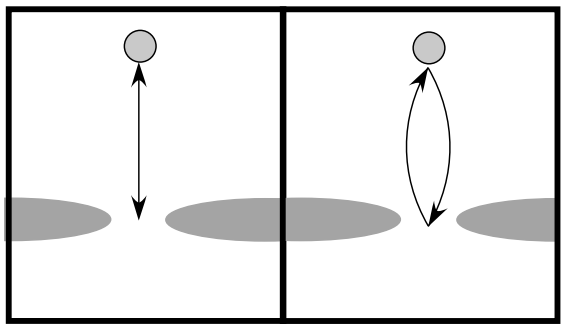

Figure 4.1: The effect of a magnetic field on backscattering. (A) Without a magnetic field, an electron will follow back its time reversed path and return to the QPC of origin. (B) A small magnetic field allows an electron to scatter into a path that still reaches the QPC of origin. As the field is increased, fewer electrons will be able to return to the QPC. Phase accumulates due to enclosed magnetic flux and the change in pathlength from the zero magnetic field case.

Figure 4.1 sketches the change in the backscattered path when a magnetic field is applied. The electron begins to follow a curved trajectory determined by the cyclotron radius

$$r_c = \frac{\hbar k_F}{eB} \quad . \tag{4.1}$$

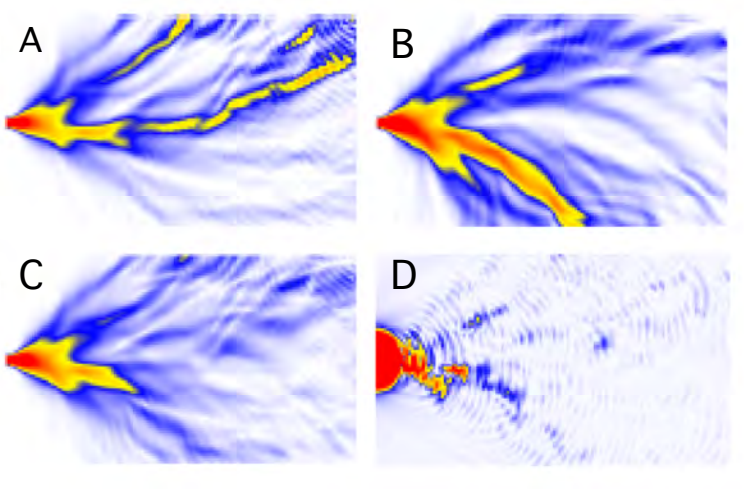

Figure 4.2: Expected backscattering tip scan image in a magnetic field. (A) and (B) Flux of electrons at magnetic field of $\pm 100\ mT$. (C) The "intersection" of the two flow patterns in A and B. The square root of the product of the two datasets is plotted. (D) Simulation of a tip scan at B = 100 mT (which is identical to the scan at -100 mT). The tip scan corresponds to the product of the positive and negative flow, as opposed to either set individually. Image is 1 micron x 0.6 micron. (Reproduced from Shaw's thesis [39].)

For small fields and a tip that is closer than r_c, some electrons will be scattered back into a path that returns to the QPC, enclosing a football shaped area. Returning to the QPC becomes more and more unlikely as the magnetic field is increased. As the outgoing and return path change in length and enclosed flux, the phase accumulated along the round trip changes from the zero field case.

When the smooth background potential is taken into account, the outgoing and return paths cannot be visualized as a football shape, but become more complex. One can consider the electron trajectories that exist for positive magnetic field as electrons exit the QPC, and the trajectories that exist for the reverse field for electrons exiting the QPC. Where these sets of trajectories overlap, a backscattering signal will be observed. The electrons need to have a reversed path available to return to the QPC.

This is shown in Figure 4.2, which is reproduced from the thesis of Scot Shaw [39]. The top two panels (A and B) show the flow from a quantum point contact (which is off to the left of the image) in +100 mT and -100 mT magnetic fields. We see some curved branches, and others that are less affected. The bulk of the flow in Fig. 4.2A is to the top of the image area, and the bulk Fig.4.2B is to the bottom, showing the effect of the reversed field. Where these two sets of paths intersect (Fig. 4.2C), we will be able to see a backscattered image, as simulated in Fig. 4.2D. The electron follows a branch to the tip, where its direction is reversed. A viable path must exist for the electron to return. This path is through a branch that exists for electrons exiting the QPC in the reverse field. We will see a backscattered image only when both of these paths exist at the location of the tip.

4.1.1 Experimental Data

One expects to see the backscattered signal disappear when the distance from the QPC to the tip is equal to the cyclotron radius, which is true for electrons emerging perpendicular to the QPC. It would not be surprising to find that the measured backscattered signal decays before this limit is reached, because the electrons need a path to return to the QPC in the magnetic field. Quantifying the decay of the signal is challenging, as it depends partly on the branches that exist.

Figure 4.3 shows experimentally obtained images for positive and negative magnetic fields. The quantum point contact is at the first plateau, and these images are taken at 4 K. Fig. 4.3C is obtained with no magnetic field. Fig. 4.3B and D are taken at ±24 mT, and A and E are taken at ±48 mT. The QPC is 600 nm below

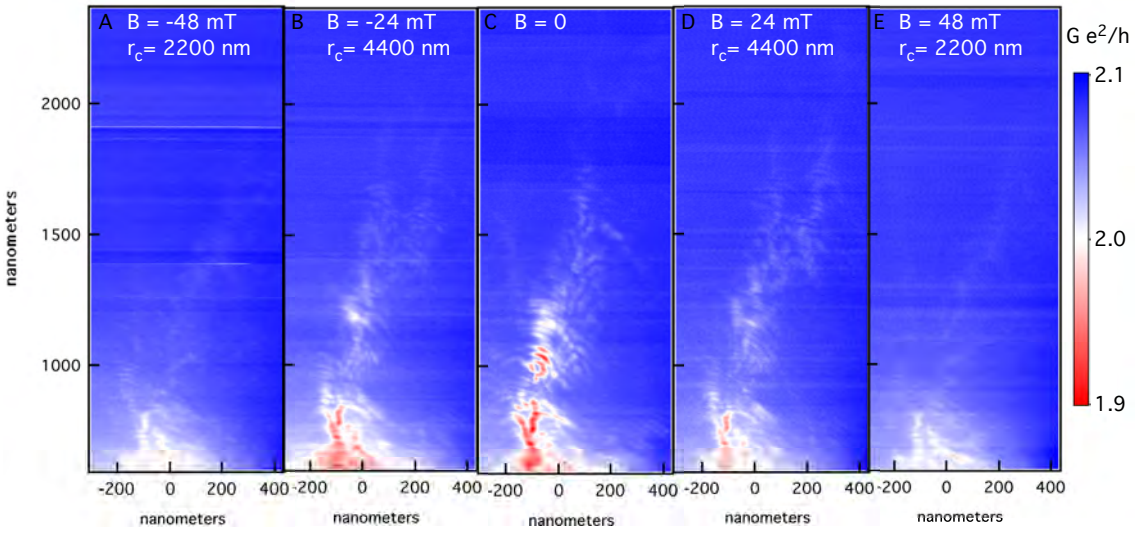

Figure 4.3: Experimental images obtained by backscattering to the QPC or origin. (A) -48 mT (B) -24 mT (C) 0 T (D) 24 mT (E) 48 mT. The images taken at corresponding fields, but in the opposite direction, are very similar as is expected.

the images, and the Y scale is numbered to show the distance from the QPC. The top edge of the images is at about 2300 nm from the QPC. This is comparable to the cyclotron radius at 48 mT, where $r_c = 2200$ nm. We see that the flow decays faster when farther from the QPC, as expected. We also see that the images taken for the two directions of magnetic field are quite similar, as they should be. While it is tempting to think that you see the electrons bending along a curved trajectory in the image, you must remember that it is the same curvature for both positive and negative magnetic fields. When there is a backscattered signal, we know that trajectories exist that go out to the tip at that point, reverse direction, and still return to the QPC. For the opposite field, the outgoing path and return path are swapped, and the image will look identical.

Figure 4.4 is another set of images taken by backscattering electrons into the QPC of origin. The area of the scan is smaller, and closer to the QPC (about 275 nm

above the QPC). The QPC is rather open, at the 5th plateau, to increase the flow pattern that is visible. These images are all taken at 1.7 K, and fringes are apparent throughout. Only one direction of magnetic field is shown. Fig. 4.4D is taken at 150 mT, which corresponds to a cyclotron radius of about 700 nm. Again, the upper part of the figure is comparable to r_c in distance to the QPC. We again see that the flow is less visible at the top of the image, though still relatively strong closer to the QPC.

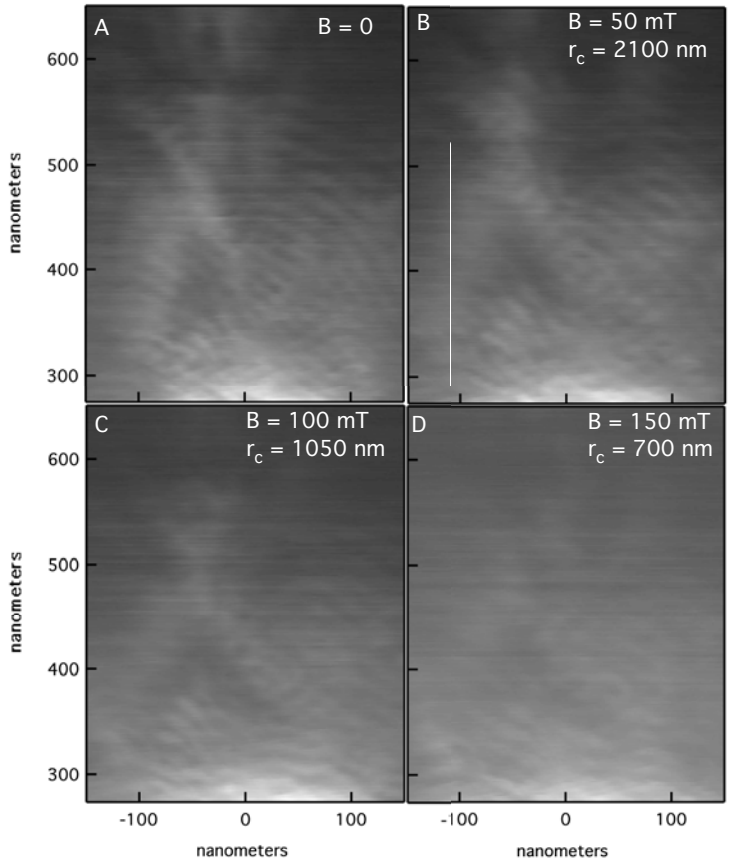

Figure 4.4: Experimentally obtained images by backscattering electrons to the QPC of origin in a magnetic field. (A) B = 0 (B) B = 50 mT (C) B = 100 mT (C) B = 150 mT. These images are taken at 1.7 K.

One expects both the fringe spacing and location to change with magnetic field.

As derived in Rob Parrot's thesis [33],

$$\Delta r = \frac{\lambda}{2} \frac{2r_c}{\sqrt{(2r_c)^2 - y^2}} \tag{4.2}$$

where Δr is the spacing of the fringes, r_c is the cycltron radius, and y is the distance between the tip and the QPC. Near the QPC, the spacing $\Delta r \rightarrow \lambda/2$, and the spacing grows larger with increasing distance. Unfortunately, I have been unable to obtain images that display this behavior. I believe with the right flow pattern it would be visible, but it is challenging given some variation in density (wavelength), the difficulty of obtaining a very accurate measurement of the fringe spacing when there are only a few periods visible, and the small change in the spacing. Additionally, one expects from a simple model with the football shaped orbits of Figure 4.1, that the fringes will shift in location as the magnetic field is changed. I was unable to find this behavior in the images as well. It is not surprising, in that the actual paths are rather different from the simple football shaped model, and to complicate matters, there is often a small drift in the position of the piezo tube. The application of a magnetic field seems to worsen this drift, though not significantly for the small fields (< 200 mT) of interest here. It may be worth repeating these measurements while scanning a topographic reference point between each electrical image.

4.2 Imaging magnetic focusing

To better image electron motion in a magnetic field, I used the magnetic focusing geometry and measured a change in transmission between two QPCs. Electrons are sourced from one QPC and the transmission through the second is measured (see

Chapter 2.4 for details). The tip is used to deflect the trajectories and change the transmission through the second QPC. We are able to image the natively transmitted trajectories as well as enhance interference fringes. This imaging technique is flexible in that it can image transmitted electrons between any two points (defined by QPCs) with or without a magnetic field. The tip potential in the 2DEG is used as an adjustable strength scatterer, such that when it lightly deflects the electrons the native transmission is imaged, and when it strongly scatters the electrons, interference effects are enhanced.

4.2.1 Background

Electrons in a magnetic field move in circles, given by the cyclotron radius (Eq. 4.1). Electrons will not participate in transport unless this circular motion is interrupted by a boundary. The electron bounces off the boundary, creating a skipping orbit that can carry a current across a sample. Magnetic focusing will occur when many electrons start at a single position, but take different trajectories spanning many initial angles. The magnetic field causes all these electrons to trace a circle back to their original position, focusing them back to the original point. When the electrons are limited in their initial spread of angles (e.g. collimated flow from a quantum point contact), then they will come to a point of near convergence after one half of an orbit.

The effect of a magnetic field on electrons emerging from a QPC is to focus the flow to a point of convergence at a distance $D = 2r_c$ from the source QPC. In the magnetic focusing geometry (Fig. 4.5), a target QPC is present a distance L from the source, and between the two there is an effective wall along which the electron

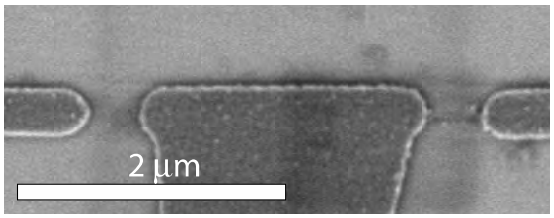

Figure 4.5: Scanning electron micrograph of a magnetic focusing device.

bounces until it reaches the target QPC, producing a skipping-orbit motion. When the magnetic field strength is such that the point of convergence intersects the target QPC (Fig. 4.6), there is a peak in the conductance. Taking into account multiple bounces, peaks will occur the QPC spacing $L = 2nr_c$, so at field values

$$B_n = \frac{2n\hbar k_F}{eL}. \tag{4.3}$$

The clarity and spacing of the focusing peaks provides information about the material properties of the sample and how ballistic the electron flow is.

Figure 4.6 is a ray-tracing simulation of the transmission versus magnetic field in a clean system, showing the electron trajectories near the first and second peaks. There is an increase in the width of subsequent peaks even in a perfectly clean system because there is not a perfect focus after half a cyclotron orbit, as can be seen in the trajectories plotted below. The subsequent bounces get wider, resulting in wider transmission peaks. This simulation was done by Rob Parrott, using ray-tracing techniques. Collimated electrons are launched from the left QPC and the trajectories are followed through the system.

Van Houten et al. [48] published a thorough analysis of magnetic focusing in a two-dimensional electron gas in 1989. They showed clear experimental focusing peaks

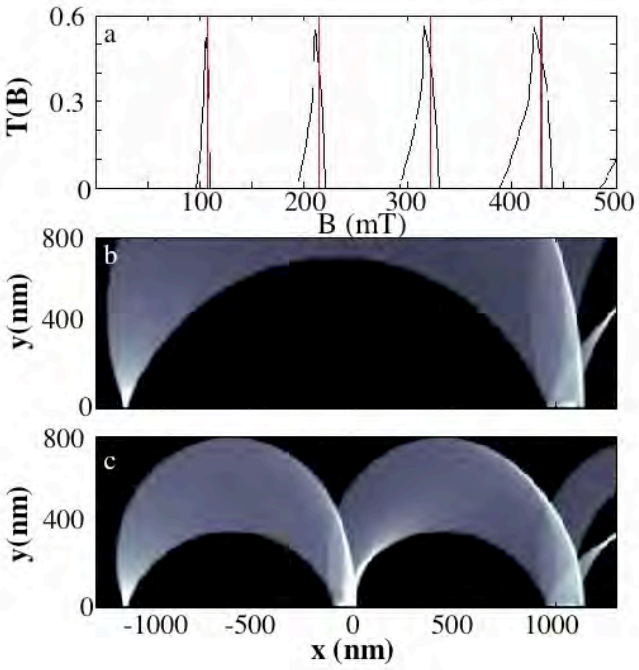

Figure 4.6: Simulation of focusing peaks in transmission versus magnetic field in a clean system. (A) Transmission versus magnetic field. (B) Electron trajectories at the first peak in transmission. (C) Electron trajectories at the second peak in magnetic field. (Reproduced from [1]).

at temperatures from 7 K to 50 mK. Conductance fluctuations are observed, which they attribute entirely to interference effects. They also provide a figure showing the caustics that develop in a clean system; however, they do not collimate the electrons emerging from the quantum point contact. In our present work, we have taken into account both the collimation of the electrons and the disordered system in defining the trajectories of electrons as well as in observed conductance fluctuations.

4.2.2 Imaging technique

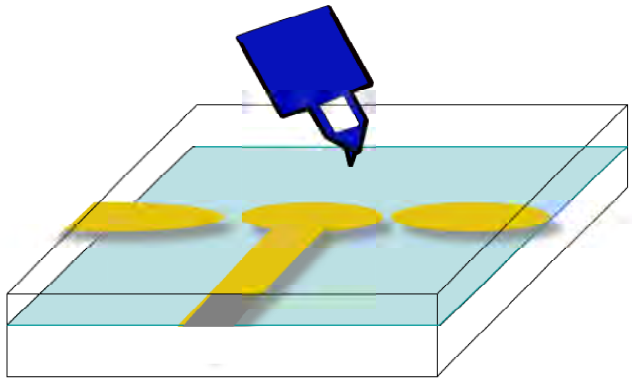

Figure 4.7: Schematic of imaging technique.

To image magnetic focusing, we introduce an SPM tip above a typical device (Figure 4.7), and measure the transconductance from source to target QPC as a function of tip position. A voltage is placed on the tip such that the electrons beneath are altered in density. This area acts as a lens, diverging when a negative voltage is on the tip and converging if a positive voltage is on the tip (Fig. 4.8). The voltage on the tip changes the focus of this lens and the strength of the scattering. This adjustable scatterer measurement technique can image transconductance between any

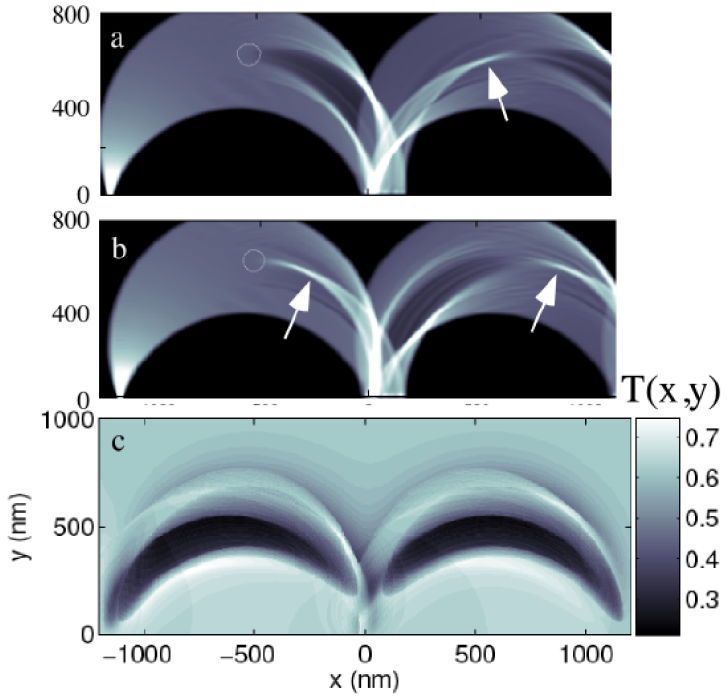

Figure 4.8: Classical simulation of the effect of the tip on electron trajectories. (A) A negative voltage on the tip acts as a defocusing lens. (B) A positive voltage on the tip acts as a focusing lens. The white arrows denote the focus of the potential created by the tip. (C) Classical simulation of a full tip scan near the second focusing peak. The double crescent with the single bounce along the gate is clearly visible. (Reproduced from [1].)

two QPCs, mapping the transmitted trajectories of electrons beneath the surface of the heterostructure.

Figure 4.8 shows the effect of the tip on the electron trajectories. Fig. 4.8A simulates a slightly negative tip, acting as a defocusing lens. The focal point is behind the lens, and recreated after the bounce along the center region, indicated by the white arrow. Fig. 4.8B depicts the effect of a slightly positive voltage on the tip, increasing the density of electrons directly beneath. This acts as a focusing lens, with the focal point indicated by the white arrows. The transmission between the left and

right QPC is changed by the location of the tip. For a defocusing tip, a shadow region is created behind the tip. If this shadow falls on the second QPC, the transmission will be decreased. The shadow area is bordered by caustics. If these fall across the second QPC, the transmission will be enhanced.

Figure 4.8C is a classical simulation of a full tip scan with a defocusing tip. Each point is generated by a simulation akin to the top two panels. The tip is placed at a specific point, electron trajectories are launched from the left QPC and propagated through the system, and the resulting change in transmission is plotted at that point. We see the crescents reproduced in this tip scan, with a clear bounce along the middle gate. The center of the crescents is dark, corresponding to the shadow falling across the second QPC. These dark central areas are bordered by areas of enhanced transmission, corresponding to the caustics falling across the second QPC.

4.2.3 Experimental results

This section describes how the samples were made and measured, and displays the images that were obtained. The images of magnetic focusing reveal clear signatures of the classical skipping-orbit patterns expected in this geometry. Branches of electrons are visible, creating structure in addition to the semicircular bouncing orbits. These branches contribute to conductance fluctuations observed in this geometry. We show that for weakly energized tips, this adjustable strength scatterer can be used to image the natively transmitted flow through the system. For more strongly scattering tips, coherent fringes are visible.

The GaAs/AlGaAs heterostructure used for these measurements contains a two-

dimensional electron gas 47 nm below the surface, with density, $n = 4.2x10^{11}cm^{-2}$ and mobility, $\mu = 500,000\ Vcm/s^2$, with the following composition: a 5 nm GaAs cap layer, followed by 20 nm $Al_{0.3}Ga_{0.7}As$ barrier, a delta-doped Si layer, then another 22 nm $Al_{0.3}Ga_{0.7}As$ barrier that forms the interface with GaAs where the 2DEG exists. We use electron beam lithography to define the gates of our device, which consists of two QPCs lithographically separated by 2.5μ (Fig. 4.5). We source a current through one QPC and measure the voltage across the second using standard lockin techniques. Both QPCs are set by the voltages on the gates to be in the quantized conductance regime, and there is no net flow of electrons through the second QPC. When electrons are ballistically injected into the second QPC, a voltage develops to drive a current that balances out the influx of electrons. Measuring this voltage records the transmission from one QPC into the second. With no magnetic field, one would expect few electrons to to be transmitted. We use a liquid helium cooled scanning probe microscope and bring a charged tip 10 nm above the surface of the heterostruture and scan the device. Each point in the resulting images is the change in transmission between the QPCs when the tip is centered at that point. The images shown here are all at 4 K unless otherwise noted.

Figure 4.9 shows the transport measurements of magnetic focusing conductance peaks. Transmission is plotted against magnetic field. It is straightforward to convert the recorded voltage to transmission. The current through the first QPC is known based on the conductance and voltage supplied from the lockin, and the voltage across the second is converted to a current with knowledge of the conductance of the second QPC. The ratios of these currents gives the transmission.

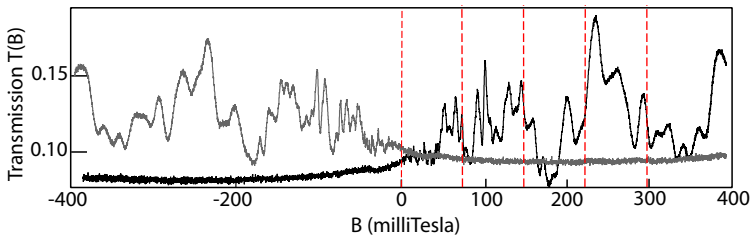

Figure 4.9: Experimental magnetic focusing peaks. Transmission versus magnetic field is plotted. The dark plot is obtained when one sources electrons from the right and measures the voltage across the left. The lighter plot is obtained when sourcing from the left and measuring voltage across the right. For opposite fields, there are the same fluctuations in transmission.

Fig. 4.9 is taken with both QPCs on the 2nd plateau. The darker plot is taken when sourcing electrons from the right and measuring transmission across the left. The lighter trace is obtained when sourcing electrons from the left and measuring across the right. Upon reversing the voltage leads and the magnetic field, one reproduces the same fluctuations in conductance. There is reciprocity between the two, as expected by the Onsager-Casimir symmetry relations in the diffusive regime [32] and extended to ballistic transport by Buttiker [10]. Buttiker shows that

$$R_{12,34}(B) = R_{34,12}(-B) \tag{4.4}$$

where the paired subscripts indicate the current and voltage leads, respectively, in a four terminal measurement. The fluctuations we see in our transmission plots are the result of both the branching of electron flow (discussed more in Section 4.2.4) and interference.

We immediately see in Fig. 4.10 the crescent shape of electrons moving in semi-circular orbits, with $r_c = 1.4\mu m$, near the first focusing peak. In the lower panels (Fig. 4.10C and D) we see that the center is mostly dark, and the bottom edge is light,

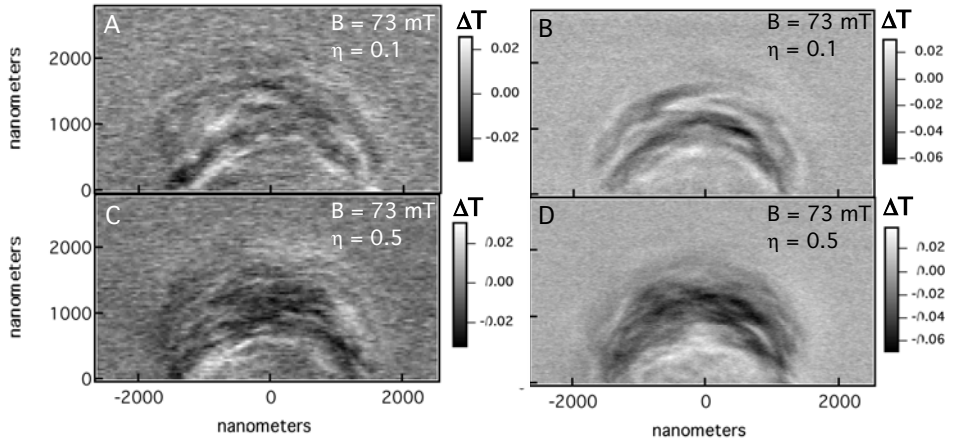

Figure 4.10: Experimental images for both right to left and left to right transmission near the first focusing peak. (A) Electrons sourced from the right QPC, $\eta = 0.1$, B = 73 mT. (B) Identical image but with electrons sourced from the left, and twice as many points taken. (C) Electrons sourced from the right QPC, $\eta = 0.5$, B = 73 mT. (D) Identical to C but with electrons sourced from the left and twice as many points.

similar to the expectation of a dark center surrounded by bright areas that is predicted in Fig. 4.8. Fig. 4.10 shows experimental images obtained with both QPCs at the 5th conductance plateau, for two different voltages on the tip. We see additional structure in the images of Figure 4.10, particularly noticeable in the images taken with a smaller voltage on the tip. There are locations of enhanced and decreased transmission throughout the crescent. We understand these features to be the result of the branches of electrons that develop in the 2DEG, and which will be discussed in section 4.2.4.

Figure 4.10A, B and Figure 4.10C,D are identical to one another except for the direction of electron flow. Additionally, there are twice as many points taken in B and D, which explains the change in the coarseness of the appearance. A and C are taken with electrons being sourced from the right and the transmission through the left QPC is measured. B and D are taken with electrons sourced from the left,

and the transmission through the right being measured, for the opposite direction of magnetic field. We see essentially the same features, though they are not identical. The gates have been ramped to zero and back, and the images are taken on different days. (Immediately repeating an image creates an identical image. Sweeping the gates to zero and back sometimes results in a slight change, and often some changes are observed day to day.) The transmitted trajectories from right to left and from left to right must be identical (Eq. 4.4), though the non-transmitted trajectories can differ. These non-transmitted trajectories do affect the image.

We characterize the strength of the tip voltage by the parameter η, given by

$$\eta \equiv \frac{V_0}{E_F} \tag{4.5}$$

where V_0 is the maximum amplitude of the effective potential created by the SPM tip (which we model with a Gaussian) and E_F is the Fermi energy. Thus when $\eta \geq 1$, the 2DEG is fully depleted underneath the tip, and the electron can backscatter from it. We have estimated the tip voltage at which the 2DEG is depleted with the aid of Mike Stopa's SETE program. The value is height dependent, and is approximately -0.9 V for a tip 10nm above the surface, and -1.4V for a tip 35 nm above the surface for this heterostructure. In calculating η we assume a contact potential offset plus the offset from the bias for the bridge circuit, which together appear to be around +0.2 V, though this has not been measured carefully. For the top panels of Fig. 4.10, the tip is 35 nm above the surface with zero volts placed on the tip. This voltage acts as a negative voltage of about -0.2 V. This leads to an estimate of $\eta = 0.1$, and $\eta = 0.5$ for the bottom two panels of Fig. 4.10.

An experimental determination of both the offset and the point at which the

electrons are depleted would be better. The SETE program can be "calibrated" to the structure because we know when the gates on the surface deplete by looking at a standard QPC conductance measurement. We then use this as a reference point, and often see that there is some mismatch that can be effectively corrected for by changing the density of electrons in the program. Still, the offset voltage is not known from the simulation. Experimentally determining the offset voltage can be done with careful scanning of the QPCs near zero effective voltage, looking for the smallest change. The depletion point of the electrons can be determined with backscattering measurements in zero magnetic field, where the flow is only visible when the tip is depleting the electrons. Both would be more accurate than the simulation.

Figure 4.11 shows the evolution of the experimental images with increasing magnetic field. These are taken with $\eta = 0.4$, and with the tip 35 nm above the surface. The center of the QPCs are located at the black and white dots. Electrons are being sourced from the left QPC, which is on the first plateau, and transmitted to the right QPC, biased at the third plateau. (The left QPC is dark because the tip pinches it off when directly above, reducing the total transmission to zero, and the right is white because when the right QPC is pinched off by the tip directly above, the section of the 2DEG below that QPC is floating, such that measuring the voltage across the QPC results in the lockin overloading.) Fig. 4.11A is taken slightly past the first focusing peak, at 100 mT, which corresponds to a cyclotron radius of 1.0 μm. We again see the crescent shape. Fig. 4.11B is taken near the second focusing peak, with $r_c = 590\ nm$ and a beautiful bounce is seen at the middle of the center gate. Two crescents are reproduced, showing the expected pattern of electron paths. Fig. 4.11C

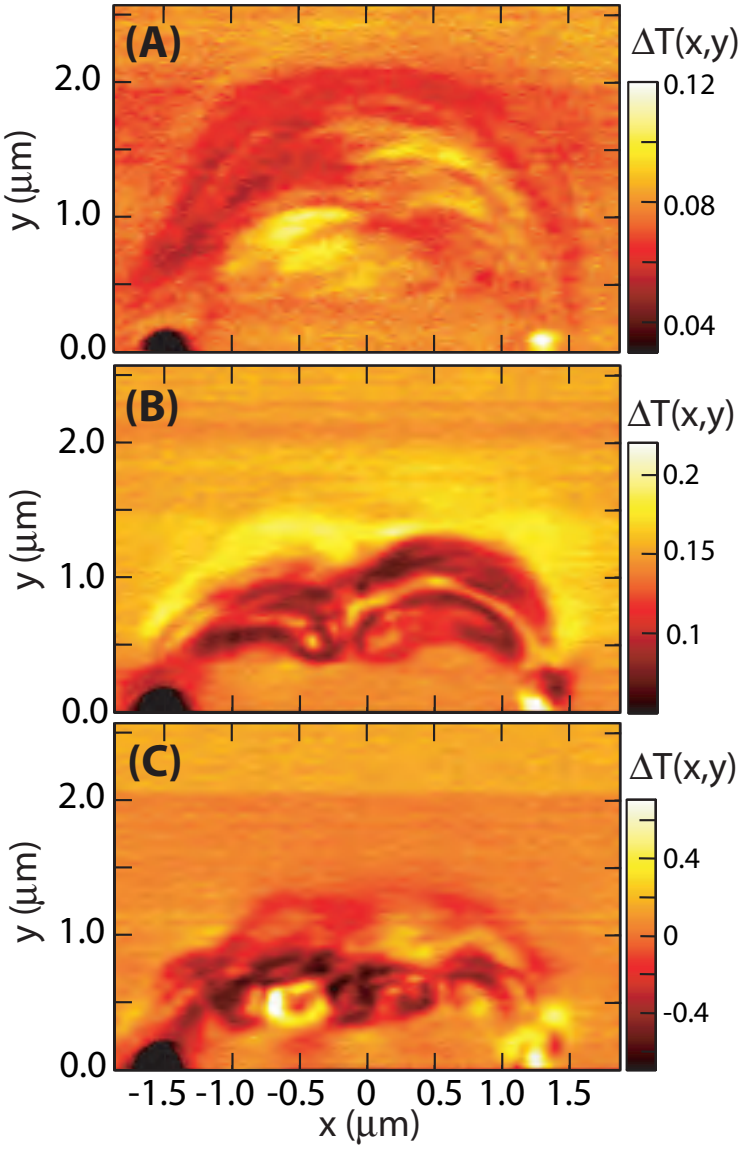

Figure 4.11: Experimental images obtained at three magnetic fields. (A) 100 mT, past the first focusing peak. (B) 174 mT, near the second focusing peak. (C) 262 mT, near the third focusing peaks. The electrons are sourced from the left QPC, biased at the first plateau, and transmitted across the right QPC, biased at the third plateau.

is taken near the third focusing peak. We cannot identify two clear bounces as would be naively expected, but we do see that the extent of the electron trajectories is limited close to the gates, with the strongest features extending about a cyclotron radius (390 nm) from the gate. This figure (4.11) shows the evolution of skipping orbits, which become the edge states of the quantum Hall regime.

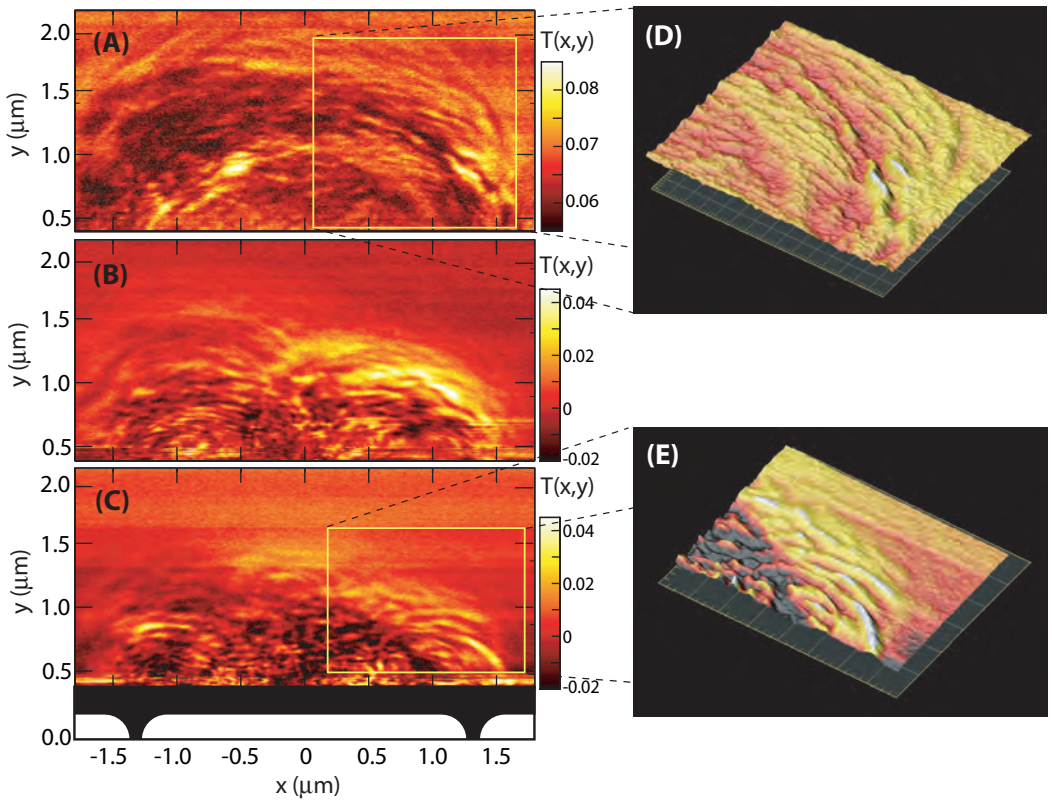

Figure 4.12: Experimental images at three magnetic fields, with $\eta = 0.8$. (A) Near the first focusing peak, B = 74 mT. (B) Near the second focusing peak, B = 169 mT. (C) Near the third focusing peak, B = 254 mT. (D) The boxed area in A is rendered such that the fringe structure is more visible. (E) The boxed area in C is rendered such that the fringes are more visible.

Figure 4.12 shows experimental images obtained when the tip is closer to the surface (10 nm), with $\eta = 0.8$. The location of the QPC gates are sketched below

Fig. 4.12C. Because the tip is only 10 nm above the surface, it can no longer be scanned directly above the QPCs. Electrons are being sourced from the left QPC to the right QPC, and both QPCs are on the 2^{nd} plateau. We once again see the semicircular structure with zero, one, and two bounces occuring along the gate (though we cannot see the location of the bounce). The images are taken at 74 mT, 169 mT, and 254 mT, respectively, which correspond to near the first, second, and third focusing peaks. We are immediately struck by the additional finer features that exist in the images, compared to the lower η images shown previously (Fig. 4.11). Fig. 4.12D and E enhance these higher frequency features, such that they can be more clearly seen as interference fringes. They will be described in detail in section 4.2.5.

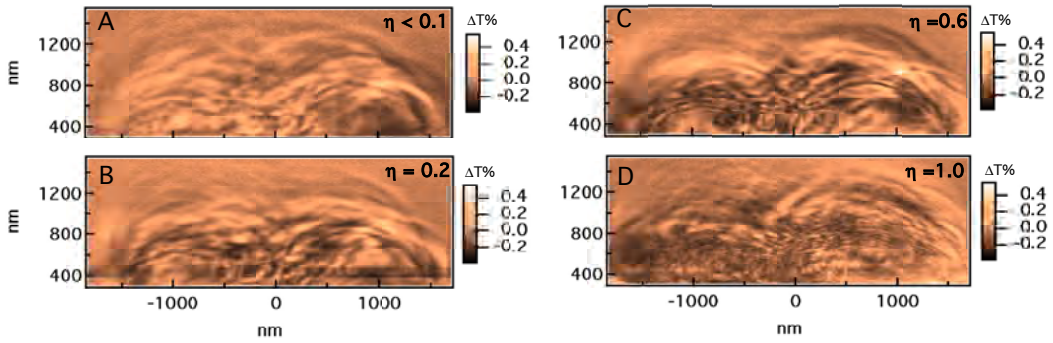

Figure 4.13: Experimental images near the second focusing peak taken with different voltages on the tip, (A) $\eta < 0.1$, (B) $\eta = 0.2$, (C) $\eta = 0.6$, (D) $\eta = 1.0$.

Figure 4.13 shows a series of images taken near the second focusing peak, with different tip voltages. This series clearly shows the development of finer features with increasing tip voltage. Fig. 4.13A is taken with $\eta < 0.1$, such that the tip just nudges the electrons into or out of transmission. By the time we reach $\eta = 1.0$, we see finer features that are the result of interference at the second QPC.

Figure 4.14 shows a series of images taken near the first, second, and third focusing

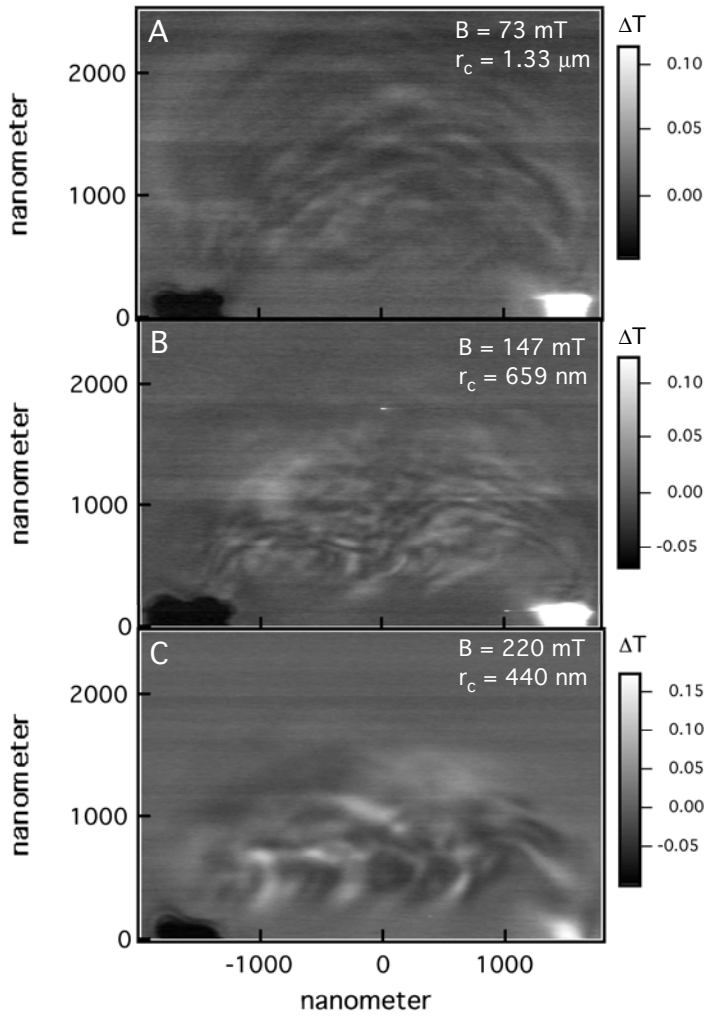

Figure 4.14: Experimental data at 1.7 K, sourcing electrons from the left QPC biased at the first plateau, measuring transmission across the right QPC biased at the second plateau. (A) B = 73 mT, (B) B = 147 mT, (C) B = 220 mT.

peak at 1.7 K. In these images, $\eta \approx 0.35$. Given this value of η, we do see more interference than at 4 K, at least in Fig. 4.14B. Fig. 4.14C does not have any apparent fringing, which is bit surprising. If there was any vibration from the pump that cools the system to 1.7 K, it could explain the absence, though one would expect it to be consistent throughout the series rather than reduce the visibility of the fringes for higher magnetic fields. The tip is now 35 nm above the surface, such that the area is over the gates. The location of the QPCs are at the black and white spots, and the gate is clearly visible where the tip has no effect, between the QPCs. There is a slight drift downwards throughout the series, such that the electrons bounce at lower location in the third image. The left QPC is on the first plateau, and the right is on the second.

4.2.4 The role of branches

The experimental images of the magnetic focusing of electron waves show two types of features beyond what would naively be expected for electron trajectories in the magnetic focusing geometry. We do see the overall semi-circular shapes associated with the skipping orbits of electron motion in a magnetic field. We also see relatively low frequency variations that result from branches, which are more easily identified when imaging with lower values of η. Branches are discussed in this section. The higher frequency modulations on top of the other features are associated with interference, and are the topic of the next section 4.2.5.

Figure 4.15 is a ray-tracing simulation of the trajectories that exist in a sample with a smoothly varying background potential. The figure shows how branching

occurs in a magnetic field and leads to fluctuations in the transmission. The model for this potential has been described in detail elsewhere [39, 44, 45]. The heterostructure we use contains a sub-monolayer of silicon donor atoms that are located typically 25 - 40 nm away in the GaAs/AlGaAs structures that we use (see section 1.2.2). About half of these silicon atoms are ionized, with some correlation. This creates positive charges that affect the potential felt by the electrons in the 2DEG. This smoothly varying potential results in small angle scattering that creates branches through which the electrons flow. The best analogy is to a swimming pool on a bright, sunny day. If you look down to the bottom of the pool, you will see constantly changing bright and dark patches that result from the bending of the light through the water. In the same manner, electron trajectories are bent as the electrons travel through the 2DEG. We have seen these branches in zero magnetic field, as shown in Chapter 3 and in the first section of this chapter (4.1).

When a magnetic field is applied, the electrons follow a curved trajectory defined by the cylcotron radius (Eq. 4.1). The smooth background potential will bend the electron paths away from a perfect circle. It is best to think about the branches formed in zero magnetic field as bending over, as the background potential allows. (See Scot Shaw's thesis for a more detailed description [39].) As these branches are bent over, they are swept across the second QPC, resulting in fluctuations in the transmission, as shown in Figure 4.15. The typical non-imaging method for measuring the magnetic focusing device is to plot transmission versus magnetic field, as shown in Fig. 4.9. A simulation by Rob Parrott reproduces such a plot for a 2DEG (Fig. 4.15A) with a representative background potential. The lower three panels (Fig. 4.15B,C,D) show

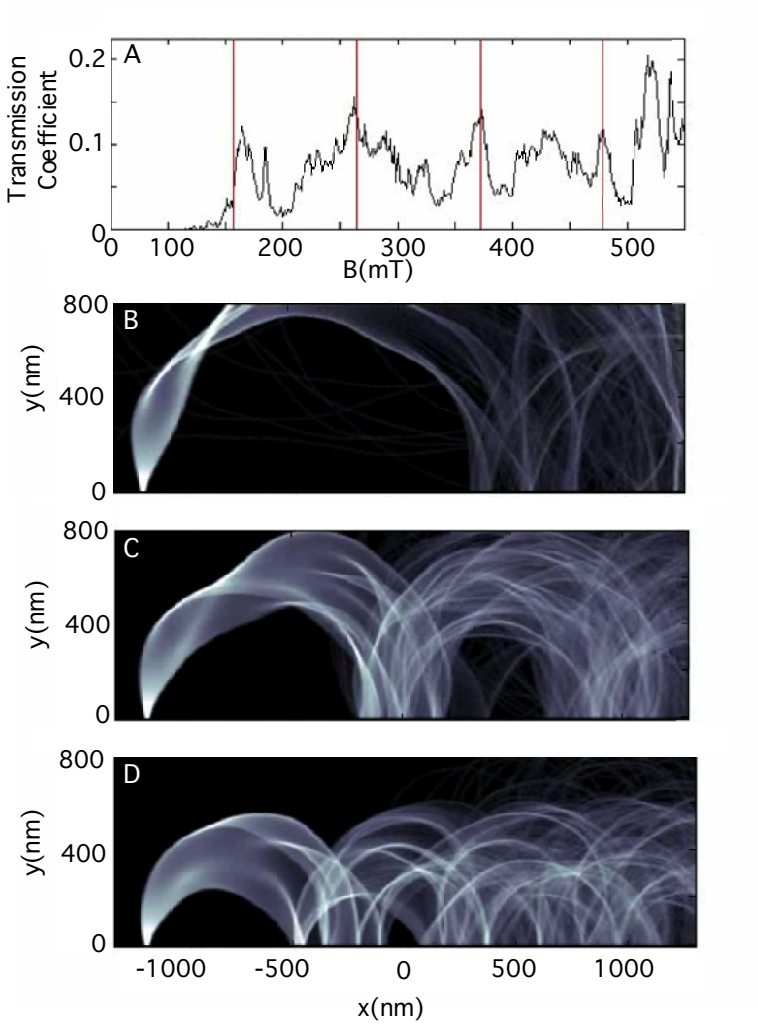

Figure 4.15: Simulation of magnetic focusing with a disordered background potential. (A) Transmission vs. B. The red vertical lines indicate the expected location of the peaks. (B) The electron flow pattern at the first focusing peak. (C) Electron flow pattern at the second peak. (D) Electron flow pattern at the third focusing peak. The fluctuations in the transmission correspond to the branches intersecting the second QPC.

the electron trajectories that exist at the first, second, and third focusing peaks, as defined by Eq. 4.3. These panels are ray-tracing simulations performed as in Fig. 4.6. Electron trajectories are traced in a magnetic field and in the presence of a background potential. Fig. 4.15A plots the transmission versus magnetic field, which is calculated by the ray-tracing procedure of the lower panels. Each point is the result of a trajectory simulation at that magnetic field. The red vertical lines indicate the magnetic field at which a focusing peak is expected, as in Fig. 4.6. We see rough agreement with the locations of the expected focusing peaks, but the additional structure is dominant. Looking at the panels below, we immediately understand the source of this structure; branches sweeping across the second QPC cause the bumps and dips in the transmission.

It is worth taking a moment to answer the question "What is the role of branches in conductance fluctuations?" Figure 4.15 is generated through ray-tracing, a "classical" process that contains no information about the phase of the electrons involved. I put classical in quotes because "classical" is often misused or carries connotations that are not intended. We see a great deal of seemingly random variation in the transmission that is completely repeatable and reproducible upon switching the voltage and current leads and the direction of the magnetic field. Comparing the theory (Fig. 4.15A) to the experimental data (Fig. 4.9) shows qualitative agreement. We would be tempted to attribute all of the fluctuations in transmission to the branching, without neediing to include the phase of the electron. However, when looking at transport within the coherence length (which is estimated to be 10 - 20 μm and has been shown to be over 6 μm by previous imaging work [45]), we must take into account the phase

of the electron. Generally when one talks about "conductance fluctuations", one is thinking about the phase of the electron, and "universal conductance fluctuations" can be derived and experimentally seen at "universal" values that depend on the exact system. This is true for diffusive transport in dirty systems that contain many modes. We are looking at ballistic transport with one or two open modes in a quantum point contact. The fluctuations we see, while the result of both interference and branches, can largely be described by the branches. See Rob Parrott's thesis [33] for a more thorough comparison of conductance fluctuations that result from branches and quantum simulations that include the phase of the electrons. The quantum mechanical simulations, which include a more realistic model of the QPCs and average over temperature, tend to broaden the fluctuations. The "classical" simulation shown here is done with a hard-wall potential with gaps of 100 nm representing the QPCs, which results in somewhat sharper fluctuation features.

It is worthwhile to reconsider the model of the SPM tip potential acting simply as a lens that creates a shadow behind it, bordered by caustics. Figure 4.16A shows the effect of the tip in a clean system in a somewhat different geometry, that of two QPCs facing one another and no magnetic field. We see the same defocusing effect of the lens, creating a shadow behind the tip bordered by caustics (the bright caustic that hits the lower right hand corner is a reflection off the top gate). When the shadow falls across the top QPC, the transmission from the bottom to the top is reduced. When the caustic falls across the top QPC, the transmission is enhanced. This is plotted by the green line in Fig. 4.16D, in which the transmission is plotted versus the X position of the tip. The dotted vertical line indicates the location of the tip

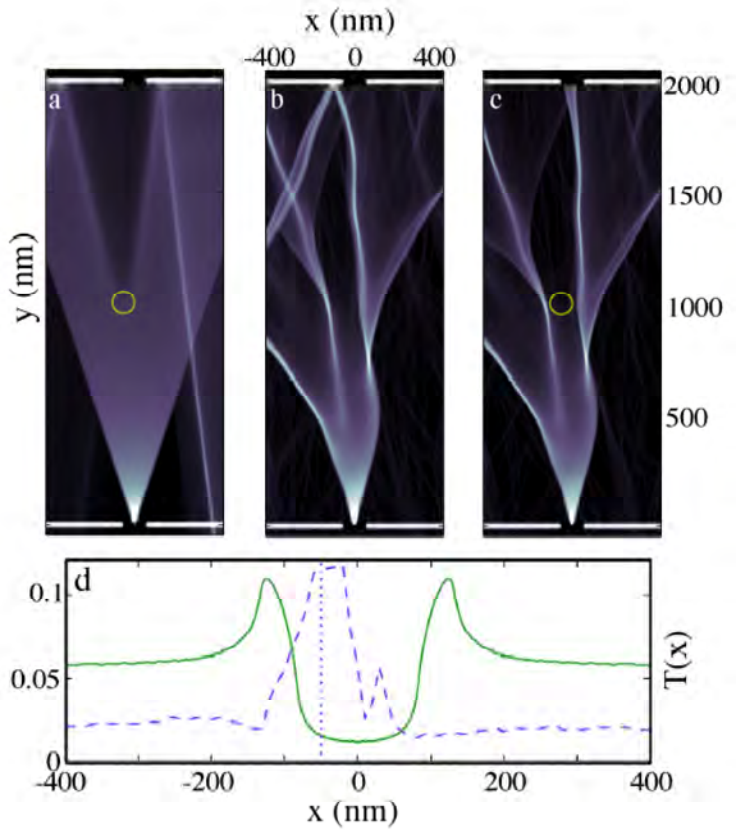

Figure 4.16: Simulation of the effect of the tip in a clean and disordered system. Electrons are flowing from the bottom QPC and the transmission across the top QPC is measured. (A) The tip acts as a simple defocusing lens in a clean system, creating a shadow behind it. (B) The electron flow without the presence of the tip. (C) Electron flow with the tip located as sketched, knocking the large branch into transmission. (D) Transmission versus tip position in X, for the Y position shown in A and C. The green curve is for the clean case, the dotted blue curve for the disordered case. (Reproduced from [1].)

in Fig. 4.16A and C. The green trace shows that without the tip (before it affects transmission) about 6% of the flow is transmitted. As the tip is scanned across X for the Y position shown in A, first the transmission increases as the caustic is swept past the second QPC, then the transmission is decreased, and enhanced again as the second bordering caustic is swept by. The situation changes when the smooth background potential is included, forming the branches displayed in Fig. 4.16B. We see that there is a strong branch that just misses the top QPC (and is reflected off to the left). The transmission without the tip is lower than the clean case (around 2%). As the tip is scanned along X, at some point it "knocks" the branch into the second QPC, causing a large increase in transmission. The same lensing effect is in action, but the result is a fairly sudden change in the transmission at a specific location. The dotted blue trace in Fig. 4.16D is the transmission versus X position in the bumpy background case. We see a large peak in transmission at the location of the tip displayed in C, where the branch is deflected into transmission. Our simple picture of the effect of the tip is still valid, but slightly more complex in the presence of branches.

We can understand the structure within the crescent shapes, seen in Figure 4.11, as the result of branches created by small angle scattering. As the tip is scanned, it deflects trajectories and in some cases will knock branches in and out of transmission. The dark areas are where transmitted trajectories are deflected out of transmission. We are able to image the branches that are transmitted before the tip is introduced (the native transmission). To demonstrate this more convincingly, we compare a simulated image to the classical trajectories. Figure 4.17 is a quantum mechanical

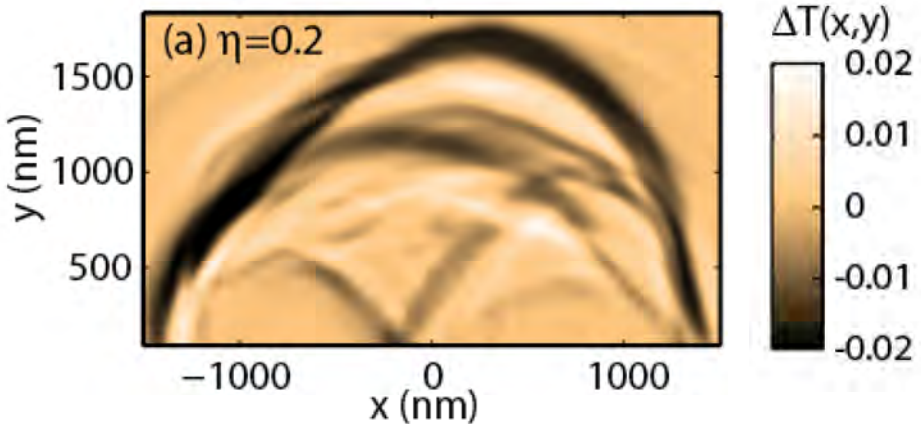

Figure 4.17: Quantum mechanical simulation of a full tip scan, with $\eta = 0.2$.

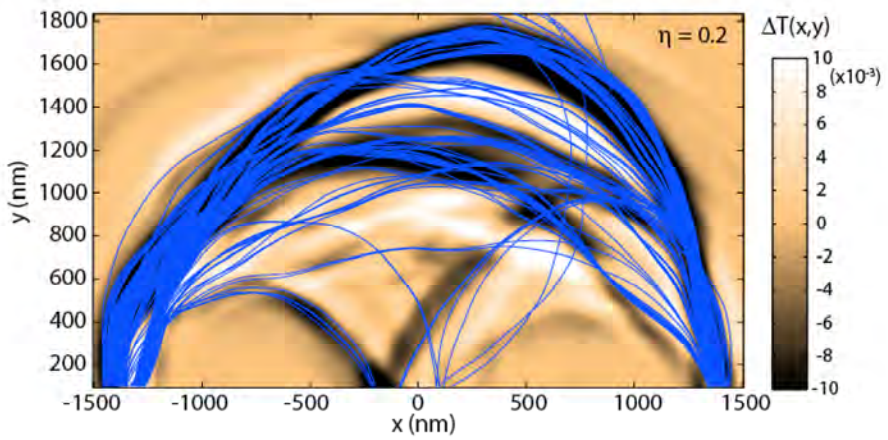

Figure 4.18: Quantum mechanical simulation of a full tip scan, with electron trajectories overlaid in blue.

simulation performed by launching wavepackets from the left QPC, propagating them through the system, and calculating the transmission through the right QPC. The tip is then centered at a point in the image, and the wavepacket is launched. The resulting change in transmission is plotted at that point. The center of the tip is moved one pixel and the simulation repeated. A full simulation of a tip scan is reproduced in this way. We see the dark and light areas of decreased and enhanced transmission, as the experimental data show. Conveniently, since we created the background potential, we can answer the question, "What are the natively transmitted trajectories?" A ray-tracing simulation is performed for the same background potential, and the transmitted trajectories are plotted in blue on top of the quantum mechanical tip scan simulation in tan for Figure 4.18. For a better comparison, these same trajectories are plotted as the red ropes in Figure 4.19. Fig. 4.19 shows in blue the potential as seen by the electrons, in transparent tan the simulation of the tip scan, and the natively transmitted trajectories in red. The transparent tan is identical to Fig. 4.17, but with the negative values (decreased transmission) cut out and the rest made slighty transparent to see the background potential below. The ray-tracing trajectories line up nicely with the dark areas of the scan simulation. This is expected because in order for the tip to decrease the transmission, electrons must have orginally been transmitted through that location.

These simulations show that our imaging technique successfully images the trajectories that were transmitted before the tip is present. We are also able to image some of the trajectories that exist but are not transmitted (the bright areas of enhanced transmission). Turning up the strength of the tip scattering leads to interference

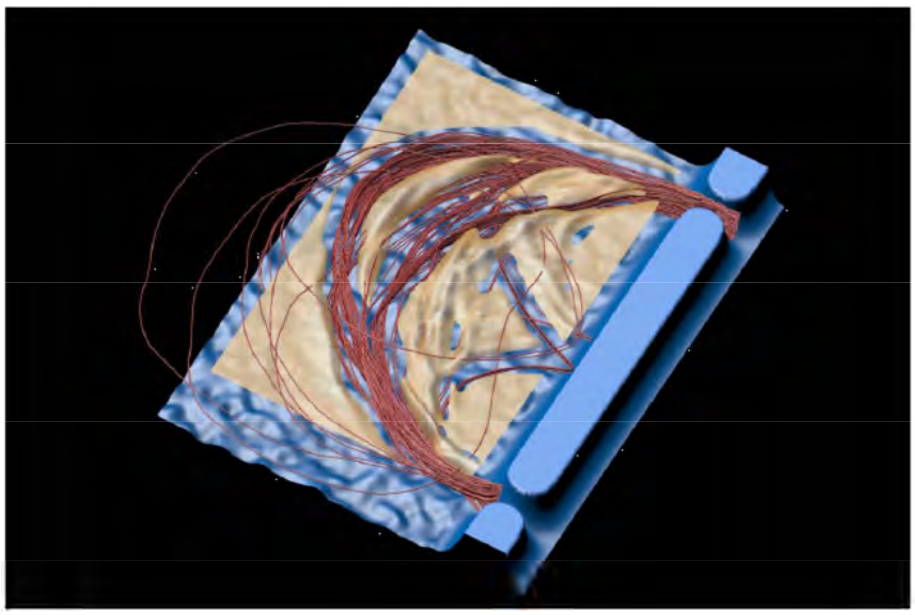

Figure 4.19: Simulation of the potential seen by the electrons (blue), the quantum mechanical tip scan simulation of Fig. 4.17 in tan with the negative values removed, and the classical electron trajectories overlaid in red.

fringes being visible, which is the subject of the next section.

4.2.5 Interference fringes

Thus far, our discussion has only included the effect of branching on the features that we see. We are well within the coherence length of electrons, and interference will occur whenever there are multiple paths for an electron to take that reconverge within the coherence length. Figure 4.20 is a schematic diagram showing why it is possible to see interference fringes. The two paths that form the black crescent are the transmitted trajectories for this magnetic field near the first focusing peak. These two trajectories will interfere, setting a reference point for the phase. When the tip is introduced, it may be in a location that deflects a trajectory that initially

misses the second QPC (the dotted line) into transmission (the green line). This adds another path the electron can travel, and changes the phase when the three paths reconverge. Both the pathlengths and the enclosed flux contribute to the net phase that is measured, and the tip can change both of these. If the tip is moved such that there is a periodic change in the phase with position of the tip, fringes will be seen in the image, indicated by the purple lines (see Eq. 4.6 below).

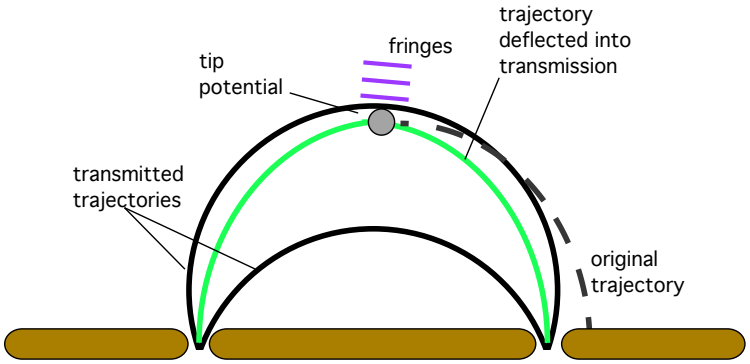

Figure 4.20: Schematic showing why we see interference fringes.

Figure 4.21 shows the simulation of a tip scan, with with $\eta = 1.2$. We see quite a few areas that display periodic structure indicating interference fringes. The simulation was done with both QPCs on the first conductance plateau and at 1.7 K, both of which increase the likelihood of seeing fringes. Multiple modes (higher conductance plateaus) lead to multiple fringe patterns overlaying, such that they are harder to see. The lower temperature increases the thermal length, allowing longer trajectories to contribute to the fringe patterns. Most of the experimental images are taken with both QPCs at the second plateau, and at 4 K. Even under these conditions, there are still parts of the images that show interference fringes (Figure 4.12 and 4.13). We

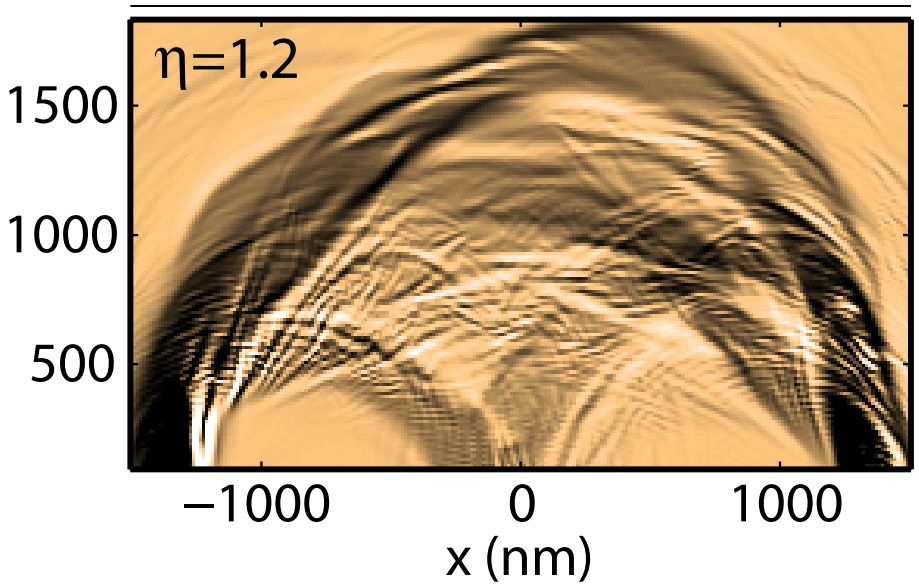

Figure 4.21: Quantum mechanical simulation of full tip scan, with $\eta = 1.2$. Fringes are seen throughout the image.

see that the schematic of Fig. 4.20 is greatly simplified. New paths may be created, and old ones may be removed. The branched nature of the electron flow makes it difficult to imagine the periodic change with tip location that must exist to see fringes in the images. However, this simulation makes it clear that we should expect to see interference fringes in parts of the image, despite these concerns.

Rob Parrott provides a more thorough discussion of the fringes in his thesis [33]. Figure 4.22 defines the scattering angle. The gray circle indicates the size of the tip, though the actual scattering event need not take place at its center, as shown. An electron travels towards the tip (p_1), where it gets deflected at some effective "point tip" that is located at q' in the diagram. This point lies at the intesection of the incoming and outgoing trajectories, though the electron will actually turn around at a point, q, in front of the point tip. The important message from this diagram

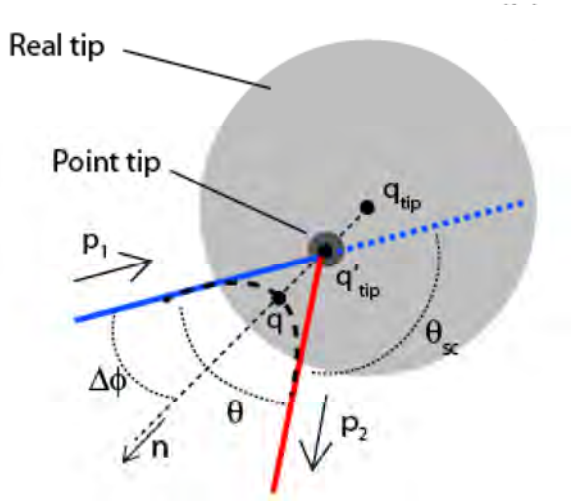

Figure 4.22: Diagram of tip scattering

is that though the tip is relatively large, we can identify an effective point that is associated with the scattering, and the history of the electron path does not affect this local scattering and the fringe spacing. Additionally, the scattering angle, θ_{SC}, is defined, as well as the normal, n that bisects the angle between the incoming and outgoing trajectories and which indicates the direction of the fringes. One can derive the spacing of the fringes as

$$\Delta r = \frac{\lambda}{2}\left|csc\frac{\theta_{SC}}{2}\right| \tag{4.6}$$

with the fringes running perpendicular to the normal, n, that bisects the incoming and outgoing trajectories. When the electron backscatters, scatters by π, we obtain a fringe spacing of $\frac{\lambda}{2}$ as in the backscattering of flow to the original QPC. When the scattering angle is zero, the fringe spacing is ∞, or rather, there are no fringes. By measuring the fringe spacing, we know the scattering angle of the electrons. By measuring the perpendicular to the fringes, we are able to back out the local initial

and final trajectory of the electrons.

With the knowledge that the greater the scattering angle, the smaller the spacing of fringes, we can better understand the effect of the tip voltage on the presence of interference in the images. A small voltage on the tip (low η) can only scatter electrons into a limited set of angles. The likelihood of seeing a set of fringes is small, because a regular change in phase would have to exist over a large area. With a large voltage on the tip (large η), the electrons can scatter into a much wider set of angles, reducing the spacing of the fringing, and increasing the likelihood of seeing fringes. We will always have interference among the converging paths at the second QPC; the question is whether we can see a tip location dependent variation in the image (i.e. fringes). For a more thorough discussion and examples of trajectories introduced by the tip, I again refer you to Rob Parrott's thesis [33].

Figure 4.23 directly compares quantum mechanical simulations of different tip strengths to experimental images. Fig. 4.23A is an experimental image with $\eta = 1$, with the black box indicating the area that is plotted in E - G for different voltages on the tip. (This is the same data as in Fig. 4.13D.) Fig. 4.23B,C,D are QM simulations at three values of η, 0.2, 0.6, and 1.0, corresponding to the experimental images below. We see excellent agreement between the experiment and simulation, with the average feature size decreasing as the strength of the scattering from the tip increases. We see distinct fringes in D and G, and no apparent fringes in B and E. It can be difficult to separate the interference effects and the "non-phase related" effects of the tip, for example in C and F. As the tip deflects trajectories into greater angles, different trajectories are accessible to the electrons. Some of the changing features are simply

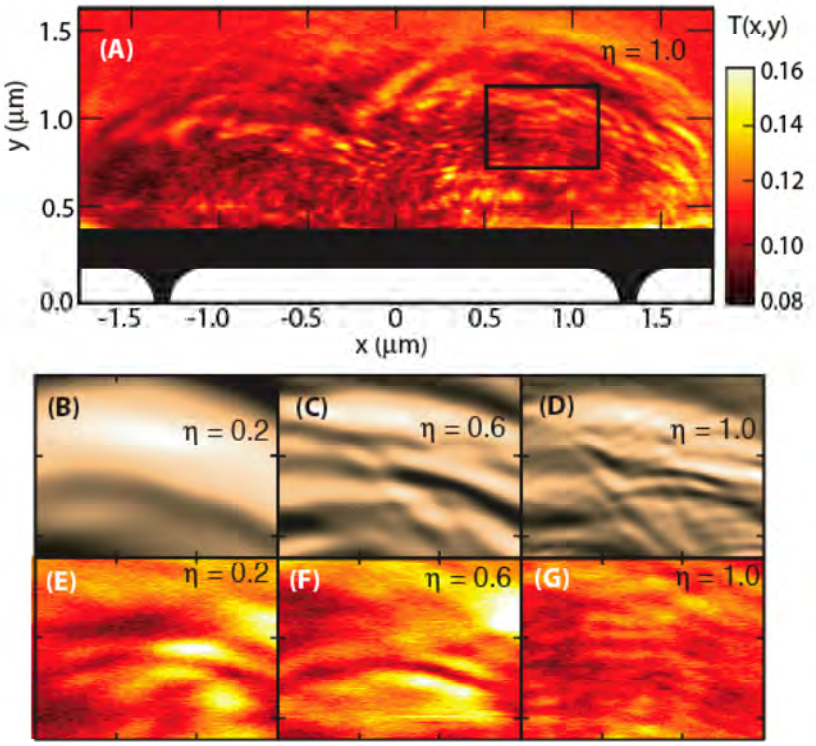

Figure 4.23: Direct comparison of experiment to theory for different tip voltages. (A) Experimental image with $\eta = 1.0$. The black box indicates the area shown in E, F and G. (B) Simulation of a tip scan with $\eta = 0.2$. (C) Simulation of a tip scan with $\eta = 0.6$. (D) Simulation of a tip scan with $\eta = 1.0$. (E) Experimental image with $\eta = 0.2$. (F) Experimental image with $\eta = 0.6$. (G) Experimental image with $\eta = 1.0$. There is excellent agreement between the simulated and experimental images.

the result of the smooth disordered background potential, and is not indicative of flow before the tip was present or of tip-dependent interference patterns. Only when a clear periodic structure is visible can we confidently identify the effect of interference in the image. This generally occurs for $\eta \gtrsim 1$.

4.3 Summary

Imaging electrons in magnetic fields is important both for the understanding of fundamental physics and for more practical applications in the design of devices that must function in a magnetic field. The presence of a magnetic field perpendicular to the two-dimensional electron gas creates additional challenges. On the technical side, the SPM must be stable in magnetic fields, which it is for the fields under discussion here, though higher magnetic fields do appear to lead to drift in x, y, and z that must be taken into account. On the imaging side, the reliable and high resolution imaging technique of backscattering to the point of origin (Ch. 3) is no longer available.

For small magnetic fields, we observed the decay of the backscattering signal (Section 4.1). We looked for an expected change in fringe spacing and location of fringes, but without success, for presumably uninteresting reasons (difficulty in measuring fringe spacing and location with sufficient accuracy).

To image electron waves in higher magnetic fields, a new technique was developed. Instead of backscattering to the QPC of origin, the electrons scatter off the tip and the transmission to a second QPC is measured. This technique provides the flexibility to image with or without a magnetic field between any two points. We produced the first images of skipping orbits of electrons in the magnetic focusing geometry. The

expected semicircular trajectories are clearly visible, along with additional structure due to branches and interference. We demonstrated that we are able to image the natively transmitted trajectories if the tip is a weak scatterer and we are able to see interference of electrons as the scattering strength of the tip is increased.

Chapter 5

Future Directions and Summary

5.1 Summary

When I entered the Westervelt lab in 2001, there was one scanning probe microscope that operated at temperatures down to 1.7 K and did not have the capability of applying a magnetic field. Desire to work with physical systems that require lower temperatures and magnetic fields, as well as to have a second operational system for simultaneous experiments, drove the construction of the new microscope. The new SPM operates directly in liquid helium and can go down to 470 mK, and has two separate magnets that can be used to apply either up to a 7 Tesla perpendicular magnetic field or up to a 3 Tesla parallel magnetic field.

In the older system, we imaged a V-shape interferometer, by backscattering electrons to the QPC of origin. The QPC is the vertex of the V, the tip reflects one path, and a metal gate on the surface acts as a mirror and reflects the other, back to the QPC where the paths interfere. If the interfering paths are similar in length, to

within the thermal length, strong interference fringes will be seen. Electrons that go from the QPC, to the reflecting gate, and back to the QPC interfere with electrons that go to the tip and back, when the tip is within a thermal length of reflecting gate. Electrons that go from the QPC and bounce twice off the reflecting gate before returning through the QPC of origin travel twice the distance. These paths interfere with a path that goes from the QPC to the tip and back, if the tip is twice as far as the reflecting gate. We can identify these different paths by changing the position of the reflecting gate (by changing the applied voltage). The interferometer allows us to identify pathlengths that differ by more than the thermal length. Raising the temperature decreases the thermal length and actually increases this time/distance resolution.

In the new system, we first looked at using the same backscattering technique to image electron flow from a QPC in a perpendicular magnetic field. As expected, when the field is increased, the backscattered signal decreases because the perpendicular field breaks time reversal symmetry. A new method to image electrons in a magnetic field was required, and we developed a technique that can image between any two points in a system, with or without a magnetic field. We measure the transmission between two QPCs, such that the tip will deflect trajectories into or out of transmission. Backscattering is no longer necessary, and at times undesirable. We have demonstrated that we are able to image the transmitted electron trajectories between the two points, by placing a small voltage on the tip and just slightly deflecting the electron trajectories. We are able to enhance the interference fringes in the images by using a strongly scattering tip. We see features that are the result of the branches

with which we are familiar from our backscattered images, as well as finer features that are the result of interference.

Many experiments are now possible on one or both of the SPM systems. Parisa Fallahi and I took images of a single electron dot in magnetic fields up to 6 T [17], and more work deserves to be done there. I have been involved in preliminary work in collaboration with Stefano Roddaro, from the Scuola Normale Superiore in Pisa, Italy, on quantum Hall edge states [36]. I also have done mostly background research to study spin-orbit coupling in two-dimensional systems (for a good overview of spin-orbit coupling in two-dimensional systems, see [52]), first looking to InAs as a good candidate, and only recently developed a collaboration with Leonid Rokhinson to study his magnetic focusing device that shows spin-splitting due to spin-orbit coupling in a GaAs/AlGaAs hole gas [37]. I hope to see stunning images result from these collaborations as they are pursued by the younger students in the lab.

Bibliography

[1] K.E. Aidala, R.E. Parrott, E. J. Heller, and R.M. Westervelt. Imaging electrons in a magnetic field. *Physica E*, 34:409, 2006.

[2] K.E. Aidala, R.E. Parrott, T. Kramer, E.J. Heller, R.M. Westervelt, M.P. Hanson, and A.C. Gossard. Imaging magnetic focusing of electrons in a two-dimensional electron gas. *submitted*, 2006.

[3] N. Aoki, C.R. da Cunha, R. Akis, D.K. Ferry, and Y. Ochiai. Imaging of integer quantum hall edge state in a quantum point contact via scanning gate microscopy. *Physical Review B*, 72:155327, 2005.

[4] Nobuyuki Aoki, Carlo R. Da Cunha, Richard Akis, David K. Ferry, and Yuichi Ochiai. Scannign gate microscopy investigations on an ingaas quantum point contact. *Applied Physics Letters*, 87:223501, 2005.

[5] D.D. Awschalom, D. Loss, and N. Samaeth, editors. *Semiconductor Spintronics and Quantum Computation*. Springer, 2002.

[6] C.H. Bennett and D.P. DiVincenzo. Quantum information and computation. *Nature*, 404(6775):247, 2000.

[7] G. Binnig, C.F. Quate, and Ch. Gerber. Atomic force microscope. *Physical Review Letters*, 56(9):930 – 933, 1986.

[8] G. Binnig, H. Rohrer, Ch. Gerber, and E. Weibel. Surface studies by scanning tunneling microscopy. *Physical Review Letters*, 49:57 – 61, 1982.

[9] A.C. Bleszynski. *Imaging electrons in nanostructures?* PhD thesis, Harvard University, 2006.

[10] M. Buttiker. *Physical Review Letters*, 57:1761, 1986.

[11] I. Chan. *Quantum dot circuits:Single-electron switch and few-electron quantum dots*. PhD thesis, Harvard University, 2003.

[12] Hong Chen, J. J. Heremans, J. A. Peters, A. O. Govorov, N. Goel, S. J. Chung, and M. B. Santos. Spin-polarized reflection in a two-dimensional electron system. *Applied Physics Letters*, 86:032502, 2005.

[13] R. Crook, C. G. Smith, A. C. Graham, I. Farrer, H.E. Beere, and D. A. Ritchie. Imaging fractal conductance fluctuations and scarred wavefunctions in a quantum billiard. *PRL*, 91:246803, 2003.

[14] R. Crook, C. G. Smith, M. Y. Simmons, and D. A. Ritchie. Imaging cyclotron orbits and scattering sites in a high mobility two-dimensional electron gas. *PRB*, 62:5174, 2000.

[15] J.H. Davies. *The physics of low-dimensional semiconductors: an introduction*. Cambridge University Press, 1998.

[16] M.A. Eriksson. Cryogenic scanning probe microscopy for semiconductor nanostructures. *Harvard University Thesis*, 1997.

[17] P. Fallahi. *Imaging Electrons in Few-Electron Quantum Dots*. PhD thesis, Harvard University, 2006.

[18] P. Fallahi, A. C. Bleszynski, R. M. Westervelt, J. Huang, J. D. Walls, E. J. Heller, M. Hanson, and A. C. Gossard. Imaging a single-electron quantum dot. *Nano Letters*, 5:223, 2005.

[19] J. A. Folk, R. M. Potok, C. M. Marcus, and V. Umansky. A gate-controlled bidirectional spin filter using quantum coherence. *Science*, 299, 2003.

[20] E.J. Heller, K.E. Aidala, B.J. LeRoy, A.C. Bleszynski, A. Kalben, R.M. Westervelt, K.D. Maranowski, and A.C. Gossard. Thermal averages in a quantum point contact with a single coherent wave packet. *Nano Letters*, 5(7):1285, 2005.

[21] M. Khodas, A. Shekhter, and A.M. Finkel'stein. Spin polarization of electrons by nonmagnetic heterostructures: The basics of spin optics. *Physical Review Letters*, 92:86602, 2004.

[22] S. Kicin, A. Pioda, T. Ihn, K. Ensslin, D.C. Driscoll, and A.C. Gossard. Local backscattering in the quantum hall regime. *PRB*, 70:205302, 2004.

[23] B.J. LeRoy. *Imaging Coherent Electron Flow Through Semiconductor Nanostructures*. PhD thesis, Harvard University, 2003.

[24] B.J. LeRoy, A.C. Bleszynski, K.E. Aidala, R. M. Westervelt, A. Kalben, E.J. Heller, K.D. Maranowski, and A.C. Gossard. Imaging electron interferometer. *Physical Review Letters*, 94(12):126801, 2005.

[25] B.J. LeRoy, M.A. Topinka, R.M. Westervelt, K.D. Maranowski, and A.C. Gossard. Imaging electron density in a two-dimensional electron gas. *Applied Physics Letters*, 80(23):4431, 2002.

[26] A. Lewis, M. Isaacson, A. Harootunian, and A. Muray. Development of a 500-a spatial resolution light microscope. *Ultramicroscopy*, 13(3):227, 1984.

[27] J. Martin, S. Ilani, B. Verdene, J. Smet, V. Umansky, D. Mahalu, D. Schuh, G. Abstreiter, and A. Yacoby. Localization of factionally charged quasi-particles. *Science*, 305(5686):980, 2004.

[28] Kent L. McCormick, Michael T. Woodside, Mike Huang, Mingshaw Wu, Paul L. McEuen, Cem Duruoz, and Jr. J.S. Harris. Scanned potential microscopy of edge and bulk currents in the quantum hall regime. *Physical Review B*, 59(7):4654, 1999.

[29] Ernst Meyer, Hans Josef Hug, and Roland Bennewitz. *Scanning probe microscopy: the lab on a tip*. Springer, 2004.

[30] APEX Microtechnology. Application note 1.

[31] Michael A. Nielsen and Isaak L. Chuang. *Quantum computation and quantum information*. Cambridge University Press, 2000.

[32] L. Onsager. *Physical Review B*, 38:10162, 1931.

[33] Robert E. Parrott. *Topics in electron dynamics in moderate magnetic fields*. PhD thesis, Harvard University, 2006.

[34] A. Pioda, S. Kicin, T. Ihn, M. Sigrist, A. Fuhrer, K. Ensslin, A. Weichselbaum, and W. Wegscheider S.E. Ulloa, M. Reinwald. Spatially resolved manipulation of single electrons in quantum dots using a scanned probe. *PRL*, 93:216801, 2004.

[35] D.W. Pohl, W. Denk, and M. Lanz. Optical stethoscopy - image recording with resolution lambda/20. *Applied Physics Letters*, 44(7):651, 1984.

[36] S. Roddaro, V. Pellegrini, F. Beltram, G. Biasiol, L. Sorba, R. Raimondi, and G. Vignale. Nonlinear quasiparticle tunneling between fractional quantum hall edges. *Physical Review Letters*, 90(4):46805, 2003.

[37] L. P. Rokhinson, V. Larkina, Y. B. Lyanda-Geller, L. N. Pfeiffer, and K. W. West. Spin separation in cyclotron motion. *PRL*, 93:146601, 2004.

[38] Y. V. Sharvin and L. M. Fisher. Observation of focused electron beams in a metal. *JETP Letters - USSR*, 1:152, 1965.

[39] Scot E. J. Shaw. *Propagation in Smooth Random Potentials*. PhD thesis, Harvard University, 2002.

[40] S.E.J. Shaw, R. Fleischmann, and E.J. Heller. Quantum coherence beyond the thermal length. *cond-mat/0105354*, 2001.

[41] A. Shekhter, M. Khodas, and A.M. Finkel'stein. Diffuse emission in the presence of an inhomogeneous spin-orbit interaction for the purpose of spin filtration. *Physical Review B*, 71:125114, 2005.

[42] G. A. Steele, R. C. Ashoori, L. N. Pfeiffer, and K. W. West. Imaging transport resonances in the quantum hall effect. *PRL*, 95:136804, 2005.

[43] M. A. Topinka. *Imaging coherent electron wave flow through two-dimensional electron gas nanostructures*. PhD thesis, Harvard University, 2002.

[44] M. A. Topinka, E. J. Heller, and R. M. Westervelt. Imaging electron flow. *Physics Today*, 56:12, 2003.

[45] M. A. Topinka, B. J. LeRoy, R. M. Westervelt, S. E. J. Shaw, R. Fleischmann, E. J. Heller, K. D. Maranowski, and A. C. Gossard. Coherent branched flow in a two-dimensional electron gas. *Nature*, 410:183, 2001.

[46] M.A. Topinka, B.J. LeRoy, R.M. Westervelt, S.E.J. Shaw, E.J. Heller, K.D. Maranowski, and A.C. Gossard. Imaging coherent electron flow from a quantum point contact. *Science*, 289:2323, 2000.

[47] V.S. Tsoi. Focusing of electrons in a metal by a transverse magnetic field. *JETP Letters*, 19:70, 1974.

[48] H. van Houten et al. Coherent electron focusing with quantum point contacts in a two-dimensional electron gas. *PRB*, 39:8556, 1989.

[49] B.J. van Wees, H. van Houten, C.W.J. Beenakker, J.G. Williamson, L.P. Kouwenhoven, D. van der Marel, and C.T. Foxon. Quantized conductance of point contacts in a two-dimensional electron gas. *Physical Review Letters*, 60(848), 1988.

[50] P. Weitz, E. Ahlswede, J. Weis, K. Von Klitzing, and K. Eberl. Hall-potential investigations under quantum hall conditions using scanning force microscopy. *Physica E*, 6:247, 2000.

[51] D.A. Wharam, T.J. Thorton, R. Newbury, M. Pepper, H. Ahmed, J.E.F. Frost, S.G. Hasko, D.C. Peacock, D.A. Ritchie, and G.A.C Jones. One-dimensional transport and the quantization of the ballistic resistance. *Journal of Physics C: Solid State Physcs*, 21:L209, 1988.

[52] R. Winkler. *Spin-orbit coupling effects in two-dimensional electron and hole systems*. New York: Springer, 2003.

[53] S.A. Wolf, D.D. Awschalom, R.A. Buhrman, J.M. Daughton, S. von Molna, M. L. Roukes, A.Y. Chtchelkanova, and D.M. Trger. Spintronics: A spin-based electronics vision for the future. *Science*, 294:1488, 2001.

[54] Michael T. Woodside and Paul L. McEuen. Scanned probe imaging of single-electron charge states in nanotube quantum dots. *Science*, 5570(1098), 2002.

[55] A. Yacoby, H.F. Hess, T.A. Fulton, L.N. Pfeiffer, and K.W. West. Electrical imaging of the quantum hall state. *Solid State Communications*, 111:1, 1999.

Appendix A

Fabrication

This appendix contains instructions for using only the newer equipment that has not yet been written up in previous theses.

A.1 JEOL 7000F

Instructions on using the JEOL 7000F, acquired in 2005. The taskbar at the top opens most of the menus to control the stage. There is no z control, focus moves z, as long as the working distance menu is open (usually in the lower right).

1. **Loading your sample**

   (a) Retrieve sample mount. Do not touch mount with bare hands (wear gloves). Open chamber if vented, otherwise, see vent step 6f.

   (b) Mount samples. Use a small amount of carbon paint on two edges. Remember where you place them.

   (c) Dot silver paint on the edges or near area where device will be written. Use as little as possible.

   (d) Load samples. Place holder in slot. Make sure holder is flat. Close door (lift a little to close) Latch. Verify stage is in Exchange position, x = 25, y = 35, z = 40, r = 0 If not, go to exchange position, see step 6d.

   (e) Press and hold EVAC until it starts flashing.

   (f) When EVAC is solid and lit, lower access arm to push in sample holder.

   (g) Push holder all the way in, pause, and bring out. The HLDR light will light up.

2. **Turning on the electron beam**

   (a) Go to faraday cup (Stage map and control:points file:position 1)

   (b) Turn on Beam. (SEI: ON Beam:ON, SEM mode on external control computer, HT should be bright green, Freeze:OFF Focus on/near Faraday cup (mag $<$ 100 to see it). Use ACB for autocontrast and brightness.

   (c) Set currents. Zoom in so only blackness of Faraday cup is showing. Small:$\approx$ 25 pA Med:$\approx$ 1 nA Hi:$\approx$ 15 nA

   (d) Focus on Tin balls (position 2)

   (e) Set stigmator so all three current values (or whichever youre using) are as crisply in focus as possible. Make sure Small current is the best focus if you are writing small features on Small current. Set stigmator by selecting a circular feature (mag $>$ 40,000) and twisting x knob, until best focus. Adjust focus. Twist y knob, adjust, etc.

   (f) Check offsets as needed.

      i. Find identifiable feature
      ii. Beam Off
      iii. NPGS (other computer)
      iv. Beam Blank
      v. Directory $\sim$/H/a850
      vi. Run File editor
      vii. Check the magnification (should be 850)
      viii. Process run file. Set magnification and current. Continue. This will create a box on the external control monitor.
      ix. Set zero offset to 850 mag, Small current, if this is what you are writing your smallest features at. Overwrite and continuously scan the area. Move stage until feature is lined up with white cursor. Stop (Esc).
      x. Switch back to manual control (Beam: Off, SEM, Beam: ON). Move the green cursors to line up with the feature at zero offset. Now your crosshairs are truly at 0,0 when using small current and 850 magnification.
      xi. Go back to NPGS mode and do 850 mag, Med current and run a850 again.
      xii. Move white cursor to center of feature and record offset. This is the offset to use in the run file when writing at 850 mag and Med current.
      xiii. Repeat for other currents and magnifications that you will be using (use a100 and a20 for the different magnifications) and record all offsets

3. **Aligning the chip.**

(a) Stay on Small current and find chip. Set z (focus) to about 6.8. Align top edge to be horizontal, find silver paint and focus.

(b) If this is the first feature and you must align parallel to the chip edge

i. Rotate the chip such that when you move ONLY in x, you stay along the top edge of the chip. This may look crooked to you. Measure the chip's dimensions. Set the upper right corner to (0,0) and move relative to this.

ii. Turn on scan rotation and set so that the chip looks parallel to the crosshairs. This is the rotation you wish to write with.

iii. Turn off scan rotation, and move to the desired location by typing in the coordinates relative to 0,0.

iv. Turn on scan rotation.

(c) If you are aligning to features already written, using an alignment file

i. After roughly aligning it, switch to external control, see step 4.

ii. Select your alignment pattern and process run file, setting the current, magnification, and offset as specified and determined.

iii. Repeat and overwrite the area as you run the alignment file. Change the rotation and x and y until the pattern is aligned. Stop the alignment file.

4. **Once you are confident you are positioned correctly**

(a) Beam: OFF

(b) NPGS mode (on external control computer)

(c) Beam: Blank

(d) Edit run file, set current, dose, offsets, etc. as desired. Save.

(e) Process run file.

(f) Set magnification and current for each layer.

(g) When finished, move away from the chip to avoid exposing the area.

(h) Set current to Low.

(i) Beam: OFF, SEM mode, Beam: ON.

5. **Find the next chip and repeat.**

6. **Once you are finished writing**

(a) Current: Low

(b) SEM: OFF

(c) Freeze: ON

(d) Go to exchange position. Open specimen exchange menu, holder 2BH, and select exchange. This will take you to x = 25, y = 35, z = 40, and rotation = 0.

(e) Lower access arm and slowly insert all the way. Pause when fully in. Remove slowly. The HLDR light will go off.

(f) Press and hold VENT until flashing.

(g) Once VENT is solid, open the chamber and remove sample holder.

(h) Remove samples, clean holder with IPA, replace holder, and close chamber.

A.2 Rapid Thermal Annealer

Instructions to use the rapid thermal annealer for GaAs heterostructures without a backgate. If you have a backgate, you'll have to figure out a reliable recipe.

1. Turn ON (green button, will light up).
2. Click JETFIRST on computer.
3. Click P.I.M.S, select Run Process.
4. Select recipe "parisa", download, click Process.
5. Load Sample. (Open chamber and place on stage.)
6. Check the two wires of the thermocouple are in the little hole.
7. Close chamber and start the process.
8. Wait for cooling to finish.
9. Remove samples, close chamber, exit program, turn off RTA.
10. If the annealing did not work, edit the recipe and increase the temperature or length of time. The password is "J".

Appendix B

Operation of Helium3 SPM

This appendix is to serve as a manual to operate the He3 SPM. Cooling the He3 SPM is in appendix C, and troubleshooting is in appendix D

B.1 Changing the tip

The tips that were used for many years are about to be used up, and no more are available. However, the general procedure for mounting a new tip will presumably remain similar. The current tips (from Park Scientific) did not conduct at low temperature and had to be coated with metal to assure conductivity.

1. **Removing the old tip**

   (a) Remove the four screws and spacer washers, then lift off the upper part of the head of the cage.

   (b) Carefully loosen and remove the screw that attaches to the tip mount. Grasp the maycor piece with tweezers to hold it, and reach underneath to unscrew.

   (c) Place the tip mount in its temporary holder.

   (d) Chip away at the stycast with a scalpel. I find it easier to leave the cantilever chip soldered so that it will not jump off when you get it free. Be patient, it takes time to do this without breaking the tip.

   (e) Carefully unsolder the tip. You will need to hold it down while unsoldering so that it does not fall when released.

   (f) Scratch off the stycast that is left on the mount.

(g) place the old tip in a "tip graveyard" and label it if it might still be useful.

2. **Preparing the new tip**

   (a) Carefully scratch off the resistor.

   (b) Scratch the back of the mount to prepare it for glue.

   (c) Measure and record the resistance. This value should change only slightly after the evaporation.

   (d) Place the tip on the rotating evaporator stage. (Handle stage with gloves.)

   (e) Be sure the tip is lowered as far as possible, and tighten the sliding cover at approximately the right location.

   (f) Align the tip under the microscope. Only a part of the cantilever should be visible, and it should be as close to the cover as possible without breaking off the cantilever.

   (g) Set up the rotating feedthrough in the evaporator. It is generally kept in the bin labelled "Sergio" at the lower right under the plasma cleaner. Tighten this connection well. Test the rotation before closing the vacuum chamber. The rotating stage needs extra long screws to be held in place, which should be found with the stage.

   (h) Evaporate 10 - 20 nm of Cr or Cr/Au

   (i) Measure the new resistance. It should change by a few ohms.

   (j) Visually inspect the evaporation with the optical microscope. You should be able to make out a faint line where the shadow mask was. You should not have metal on the main part of the cantilever chip, though if it did not short the leads together it's still probably okay.

   (k) **Prepare stycast 1066.**

      i. Find Part A and B in the refrigerator in 211 that are from the same date.

      ii. Measure about 10 g of Part A into a plastic beaker. Use two wooden applicator sticks and patience to get it out. Avoid getting it stuck on the side of the beaker.

      iii. The ratio is A:B 100:28 Calculate the amount of Part B you need and measure it into a separate plastic beaker. Use the plastic eyedroppers.

      iv. Pour part B into part A and mix until it's an even consitency.

      v. Place into a bell jar and pump out the bell jar.

      vi. Wait for the stycast to mostly stop bubbling, about 10-15 minutes.

      vii. Clean up any spillage in bell jar.

(l) Apply a minimal amount of stycast to roughened surfaces (from scratching) that are to be glued. Use wooden applicator stick.

(m) Allow 24 hours at room temperature, or 3 hours baking about 65^o C (set oven to 100^oC). Keep the rest of the stycast in the plastic beaker. If it's hard, then you're ready.

(n) Solder the cantilever leads to the chip. If you short the leads, you can scratch a gap in the bonding pad rather than resolder, if desired. The reistance will change while the tip is still warm, but check that the resistance is approximately correct.

(o) Place tip mount into bottom of AFM head and carefully screw it tight. Get the rotation as straight as possible, the tip must be pointing at one of the wedges for the coarse positioning screw.

(p) Place the spacer washers on (two per screw) and screw on the top of the AFM head.

(q) When you connect the new tip to the cantilever circuit

i. Change the balance resistor to be close in value.

ii. Turn the gain on the PAR113s all the way down.

iii. Turn up the gain while keeping track of the cantilever signal. Set the first preamp to 500 and the second to 200.

B.2 Changing the tube

The tube should be changed when the hysteresis in the scans is poor, or the drift to low temperature is repeatedly inconsistent. (Figure B.1 shows most of the parts.)

1. **Remove the old tube**

(a) Holding the cage upright, loosen the three hex screws on the bottom. Hold the tube in place as you remove these screws.

(b) Lift the cage straight up, avoiding contact with the sample mount and wires.

(c) Unscrew the three screws in the maycor base. If a screw is glued, try to pick at the glue with a scalpel and get a larger screwdriver to loosen the screw.

2. Carefully remove new tube from plastic packaging. Avoid touching the tube, wear gloves if necessary. There is lead in the tube.

3. Wrap the plastic bubble wrap around the tube, leaving the bottom accessible. (Fig. B.1B)Place in a small vise for soldering. Gently tighten so that the tube will is not completely free.

4. **Solder two black wires to the interior of the tube.** If they come unsoldered, they cannot be replaced after the glue has set, so use two wires. (Fig. B.1D)

   (a) Use a *small* amount of flux and do not drip it anywhere on the tube as it can lead to shorts.

   (b) Bend the ends of the wires into loops and use the manipulators to hold the wire in place. (Fig. B.1C)

   (c) Set the soldering iron temperature to 500^{o}C (50), and do not directly touch the tube with the iron.

   (d) Put a little solder on the tip of the iron and touch the wire. Wait until the solder wets the surface of the tube.

5. Prepare stycast 1066, as described in (2k)

6. Scratch the maycor and metal pieces for the tube. (Fig. B.1E)

7. Thread the two black wires through the bottom piece of maycor. Apply minimal stycast. (Fig. B.1F)

8. Bend the wires into the trough designed for them, and 60 degrees to the side as the AFM cage was machined incorrectly.

9. Screw in the three screws that hold the base of the tube. Align it so that the black wire is at the larger gap in the base. Do not get stycast under the screws. (Fig. B.1G)

10. Carefully place the cage around the tube and tighten the three hex screws on the bottom. (Fig. B.1H)

11. Apply stycast to the small maycor piece and insert into top of tube.

12. Apply stycast to metal piece and insert into small maycor piece at top of tube. (Or glue this part first, especially if the fit is tight.) Avoid pressing too hard on the tube. (Fig. B.1I,J)

13. Use the extra long screws and the alignment piece to align the sample stage correctly. The two screw holes must form a line perpendicular to one of the coarse approach screws. Tighten the long screws and twist so the alignment is correct. (Fig. B.1K,L)

14. Allow the stycast to dry. (Fig. B.2A)

15. Remove tube from cage, you can keep it on the base if you are careful.

16. Solder the exterior wires to the four quadrants. Again, use a small amount of flux, 500^{o}C, and do not touch the tube with the iron. (Fig. B.2B,C)

17. Solder the wires to a ten pin microtech connector. (We presently have to insert the metal pieces into the plastic, as shown in (Fig. B.2D).) The black wires to the interior must be on one end, and the quadrants must be attached in sequence, though clockwise or counterclockwise does not matter. Be careful not to melt the connector, and **USE SHRINKWRAP** and wrap the wires and connector with tape to avoid accidentally shorting high voltage to ground, or to yourself. Check that the connections are not shorted. (Fig. B.2E)

18. Carefully bend the wires so that they fit into the cage without touching the tube, as best you can.

19. Reassemble the cage. Be careful not to bump the stage while you lower the top down. Tighten the three screws at the bottom. (Fig. B.2F)

B.3 Mounting the sample and Assembling the AFM

1. Use GE varnish, PMMA, or silver paint to affix the sample to the sample holder. Position the sample such that the tip can reach the device when moved with the xy coarse position screws. GE varnish requires 3 hours bake to cure.

2. Press down on sample to assure it is flat. Use wooden applicator sticks to touch the edges of the sample.

3. Wirebond. Keep yourself and the sample grounded. There are connectors with all the leads soldered together to a large resistor that you should use to ground the sample.

4. Place screws through the two holes on the sample holder and through the ground plane. The wire from the ground plane should be opposite the wires to the device. The device should be near a coarse approach screw, such that the tip will be over it.

5. Extend coarse z approach screw so that tip will not snap off when you place the head.

6. Place the AFM head carefully on the three screws.

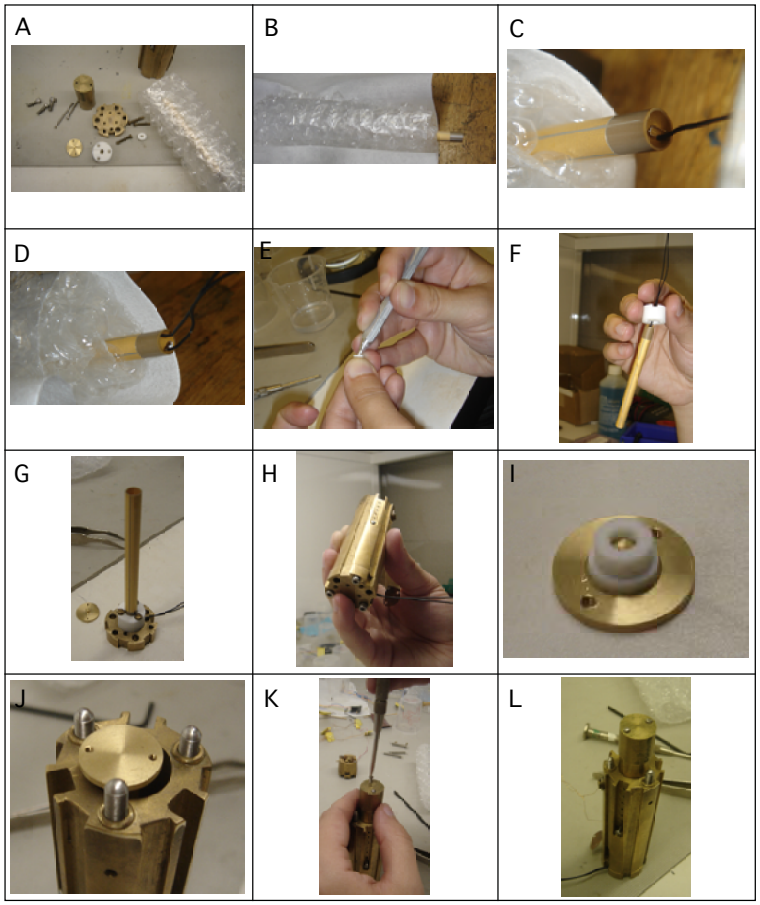

Figure B.1: Procedure for assembling a new new piezotube.

7. Hang the three springs from the eyehooks. There is a larger and smaller hook on most of the springs, use the smaller.

8. Hook all three springs *while holding the head in place* to the lower screws. If one spring is stretched, the head will spring off if not held. I use my fingers to attach the springs.

9. Align the tip. Use the optical microscope with a large working distance. Look through the larger opening in the head. Move the xy coarse positioning screws and the z coarse approach screw. Always watch while turning the z screw.

10. Check that the silicon cantilever chip is parallel to the device chip. Otherwise the edge will come into contact before the tip. (If this does happen, blow off the silicon dust before proceeding to realign.)

11. Position the tip a half turn (8 turns with gear) off the surface.

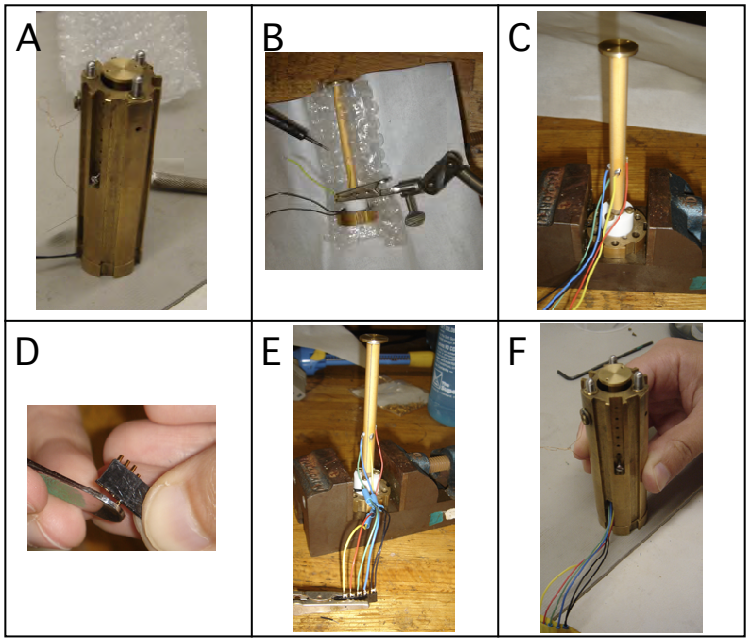

Figure B.2: Procedure for assembling a new piezotube.

12. Flip AFM upside down and tighten screws to dunker stick. Keep the sample grounded. The hex key for the z coarse approach can be difficult to insert. It will be obvious when it goes in as long as the coarse approach rod is at the correct height.

13. Connect the high voltage microtech connector. The black wire goes to the dot on the connector that attaches to the mini BNCs.

14. Connect the cantilever leads to the bridge circuit. Orientation does not matter.

15. Connect the sample leads. Write down the orientation. Check that the 24 pin switcher box is grounded. Remove the other ground connection.

B.4 Topographic scans at room temperature

1. **Turning things on**

   (a) Reference voltage (one switch)

   (b) XYZ box (two switches, ±18V and ±9V)

   (c) Voltage preamps, the PAR113s. These are usually left on and the inputs grounded. Flip the two inputs on the left preamp to DC and then the two

inputs on the right one to DC. Flip the inputs simultaneously to avoid overloading the PAR113.

(d) Voltage controlled oscillator. Turn to 1kHz.

(e) Adjust reference voltage so that the cantilever signal is near zero on the oscilloscope (which must be turned on if it is not).

(f) DAC, if not on (check the external power supplies are on)

(g) High voltage power supplies. Two of them.

(h) Check the feedback. With the cantilever signal positive, turn up (clockwise) the feedback knob on the feedback box. The multimeter measuring Z (which needs to be turned on and switched to read the input from the back if it is not) should go to $\approx$ 225V. Change the reference voltage so the cantilever signal is negative and watch the Z voltage go to $\approx$ -225V.

(i) Turn feedback down. Make sure X, Y, Z and the plane are at zero as well (check knobs are all the way counterclockwise).

(j) Connect the blue labelled connector from the high voltage box to the blue labelled connector on the dunker stick. (No high voltages should be on, you can damage the tube by suddenly applying high voltages.)

2. **Approaching the surface**

(a) Turn up the feedback (knob on XYZ/feedback box clockwise)

(b) Check that the cantilever signal is positive, about 200mV, and not drifting significantly.

(c) Turn the coarse approach screw at the top of the dunker stick counterclockwise (when looking from above), cautiously.

(d) Stop turning **IMMEDIATELY** when the pitch suddenly changes. This should be the tip coming into contact and the feedback engaging, but if something is wrong with the feedback you can avoid breaking the tip by paying close attention.

(e) Slowly turn the screw so that the Z voltage reads about 100V.

3. **Taking topographic scans**

(a) Check that you are not pushing too hard into the surface (due to cantilever drift or PAR113 drift generally). Turn down the feedback (*only if it is positive!*) and check that the cantilever signal is about 200mV.

(b) Check that the blue cursor is at (0,0) and turn up X and Y (turn knob clockwise, from above).

(c) Set the scan area with the red and green cursors. Easy: Set the box to -2 to 2 V in x and y and hit "Snap Cursors". This 4V x 4V is a conservative area, 6V x 6V will show two sets of numbers.

(d) Set the scan speed. 1 V/s is conservative, 2 V/s if you know your area is smooth. Flyback can be 2 V/s or faster if surface is smooth.

(e) Set the number of points. 40 points for a 4 x 4 V scan is reasonable to see things. Check the square pixel box.

(f) Check the appropriate box above the graphs to take data, and verify you are reading the correct input value.

(g) Double check everything. Area, speed, points, no voltages on the gates, no voltage on the tip, etc.

(h) Click "StartScan" The pitch should immediately begin to change.

(i) Click "Flatten" after the first line of the scan is complete (the program will crash if done earlier). This fits a plane to the image and autoscales it.

(j) Set scan rotation as desired. (If you are setting the drift according to a previous cooldown, use that scan rotation. But find the correct one, as you'll want to switch to that once you've cooled down so that things look straight.)

(k) **Set the analog plane with the plane box.** This is not necessary, but might save some wear and tear on the tip. It is necessary before electrically finding the device.

i. Turn up the plane with the knob on the XYZ/feedback box. The pitch may change a little as you do this, though the feedback keeps the total output voltage the same. Turn slowly.

ii. Take a small scan (0.2V x 0.2V) in a flat area. Take a coarse scan, 10 - 15 points.

iii. Hit flatten once finished. Note the x and y coefficients. Turn x or y plane knobs and repeat the scan. You could calculate the values, but the scan rotation "x" and "y" are not lined up with the grid. It's easier to just methodically turn the knobs.

iv. Set the plane so that the coefficients when you flatten are < 0.1 or so. Repeat the scan to see how reproducible they are until satisfied.

B.5 Preparation for cooling

1. **Move to the desired location**

(a) If you do not know the drift, go to within about 30 microns of the device. If you do know the drift, go to within ten microns of the desired location.

(b) Come off the surface before moving the tip with the screws, a few turns until you are very comfortable with it.

(c) Always **TURN DOWN THE HIGH VOLTAGE** before touching the AFM. Something may have shorted or you may bump a wire that isn't insulated well.

(d) Stop *immediately* if you hear a pitch change, as you've just contacted the surface. Turn up the feedback and adjust as needed.

2. **Tie up the wires with floss.** Be cautious. Avoid pulling on the tube. Take scans as you do this if you think you may have shifted things.

3. Take another scan and position the tip until you are satisfied.

4. **TURN OFF THE SURFACE** about 30 turns when you are ready to cool. The tube usually drifts about 20 turns towards to tip.

B.6 Locating the device at Helium temperature

1. Turn on cantilever circuit, feedback, and high voltage.

2. Open valve to release pressure. This is not always necessary, but pressure increase can cause drifting of the cantilever signal.

3. Contact surface.

4. Set scan area and take a scan. Watch and stop scan if you are on top of the device.

5. Raise dewar off floor as needed. Carefully crank winch. Be sure that the steel cable is wrapped well and will not slip. Adjust position of dewar if needed before fully raising so that it will not swing much upon being lifted.

6. Find a number or gate and identify your position.

7. Find two sets of numbers and calculate the microns/volt.

8. Test that the device works.

9. **Add extra voltage if needed**

(a) Remove high voltage plug from dunker stick and turn off high voltage.

(b) Calculate how much voltage you need and in what direction. The tube should not have more than 600V across it. Only add about ±150V max. Presently, we have only one extra set of power supplies per SPM, and so can only add extra voltage in one direction. You can borrow the extra set from the other SPM if it is not in use.

(c) Connect the additional power supplies, to add or subtract voltage as needed. The voltage on the extra supplies should be set at zero to begin.

(d) Turn on the four power supplies. Measure the voltages that will go to the tube to make sure everything is correct. Turn down the extra supplies to output zero, and turn down X, Y, and Z before connecting to the tube.

(e) Plug in the connector to the dunker stick.

(f) Turn up the feedback and come into contact with the surface.

(g) While in contact, *slowly* turn up the extra voltage. You want to keep the tube balanced, so add about 25V to the positive and negative supplies at a time. You will hear the tip go over bumps and such. If you come out of contact, okay. If you press in too hard, stop and move away from the surface a turn or two.

(h) Note if you went towards or away from the surface. If towards, then you can safely turn off the extra voltage overnight. If you moved away from the surface and had to mechanically approach closer, you will have to leave the power supplies on. Once everything is set, it is inadvisable to change the coarse approach rod.

(i) Find your location again topographically, still avoid scanning over the device. You may want to scan multiple times as you add the full voltage to keep track of where you are.

10. **Electrical scan to find QPC/device**

(a) Turn off the feedback (make sure it is positive!)

(b) Check that TipH is zero, and turn up TipH on XYZ/feedback box.

(c) Find the surface, use "setheight 0 0.2" You will see the z voltage ramp up to where the feedback was, and hear the tip come into contact and stop when it is pushing 200 mv (0.2V) into the surface.

(d) Subtract 3 V from the TipH value displayed, and change the TipH so that the tip is 3 V above the surface. (If TipH ramped to 5 V, make it 2 V.)

(e) Before energizing any gates or the tip, drag the tip (the blue cursor) around the area you wish to scan, to make sure it will not hit anything, or do a deflection scan.

(f) Energize the gates and the tip. For a QPC, keep it relatively open (4th plateau) and -1V on the tip should be fine.

(g) Select graphs to read in the conductance and to read in the deflection (to keep track of whether you hit anything).

(h) StartScan.

(i) Autoscale. Do not flatten. Set the coefficients to zero if they are not. You should see a circle of decreased conductance where the QPC is. Increase the voltage on the tip or cautiously get closer to the surface if you do not.

B.7 Scanned gate measurements

1. Setting "Zguide"

   (a) Turn on the plane from the XYZ box and set it if not yet done.

   (b) Select an area near the QPC that is not over the gates nor where you are likely to want to scan. Put the red and green cursors at this area. If you find that there's dirt in this area as you proceed, move to a better location. An area of about 1V x 1V is fine for this.

   (c) Run the command "flatteninside" which will call "autoflatten." You can also set the red cursor to the center of the QPC (set.var $qpcx $$redx; set.var $qpcy $$redy) and then use "redtocenter" and define the box relative to that. (movecursors r $qpcx| + 1.0| etc.)

   (d) Set Vbuffer = -3V and check the box, "Zguide." The output to Z should not change much, but now Zguide is controlling TipH.

   (e) Lower Vbuffer (less negative) to approach the surface. Go back and relocate the QPC as desired. Set Vbuffer lower and call "flatteninside" again. Look at the coefficients of the plane (written in the console window) and check that you're getting reproducible values. Continue to lower Vbuffer and find the plane until you are satisfied.

2. Select your scan area, and before energizing the gates or the tip, take a deflection scan of the area with Vbuffer relatively high. (Start at $\approx$ -1V.) Reduce Vbuffer until you begin to hit something or you reach -0.12 V. If you're within -0.2V you're probably fine. You may want to find Zguide again depending on how well the area you selected represented this area.

3. There is some drift in Z. You can call "adjustheight", which will use the same Zguide plane and add an offset. Or you can slowly reduce Vbuffer to 0 and check that the tip does indeed contact the surface at that point, and manually adjust Zoffset if not.

4. Set the QPC to a plateau. The best thing to do is charge the tip, place it in front of the QPC, and set the QPC to a plateau in that condition. This will reduce the effect of the coupling between the tip and the gates.

5. Set the tip voltage to deplete (-2.75V is probably more than needed), and take a scan measuring the conductance. You should see flow!

6. **Time constants**: for 10kHz lockin frequency, you might choose to average 3 ms. The maximum speed at which you can scan is lockin average (3 ms) * # of points per line = seconds per line ν. The volts per line divided by ν = max velocity in volts/second. If you use constantstep [ ] then when you change the size of the scan, the speed can remain the same and the number of points will automatically change.

B.8 Using gate feedback

Macro "dofeedbackscan" and "dorealscan" steps you through the process, though they have been modified for a variety of purposes. This covers the basics. For best results, perform two feedback scans, one just above the plateau and one just below. Then average them together.

1. Turn on gatefeedback box.

2. Check that it is connected to the summer along with the gate voltage and Vguide, and the sum is going to the gate.

3. "goto.feedback.control" 4.0 will activate the feedback box and set the conductance to $4e^2/h$. This happens by setting the digital.0 output to 1, which turns on the relay that allows the feedback voltage to be applied to the gate. This signal comes from the ADC box, through the small blue wire. You may want to limit the output of the feedback box when you turn it on. Do this by applying a voltage to the limit input and sweeping it to a value that allows the feedback to do its job. Set gatev to zero and turn off vguide so the total voltage going to the gate is provided by the feedback.

4. Set the tip voltage and raise the tip such that you are no longer depleting the electrons with that tip voltage.

5. Take a scan, reading in the feedback output. (Also read the conductance to see how good a job the feedback is doing. The plot should be one value, but will not be perfect.) Adjust the gain and averaging so that the feedback can follow the changes in conductance and does not begin to oscillate.

6. Multiply the feedback voltages by the appropriate constant to convert it to the correct output to the gates. scan.timesconstant c $feedbackconv

7. "goto.computer.control" sets digital.0 to 0, disconnecting the feedback and setting gatev with the DAC.

8. outputcalibration 2 $|mid.z|c$ [ ] sets the output of vguide to the average value and the step size.

9. Turn on Vguide.

10. Take a scan as usual.

Appendix C

Cooling Procedures for the He3 SPM

This appendix is to serve as a manual to cool the He3 SPM. Operating the He3 SPM is in appendix B, and troubleshooting is in appendix D

C.1 Cooling without the He3 insert

If you only need to reach 1.7K for the experiment of interest, you can cool with the "dummy" insert for the He3 system. It is the cylindrical tube with an open bottom, such that the SPM sits in the He4 liquid inside the blue dewar.

1. **Cooling the dewar from room temperature.**
   (a) Turn 30 turns off the surface.
   (b) Place dunker stick into insert.
   (c) Place insert into blue dewar. Place the sliding clamp at the bottom so that you can get the insert straight as you lower it.
   (d) Place nitrogen transfer stick into the dewar and seal it off (tie it or attach to the Lab50 nitrogen supply).
   (e) Pump out the dewar with the roughing pump.
   (f) Flush with nitrogen gas.
   (g) Repeat 2 or 3 times. Overpressurize the dewar slightly the last time so that no air is sucked in before you begin to fill.

(h) Begin filling slowly. Remove the overpressure valve and speed up the nitrogen flow as things cool down and the transfer tube freezes.

(i) Watch the resistance of the diagnostic resistors. They start at 384, 446, and 493 Ω for AB, CD, and EF respectively. EF will read about 592 Ω when it is in liquid, and CD will read $> 515\Omega$. At least cover the magnet with liquid, and fill considerably more if you are leaving it overnight.

(j) Close the dewar (make sure overpressure valve is on and open). Tie off the transfer line. Wait at least two hours, or overnight.

(k) Remove the nitrogen. Pressurize the dewar with helium gas and collect the liquid through the transfer tube. Make sure the tube reaches all the way to the bottom. When no more liquid comes out, wiggle it (gently) to be sure.

(l) Once all the liquid is gone, pump out the dewar. The needle should smoothly go to zero. Fill with Helium again and repeat to be sure all the nitrogen is out. You do not want to freeze any nitrogen.

(m) Remove the nitrogen transfer line and remove the overpressure valve.

(n) Transfer liquid helium.

(o) The resistor EF will read about 6.5kΩ when helium has condensed. Turn on the helium level meter and fill to 100%.

2. **Warming up**

(a) Turn safely away from the surface. 6 turns is sufficient.

(b) If you can wait, allow the entire dewar to warm up. You can add Helium gas to speed up the process.

(c) Pull the insert up about half way and wait for about twenty minutes, to avoid warming too quickly. Pull it the rest of the way out and wait for two hours. Be sure the insert is as high as possible.

(d) Carefully remove insert from dewar. Remove dunker stick from insert. Scan to check the position if desired.

3. **Cooling the SPM with the blue dewar already cold.** While it is preferable to cool the dewar and the SPM at the same time, slowly from room temperature, it is faster to warm up and cool down just the SPM, at the risk of having dirt from the air get on the sample or tip.

(a) Place dunker stick in insert.

(b) Place insert at the top of the dewar, clamped at the bottom.

(c) Open the top clamp that hold the dunker stick to the insert. Be cautious as the friction may not hold the insert up. Keep the overpressure valve closed. You want all the helium gas to rush out through the insert and push the air away.

(d) Slowly begin to lower the dunker stick and insert.

(e) Close the top clamp once the vapor coming out is chilled and open another valve to release the pressure. Continue to lower the insert. You can monitor the temperature with the diode thermometer and keep it at nitrogen temperature if you desire.

(f) When you reach the bottom, you're cold.

4. **Cooling to 1.7K**

(a) Run the pump line through a concrete bucket and to the large valve of the dewar. Use a plastic o-ring and KF clamp to keep the dewar and sample electrically isolated from the pump.

(b) Check the lines for leaks by pumping out the lines and monitoring the pressure. It should remain constant.

(c) Close the gate valve. Open the valve to the dewar to repressurize the lines.

(d) Slowly open the gate valve. When you hear the pump making a distinct noise that it's working, wait for the pressure to go down some. Then open the valve more.

(e) Continue pumping until you are down to the base temperature. The temperature is determined by the size of the pump. It can take a half hour to two hours depending on the pump. If you frost up the lines and the top of the dewar, you're probably going too fast. (Some frost is okay.)

(f) When you are finished or run out of helium, close valves to dewar and turn off pump. Open the overpressure valve if you closed it.

C.2 Cooling to He3

1. Place the dunker stick in the He3 insert.

2. Leak check He3 insert and lines. $10^{-}8$ torr l/s is good, $10^{-}7$ is probably okay.

3. Pump out the He3 insert at room temp for at least an hour with the turbo pump, to get down to low $10^{-}5$ torr. Place into dewar. Cool dewar if not cold.

4. Attach both the fat (out) and skinny (in) lines to the insert. Use plastic KF clamps and o-rings to keep the dewar and sample electrically isolated from the pumps. Make sure valves 1,2,3,11,12 and the valves to the insert are closed.

5. With 4,5,7,9,10 open, pump 2 hours or overnight with the turbo pump at valve 10 to reach low $10^{-}5$ or high $10^{-}6$ torr. Open valve 6 to 10 torr gauge only after the pressure is <10 torr.

6. Close valve 10 and monitor the pressure increase on the 10 torr gauge. It should be less than 0.3 mtorr/minute.

7. Reopen 10 and slowly open the big valve to the insert. There should be at most a small rise in pressure. Allow to pump a few minutes, and close valves to insert.

8. Close 10 and cap off. Remove turbo pump to free up space.

9. Close valve to 10 torr gauge. Check that 10, 2, and needle are closed. Open valves to dumps (1) and 3 to introduce He3 exchange gas. Open valves to insert. Monitor using 1000 torr gauge. Open needle valve until 20 torr (200 mV) is introduced into the insert. Close needle and valve 3.

10. Refill the He4 in the dewar if needed. Pump on the He4 bath to cool to 1.7K.

11. Condense He3 when pressure of He4 bath is <9 torr. Turn on the pump on the He3 cart and open back valve 11. Valve 4 should be open at this point. Begin to bleed He3 by opening valve 3 and cracking needle valve. Make sure valve 11 is open. Should take 20 - 30 minutes for the pressure in the dumps and the insert to equilibriate. Open 2 to condense the rest of the He3, wait about 30 minutes and reach around 30 torr. Waiting longer should condense more helium.

12. Pump on He3. Close 4,2,3 and needle valves. Valve 11 should be open. Begin pumping with the cart's sealed rotary pump. Crack the front valve 12 slowly. Take about 45 - 60 minutes to reach less than 1 torr. Base temperature is 85 - 120 mtorr.

13. Once the He3 is all pumped out (the gauge reads zero), close the valves working from the insert to the He3 pump. Close 11 before turning off the pump. Turn off the pump last.

14. If you wish to speed up pumping all the He3 out, try to use the diode to heat things up, or add a resistor to the dunker stick to generate enough heat to vaporize the helium (close the 10 torr valve if you do this).

15. The dump pressure is 850 mbar as of 04/05/06

Appendix D

Troubleshooting

This appendix is to aid newer users by describing some of the more frequent problems and how to address them.

D.1 General Remarks

1. Always listen. Going up in pitch means the tip is pushing into the surface, being deflected up. Down is snapping into the surface, deflected down. Always know why the pitch is changing. If you don't and it changed suddenly, stop whatever you're doing.

2. Be cautious with the tip. Never move things blindly (always watch in the microscope or have the feedback on). Allow extra room when assembling the SPM. Keep in mind the effect on the tip of any action that you do. Keeping the tip 8 turns off the surface (top of dunker stick) is generally safe. Once you're positioned and taking electrical scans, avoid turning the coarse approach rod and just turn down the voltage.

3. Let things go wrong twice at low temperature before you try to fix it. If it doesn't come into contact or doesn't scan, often warming up and cooling down will fix it. If you don't know how to fix something with the scanning at low temperature, changing the tip, tube, and sample generally works. The sample makes a different only if it's dirty. (You tend to get more resonances in the scanning if it's dirty.)

4. If something funny happens with output voltages from the DAC (it freezes or rails), use the "reset all" option under the Hardware menu. Be sure that you

have turned down the tube voltages and gate voltages before doing this to avoid crashing the tip or shocking the device. If you turn off the power supplies to the DAC you will need to reset the hardware or open the program after turning them on in order to initialize the outputs to zero.

5. //AutoRun in the startscript runs automatically whenever you open the program. Remember to change the DAC conversion, the scan rotation, the path, etc. and save the new script so that you don't have to redo it if the computer crashes. To set the conversions requires two commands: set.var $gateconv 0.33; voltconv $gateconv;

6. **Interpreting the cantilever signal**

   (a) Reasons that the cantilever will change pitch

      i. **Change in temperature** Turn off the HVAC in the room if needed
      ii. **Change in deflection**
      iii. **Change in illumination** Shine a flashlight on the tip to check things are responding
      iv. **Drift in the electronics** If you overload the voltage pre-amps they take some time to settle.
      v. **Pressure change** May correspond to a deflection change. I often scan at 4 K with the valve open.
      vi. **Change in resistance of the cantilever circuit** (e.g. bad connection)

   (b) **Normal scanning** You will hear and see blips and dips on the cantilever signal for a normal scan. The value should not go off the oscilloscope screen (with the vertical spacing 200 mV). If they do, you are going over something tall and may want to move locations if you are concerned. If there is a slant to the sample, you will hear the pitch slightly higher in one direction as it's generally pushed into the slope upwards, and lower in the other. Flattening with the plane box will remove this.

   (c) **Beware of drifting into the surface while you're out of the room for a while.** If you leave it in contact or taking a scan, the cantilever may have drifted towards the surface and be pushing harder than before. Generally, you turn down the feedback, reset the reference voltage, and turn the feedback back up. However, if you drift so much that zero volts in z (feedback off) keeps the tip in contact, you will set the reference voltage to "zero" this position and still be pushing into the surface. You may still be able to scan. But things should seem not quite right - it's hard to describe. If the pitch changes continuously as you turned down the feedback initially, then you're still in contact. You won't hear the same

"coming out of contact" noise that's normal. If you turn the Z coarse position, you'll hear a continuous change in pitch.

D.2 No or noisy cantilever signal

1. Check that PAR113's are on, reference voltage box is on and set correctly, cantilever is plugged in to bridge circuit, gray cable is plugged in to dunker stick.

2. Check the batteries on the reference voltage. Both should be $> 12V$.

3. Ten-pin switcher box should have A - D floating. You may not realize if they are grounded, if the reference voltage is near zero the signal may look normal, but you'll break the tip when you try to come into contact.

4. Broken cantilever. Or open solder connection on bridge circuit. You may pick up a sawtooth signal when this happens. Check the resistances across the bridge circuit (remember that you're measuring resistances in parallel).

5. Oscillations on cantilever signal, around 300 Hz. Most likely your sample is dirty in that area or you have dirt on the tip. Move locations and see if this helps (just move the blue cursor or your scan area). Sometimes you can knock dirt off the tip by scanning. Try slowing down the feedback (lower the fine gain or raise the coarse gain. Or increase the capacitor but this is rarely the right thing to do.) It's also possible that the tube is bad. If your drift has been inconsistent, change the tube.

6. Low frequency oscillations, around 6 Hz. These are most likely building vibrations. Raise the dewar off the ground. It may be helium boil-off, especially if you just filled, in which case release the pressure and check again in a little bit.

7. 60Hz noise. This is most likely electromagnetic pick up. The BNCs from the 10 pin box to the PAR113 should be twisted. Try moving around these cables, or twisting and untwisting a bit, until you hit a "sweet spot" where the noise is low.

8. At low temperature, if you've checked everything then warm up, check that the signal is there, and cool down and see if it fixes itself. Keep in mind that if there's a bad solder joint or something like that, it may go bad at low temperature and be okay at room T. If you really can't fix it, change the tip and think about resoldering things.

D.3 Tip does not come into contact

1. Know approximately how far you are from the surface when you align the tip under the optical microscope. If you turn significanly past this amount, back up and check on things. Turning too far could result in a broken tip if something isn't right.

2. Check that the coarse approach screw is turning. If it is not, check both that the gear is properly engaged and the hex key at the bottom is properly inserted.

3. Back away from the surface and remove the AFM. Check if the corner of the cantilever chip touched the sample before the tip did. Look for Si dust or other marks on one side that indicate it has touched, or lower the tip closer to the surface to better see the angle. If you did leave a bunch of Si dust near the device, take apart the the AFM and blow clean nitrogen on the sample to remove as much as possible.

4. Disassemble and reassemble. Most likely this will fix it, whatever it was. Just be careful about everything and align the cantilever carefully.

5. At low T, your options are limited. Check the resistance of the cantilever to be sure it didn't break, check that the ref voltage is close to what it was last time you cooled down to again verify that nothing funny is going on. Then warm up, verify that you can come into contact, and cool down again. Sometimes junk got on the tip and it'll come off when you cycle it.

D.4 Does not scan properly

1. Do you hear changes in pitch? **NO**

   (a) Are X and Y turned up?

   (b) Are the voltages making it to the gray connector? Check at the blue box that takes the voltages in from the HighV amplifiers in and sends them out into the cable.

2. Do you hear changes in pitch? **YES**

   (a) Are you reading in the feedback signal?

   (b) Is the graph at zero, with noise? The ADC isn't reading in the voltage correctly.

(c) If at low temperature and the image just looks wrong and it sounds like the tip can't quite stay on the surface, there is probably junk on the tip. Scan a little bit and see if it falls off. Otherwise warm up and cool back down, this usually fixes the problem.

D.5 Piezo tube problems

1. Cool down drift is inconsistent. Change the tube if it's very inconsistent. Make sure you're not accidentally banging the AFM when you load it. Check the drift going from low T to room T and see if it goes back to the original position (or close to it). Check that you're not pulling on the wires with the floss.

2. Tube drifts in x, y, or z. The tube is bad. Don't jump to this conclusion if it is drift in Z, it could be the temperature or pressure changing and legitimate feedback compensation. Some drift is normal.

3. Hysteresis in x or y. The tube is bad. A little bit is okay, determining when it's too much is up to you.

4. You hit the breakdown voltage of the tube. Don't do this! Do not scan in helium gas, you are likely to hit breakdown at some point, even if your calculations tell you that you will not.

Appendix E

Diagrams and Schematics

This appendix contains detailed circuit diagrams of the electronics that are not included in Chapter 2

E.1 Voltage Reference Box

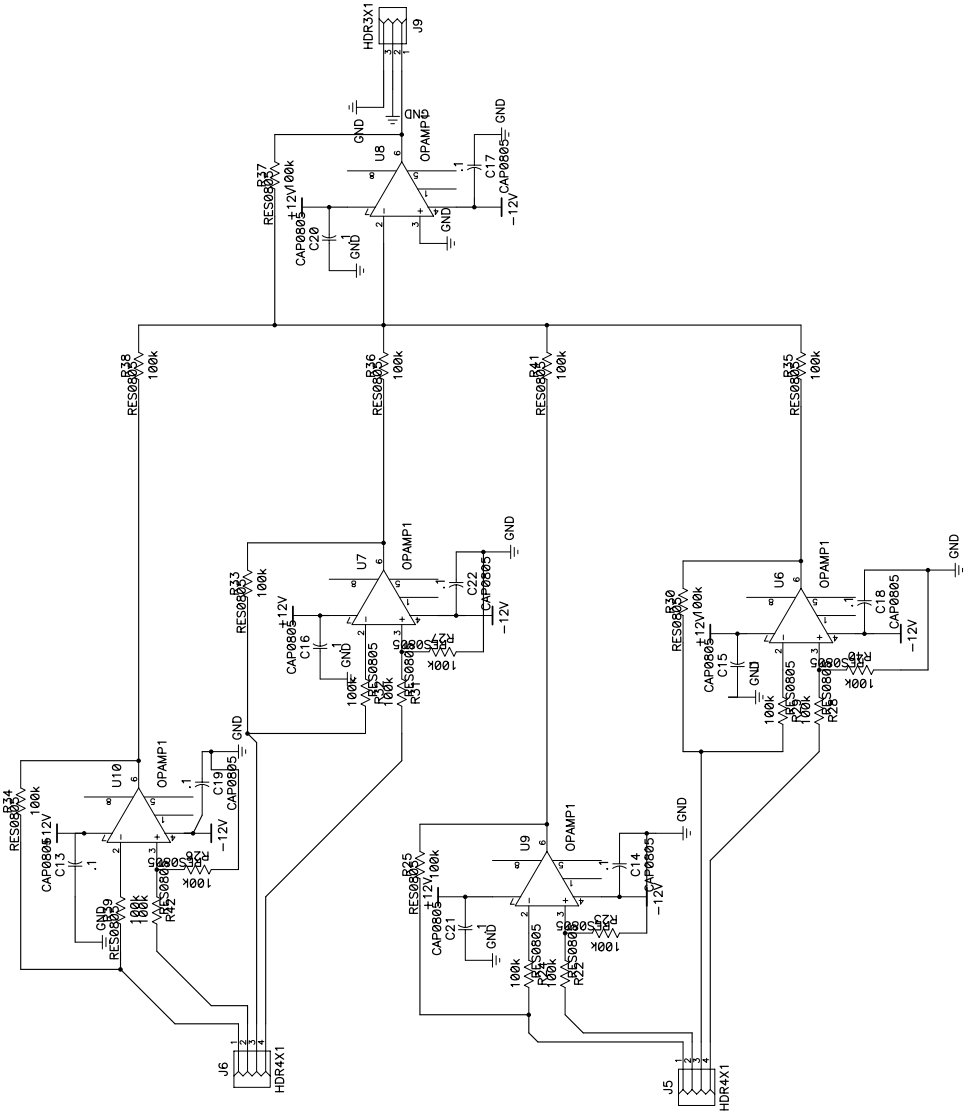

Figure E.1: This is the summer portion of the voltage reference box. Three of these circuits are on the board.

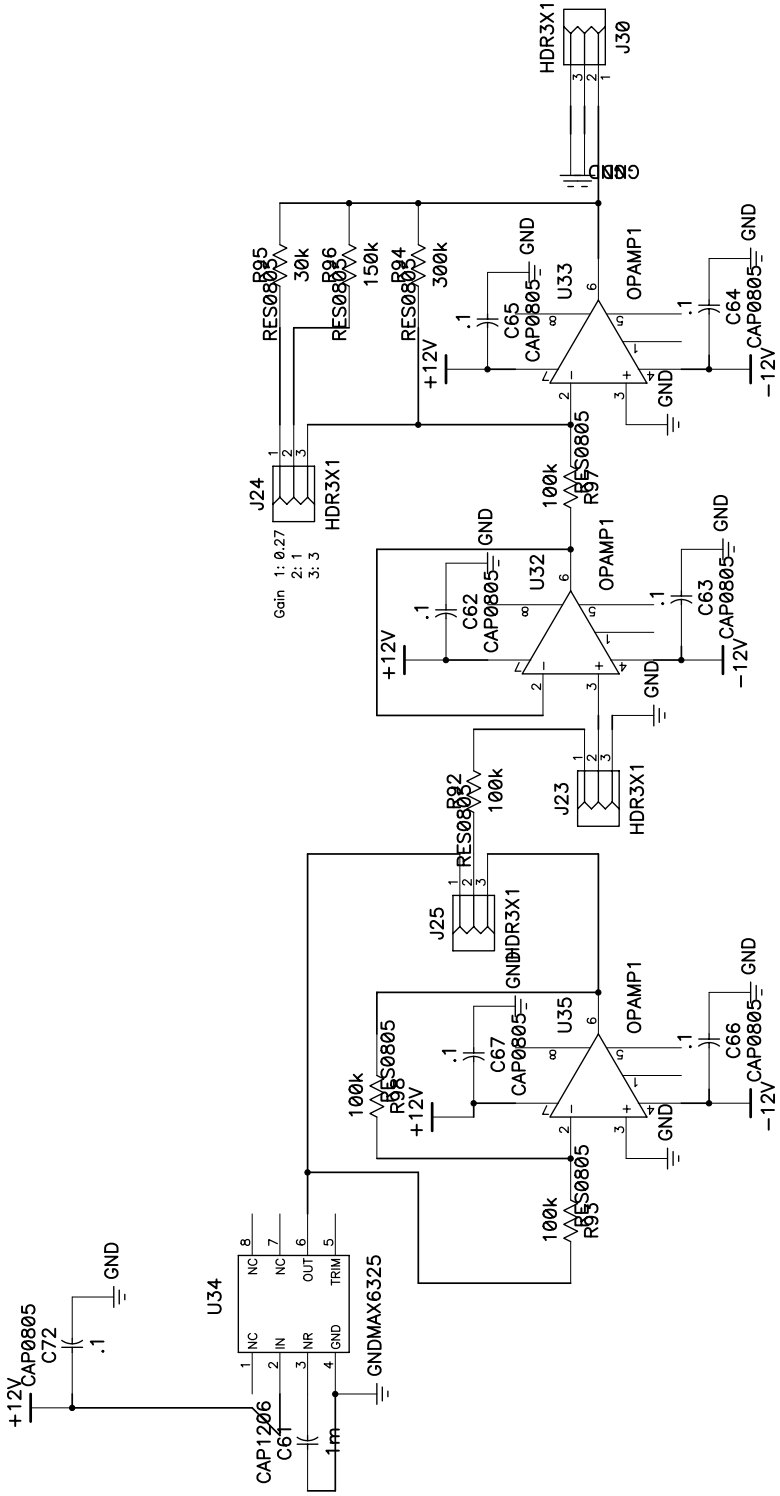

Figure E.2: This is the voltage reference portion of the voltage reference box. Five of these circuits are on the board.

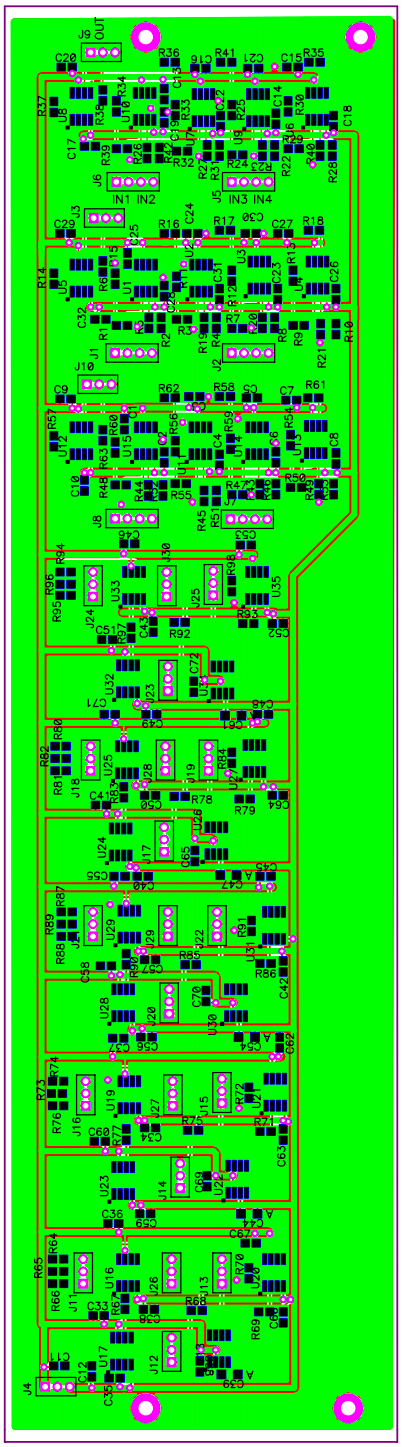

Figure E.3: The PC Board layout for the voltage reference box.

E.2 Digital Analog Converter

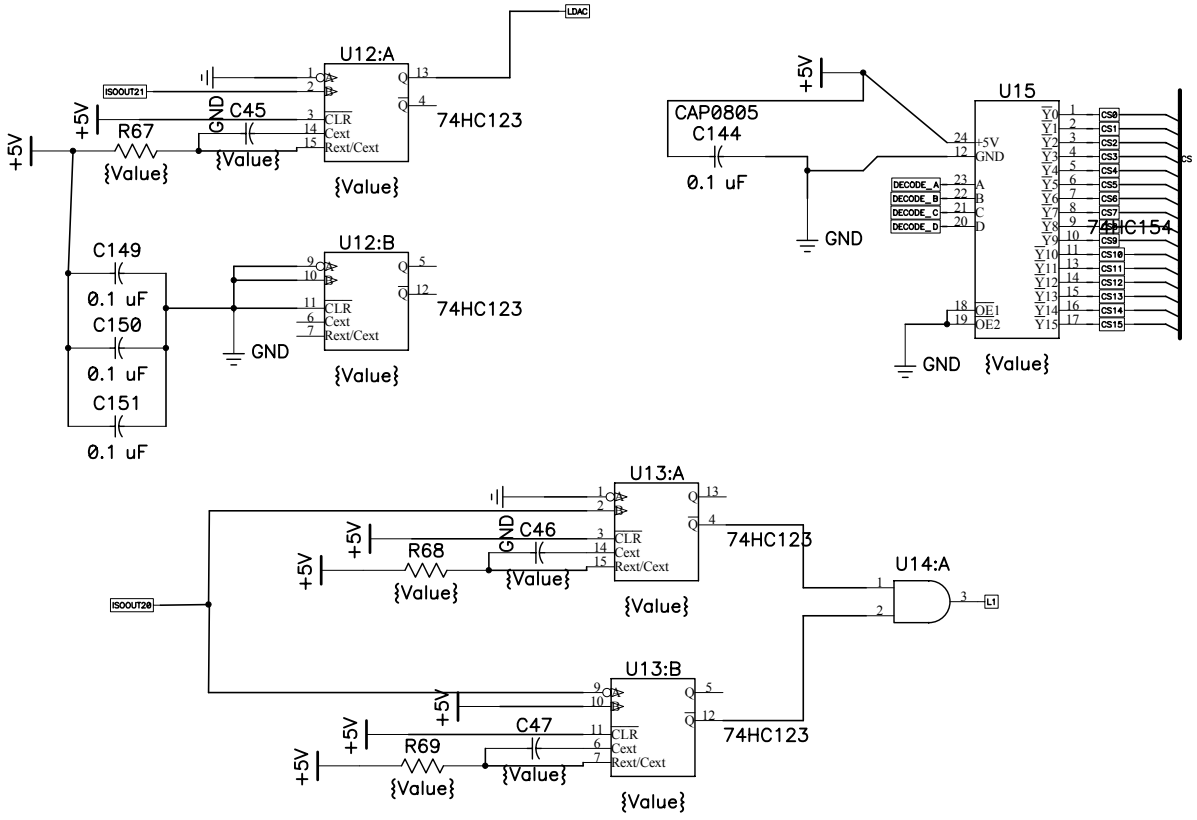

Figure E.4: This section contains the timing logic and the decoder of the DAC.

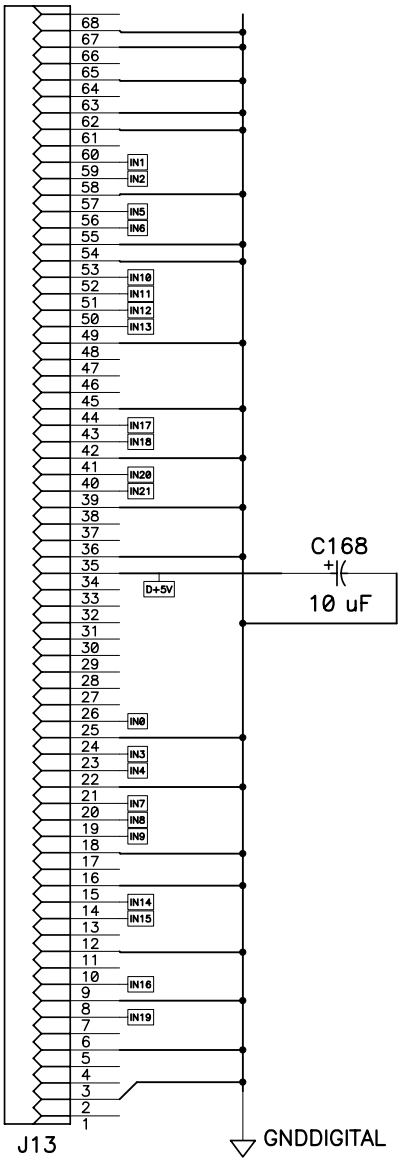

Figure E.5: This is the schematic of the connector from the computer to the DAC board.

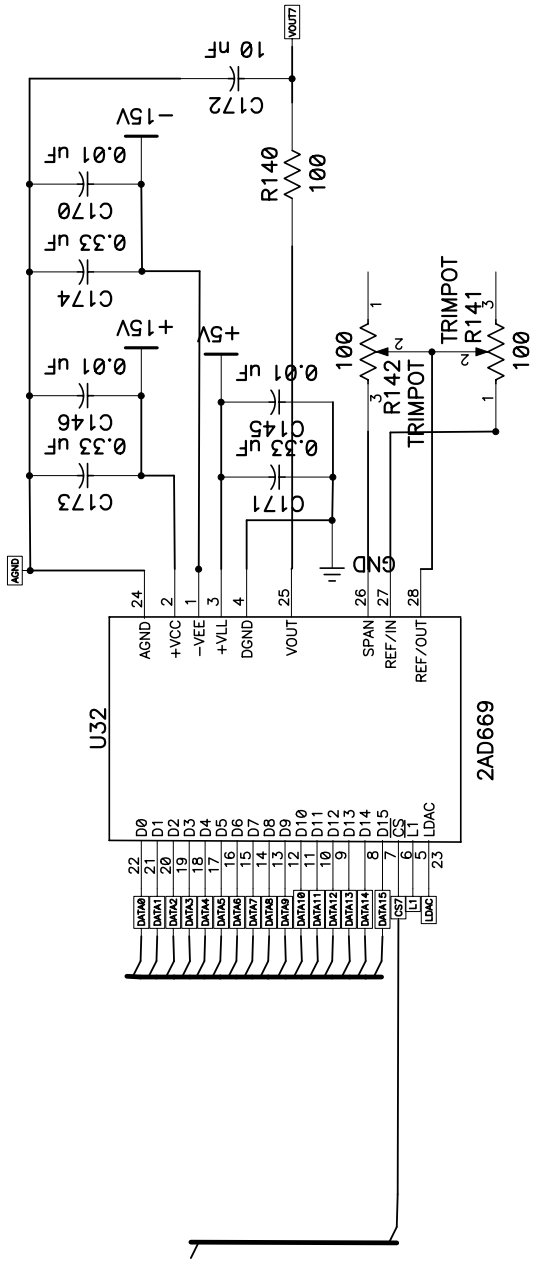

Figure E.6: This shows the pinout and connections to the DAC chip.

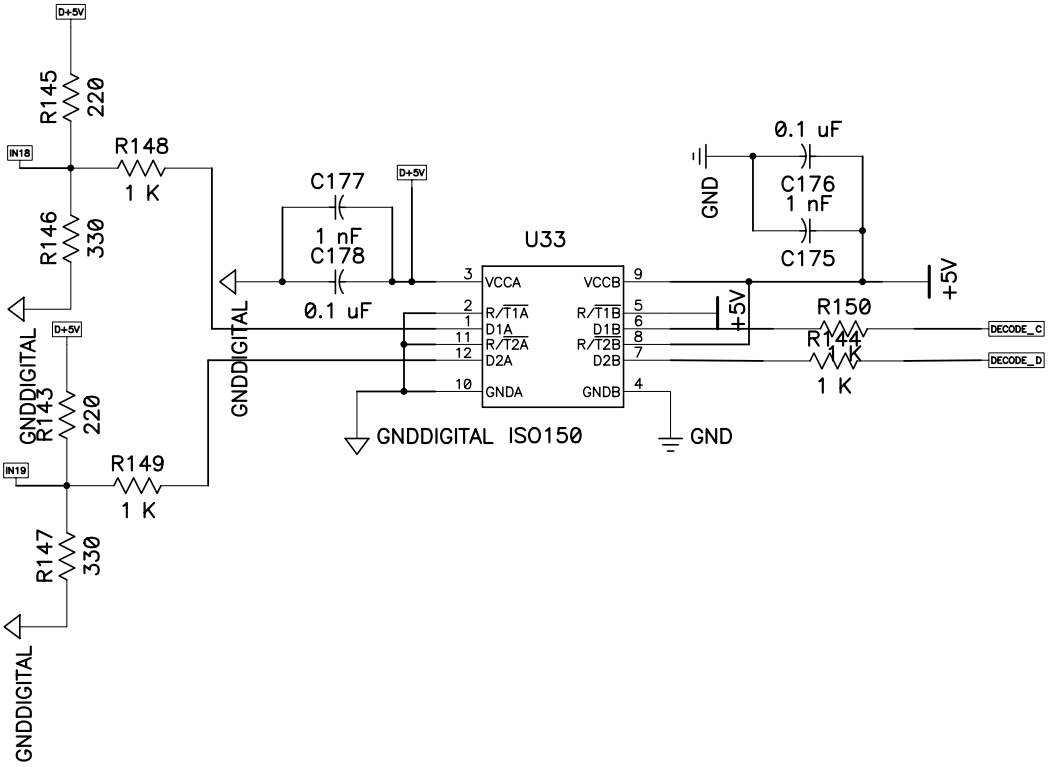

Figure E.7: This schematic shows the pinout and connections to the ISO150 chip on the DAC board.

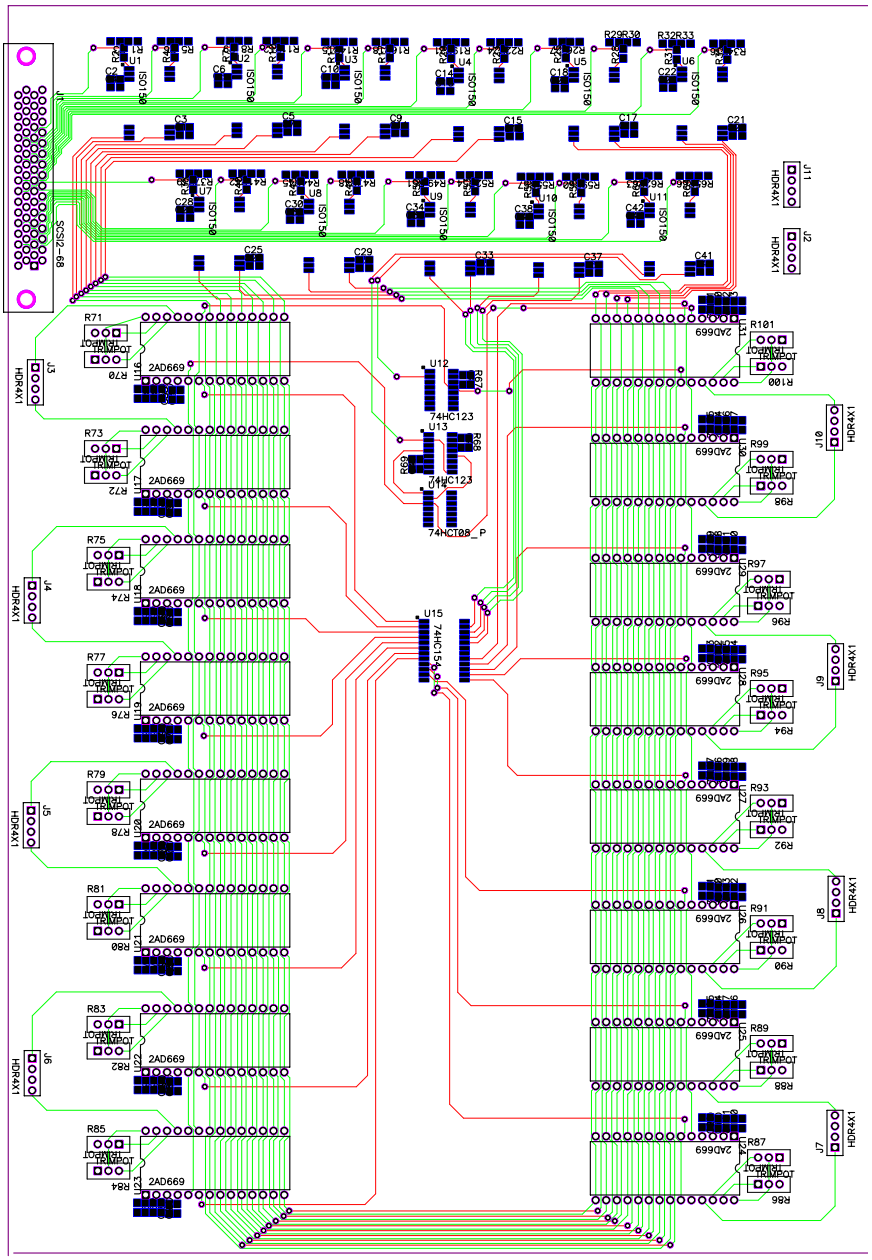

Figure E.8: This is the printed circuit board layout, if ever needed for debugging purposes. An electronic copy should be available. The top section contains the isolation chips, the sixteen DAC chips are laid out surrounding the logic in the center.

E.3 XYZ Box

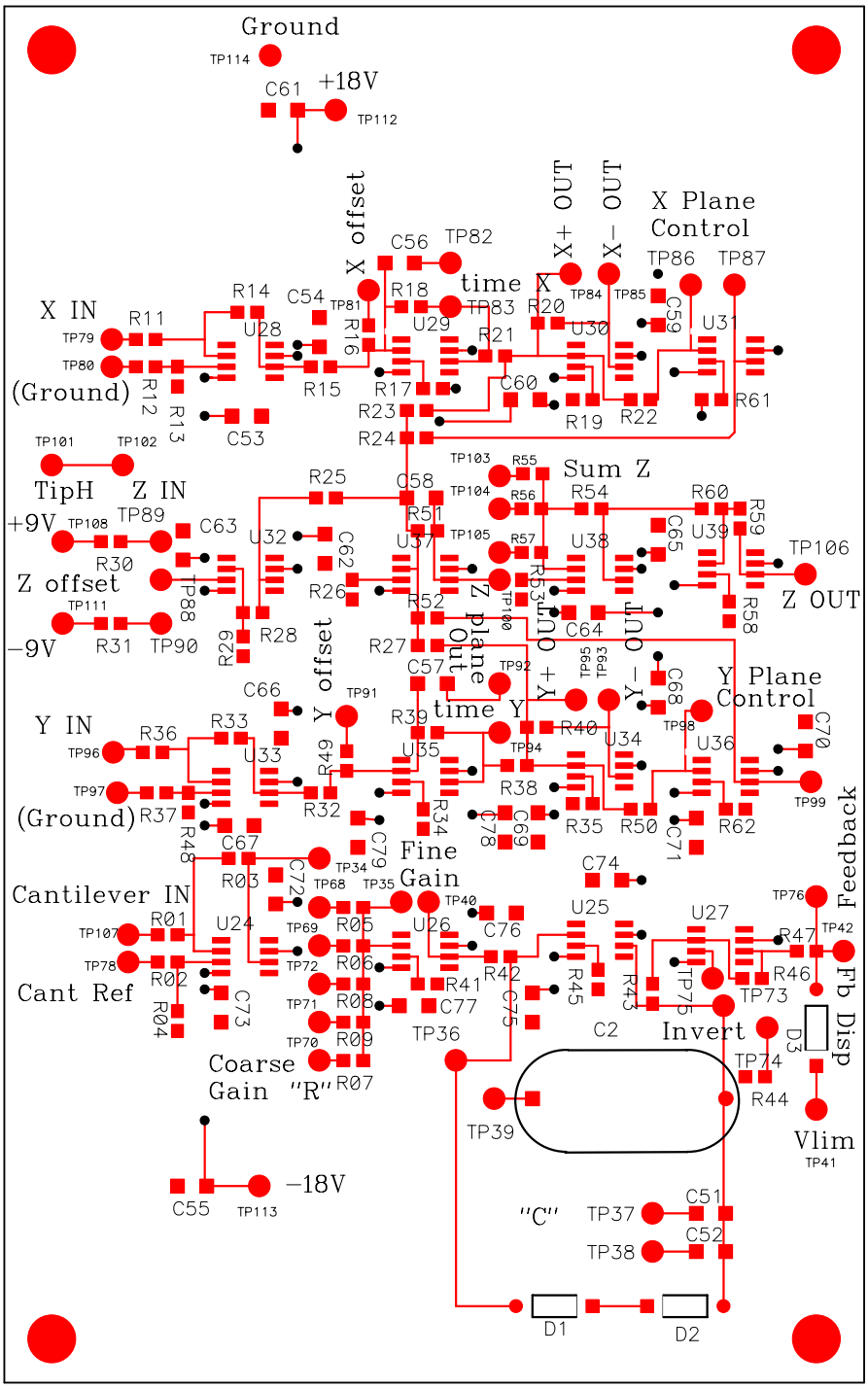

Figure E.9: Printed circuit board layout of the XYZ circuit. The schematics are in Chapter 2.